Design of Large Pore Ordered Mesoporous Silicas, Related Silica/Polymer Composites and Carbon Replicas

by

Liang Cao

A dissertation submitted to the Graduate Faculty in Chemistry in partial fulfillment of the requirements for the degree of Doctor of Philosophy, The City University of New York

2010

This manuscript has been read and accepted for the
Graduate Faculty in Chemistry in satisfaction of the
dissertation requirement for the degree of Doctor of Philosophy.

	Dr. Michal Kruk
Date	Chair of Examining Committee
	Dr. Mahesh Lakshman
Date	Executive Officer

Dr. Shi Jin

Dr. George John

Dr. Michal Kruk
Supervision Committee

THE CITY UNIVERSITY OF NEW YORK

Abstract

Design of Large Pore Ordered Mesoporous Silicas, Related Silica/Polymer Composites and Carbon Replicas

By

Liang Cao

Advisor: Dr. Michal Kruk

This dissertation includes four chapters, namely, the introduction to development and current research interests in mesoporous materials, the "soft-templating" synthesis of large pore 2-D hexagonal ordered mesoporous silicas, the synthesis of mesoporous polymer/silica composites via surface-initiated controlled polymerization, and the "hard-templating" method to fabricate ordered mesoporous carbons.

In Chapter 2, the synthesis of SBA-15 silica with 2-D hexagonal structure of large and ultra-large cylindrical mesopores is outlined. Our work on hexane and 1,3,5-triisopropylbenzene, as suitable micelle expanders, allowed us to tailor SBA-15 pore diameter up to ~15 nm and ~30 nm, respectively. Silica precursors tetraethylorthosilicate (TEOS) and tetramethylorthosilicate were both found suitable, but TEOS was preferred. We also developed a facile and rapid method to synthesize SBA-15 and other mesoporous silicas (FDU-12) in a few hours instead of at least 2 days as originally reported. We also found that the use of static conditions can induce formation of large-pore SBA-15 with platelet morphology.

In Chapter 3, the synthesis of well-defined mesoporous polymer/silica composites via surface-initiated atom transfer radical polymerization (ATRP) was described. 2-(4-chlorosulfonylphenyl)ethyltrichlorosilane was successfully proven as a cost-effective and powerful initiator to initiate polymerizations of various monomers from SBA-15 silicas. We further demonstrated the ATRP with activators regenerated by electron transfer (ARGET) as a more convenient and more environmentally friendly pathway to synthesize polymer/silica composites under mild conditions with hundred ppm levels of copper catalyst and tolerance of limited initial amount of air. In both methods, tunable surface properties, such as adjustable polymer loadings and polymer film thicknesses, can be achieved.

In Chapter 4, high quality ordered mesoporous carbons were synthesized using mesophase pitch or grafted polyacrylonitrile (PAN) as carbon precursors. The infiltration of mesophase pitch into the silica host was effective for synthesis of semi-graphitic carbons with different framework geometries, such as 2-D hexagonal array of nano-rods or cubic carbon structures, even at low carbonization temperature (850 ^{o}C). After stabilization and carbonization of silica/PAN composites, and removal of silica templates, mesoporous carbon materials had ordered structures with hollow nanoscale features, nanopipes or nanospheres from replication of SBA-15 or FDU-12 silicas, respectively.

This is

dedicated to my parents

Cao Jianmin and Zhen Huien,

(曹建明 与 甄惠恩)

my wife

Sun Fangfang

(孙芳芳)

and my son

Cao Zihao

(曹子皓)

Acknowledgments

May I have the pleasure to express my sincere thanks to my advisor, Professor Michal Kruk, for the cooperation, advice, encouragement and recommendations during my graduate study. Without his guidance, expertise, patience and kindness, this thesis would not have come to fruition. It has been an honor to work with him, and I will always be grateful for his help.

I also want to thank my research committee members, Professor Shi Jin and Professor George John for their time, advice and support. I am grateful for Professor Nan-Loh Yang, Professor Ralf Peetz, Professor Shuiqin Zhou, Professor Krishnaswami Raja, Professor Chwen-Yang Shew, Professor Alan Lyons, and Professor Qiao-sheng Hu, who helped me in different ways. I would like to convey my gratitude to Dr. Yalin Wang for his help with the TEM/SEM experiments and Mr. Tai Park for his help with thermal and molecular weight characterizations.

I especially thank my group members Dr. Xuewu Yan, Liang Huang, Xue Tian, Manik Mandal, Chin Ming Hui and Tiffany Man for the cooperation during my Ph.D study. I would also like to thank other friends and colleagues in CSI and Graduate Center.

I would like in particular to express my gratitude to my wife, Fangfang Sun, for her unconditional and endless love, support, understanding and encouragement, to my parents and my parents in law, for the support they always offer, and the new addition, my son Zihao, for bringing hope and happiness to me.

I acknowledge the financial support from College of Staten Island, Graduate Center at the City University of New York and Center for Engineered Polymeric Materials. The financial support from NSF and PRF is also acknowledged.

Table of Contents

List of Figures

List of tables

List of schemes

Chapter 1.

Introduction: Development and Selected Current Research Interests in Design of Ordered Mesoporous Materials

1.1. Ordered Mesoporous Silicas

According to the IUPAC definition,[1] nanoporous materials are classified as microporous (< 2 nm), mesoporous (2-50 nm) and macroporous (>50 nm) materials depending on their pore diameters. Mesoporous materials have been made and utilized with a long history and tradition,[2] while the ordered mesoporous materials have a fairly short history. The first family of ordered mesoporous materials were ordered mesoporous silicas (OMSs) reported by Kuroda group[3] and Mobil Company[4-7] in the early 1990s. Since then OMSs have attracted wide interest of researchers because of their high specific surface areas and pore volumes, uniform meso-structures with accessible pores, diverse chemical compositions, rich surface functionality, various morphologies (particles, films, monoliths, etc.), and so on. Therefore, thanks to these excellent properties, OMSs are candidates in applications in separations of large molecules, bio-sensing, catalysis, adsorption, microelectronics, optics, and fabrication of nano-objects.[8-11]

Synthesis of OMS is primarily based on the "soft templating" strategy;[8,9] that is, surfactants (amphiphilic molecules or macromolecules) aggregate in solution and form ordered mesostructures in which surfactant micelles template the silica framework formation. Although there is a consensus that, in the "soft-templating" synthesis, the surfactant plays a central role in directing the formation of the organic/inorganic mesostructure, two different scenarios are debated regarding silica precursor involvement in the formation of mesostructure.[5-7,12-15] The initially proposed liquid crystalline templating mechanism[5-7] suggests that the surfactant alone forms the mesophase that subsequently serves as the template. Later, hydrolyzed silica precursors deposit and polymerize on the hydrophilic domains of the mesostructure to form inorganic silica framework which copies the geometry of the liquid crystalline phase. However, this theory was questioned because relative low concentrations of surfactants do not meet the

requirement of formation of the liquid crystalline phase.[16,17] Consequently, the cooperative self-assembly formation mechanism[18-22] is proposed in which surfactant molecules, together with the silica source, form the liquid crystalline phase in which surfactant micelles template the mesopores. The debate continues because the two mechanisms, the liquid crystal templating and the cooperative formation, are valid depending on the different synthesis conditions. However, in most cases, the cooperative mechanism is likely to be operative. In either of the above synthesis mechanisms, the mesostructures strongly rely on the several parameters, for instance the chemical structure of surfactants, temperature, concentration, pH, addition of salts, in the process of formation of disordered (worm-like or form-like), lamellar, hexagonal or cubic phase. So a proper selection of surfactants and synthesis conditions is extremely important for OMS design. The choices of surfactants are from two main categories according to properties of hydrophilic head groups: 1) ionic surfactants including anionic head groups (alkyl carboxylate, phosphate, sulfate, etc.),[20,23,24] or cationic head groups (alkyl quaternary ammonium salt, *etc*.)[4,5,7,25] 2) neutral surfactants with no charged head groups,[8] including poly(ethylene oxide)/poly(propylene oxide) diblock or triblock copolymers.

Among ionic surfactants, cationic ones were first used to synthesize OMS from the so-called MCM family.[4,5,7,25] Under appropriate alkaline conditions, deprotonated silica species (anions) and surfactant molecules (cations) can form lamellar MCM-50, 2-D hexagonal MCM-41 and cubic *Ia3d* MCM-48. The MCM-41 and MCM-48 have been evaluated for industrial processes involving catalysis and adsorptions. Later, anionic surfactants[20,23,24] were applied under acidic conditions, in which anionic surfactant molecules are surrounded by positive counterions and silica species. Successful examples include AMS series of materials.

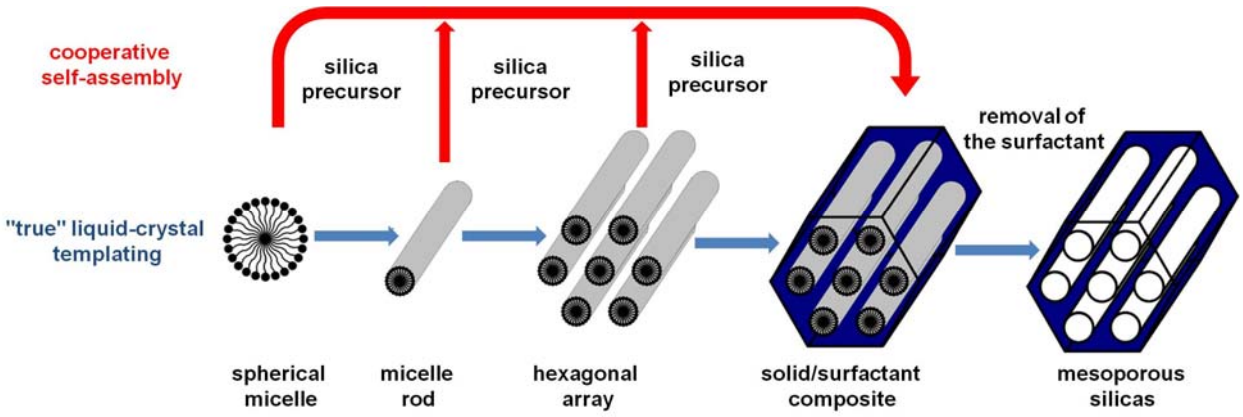

Scheme 1.1. Two different synthesis mechanism cooperative self-assembly and "true" liquid-crystal templating.

However, ionic-surfactant-templated OMSs have the limitation of typically producing small mesopores with sizes in the region of 2-7 nm due to ionic surfactants' short chains and small resulting micelle sizes and the wall thickness in the range of 0.7-1.5 nm. Therefore, the difficulty in enlarging pore diameters and improving hydrothermal stability hindered their potential applications. On the other hand, most neutral surfactants used in OMS synthesis are amphiphilic block copolymers with high molecular weights, therefore larger pore diameters (~8-30 nm) are achievable.[8] Moreover, neutral surfactants have high flexibility in tailoring pore structure, because the hydrophobic/hydrophilic block ratios can be simply adjusted by selecting different block lengths or by adding co-surfactants, by changing reaction conditions, such as temperature or pH, or/and by adding additives, such as micelle expanders.

Polymer-templated SBA-15 with 2-D hexagonal (p*6mm* symmetry) structure of channel-like (cylindrical) mesopores is one of two most popular OMSs (in addition to MCM-41) owing to its several remarkable features.[21,22] First, the synthesis of SBA-15 (pore diameter of ~9 nm) is very simple and well-reproducible. The synthesis is based on the use of readily available

poly(ethylene oxide)-poly(propylene oxide)-poly(ethylene oxide) triblock copolymer ($EO_{20}PO_{70}EO_{20}$; Pluronics P123 manufactured by BASF) and normal silica precursors (mostly tetraethyl orthosilicate) under acidic conditions.[21,22] Second, SBA-15 exhibits larger pore diameters (up to 30 nm) than those previously attainable for ionic-surfactant-templated materials, such as MCM-41 (up to ~7 nm)[26] and MCM-48 silicas (up to ~5 nm).[27] Moreover, the pore diameters of SBA-15 can easily be adjusted in a wide range by changing the synthesis and hydrothermal treatment conditions. Third, SBA-15 has thick walls between the pores, so it is inherently much more hydrothermally stable than MCM-41 and MCM-48. Forth, the cylindrical pores of SBA-15 are usually connected with one another by irregular micropore or mesopore connections, due to the occlusion of the poly(ethylene oxide) blocks of the template in the silica framework. Such a three dimensional structure creates opportunities for the use of SBA-15 as a template to synthesize ordered arrays of connected nanowires and nanotubules.

It was originally reported that the pore diameter of SBA-15 silica can be enlarged from its typical value (~9 nm) to 30 nm using 1,3,5-trimethylbenzene (TMB) as a swelling agent.[21,22] However, it was shown later that as the amount of TMB was increased, a limited pore diameter increase (up to 12 nm) with retention of the SBA-15 structure was followed by a major pore size increase with a change of the pore geometry to spherical and formation of a new material, referred to as a mesocellular foam (MCF).[28] MCFs exhibit quite narrow pore size distributions, but their structures are either weakly ordered or disordered.[29]

Several reported strategies allow one to extend the pore diameters of SBA-15 beyond the 12 nm limit. First, the selection of surfactants of appropriate size is a well-established strategy for the pore size tailoring.[30-38] Early work on the synthesis of large-pore silica with 2-D hexagonal

array of cylindrical mesopores involved poly(ethylene-co-butylene)-poly(ethylene oxide) surfactants,[30] but the structural identification of the product was based only on transmission electron microscopy and is not fully convincing. Later work involved block copolymers synthesized via the extension of poly(ethylene oxide) (PEO) block with poly(methyl acrylate) (PMA) block(s)[31-33] using atom transfer radical polymerization.[39,40] The resulting diblock (PEO-PMA)[32,41] and triblock (PMA-PEO-PMA)[33,42] copolymers were successfully used as templates for the synthesis of 2-D hexagonal silica structures (SBA-15) with d_{100} interplanar spacings up to at least 16.5 nm, and with BJH pore diameters up to 20 nm. The increase in the size of the hydrophobic block (PMA) resulted in a fairly systematic pore diameter increase. However, in the report on the use of PEO-PMA copolymers,[32] broad ranges of synthesis conditions were delineated, with no specific conditions for the synthesis of particular samples. Moreover, one of the reported isotherms[32] showed a hysteresis loop characteristic of a material with constricted (cage-like[34] or plugged[35,36]) mesopores, while another one showed a significant increase in uptake extending from the capillary condensation in primary mesopores to the saturation vapor pressure. Apparently, the structures of these materials can exhibit peculiarities not observed in typical SBA-15 silicas. Because of the fact that PEO-based copolymers with hydrophobic blocks other than poly(propylene oxide) (PPO), for instance PMA or polystyrene, can be conveniently synthesized and hold promise in the synthesis of large-pore ordered mesoporous silicas,[32,33,37,38] it is important to further investigate templating effects of these novel structure directing agents. We reported that well-defined PEO-PMA diblock copolymers with high mass fraction of the PMA block are suitable as templates for large-pore SBA-15 with an appreciable degree of structural ordering. The obtained SBA-15 silicas exhibited (100) interplanar spacings up to 17 nm and often had narrow pore size distributions. The unit-cell size and the pore diameter

increased and the degree of structural ordering decreased with the increase in size of the hydrophobic block (PMA) of the copolymer and lowering the temperature (e.g., to 10 °C).

The second strategy to synthesize large-pore SBA-15 was to use additives. Concentrated solutions of Pluronic F127, $EO_{106}PO_{70}EO_{106}$ (which has the same size of the hydrophobic PPO block as Pluronic P123, but has a much larger hydrophilic PEO blocks), in combination with appropriate cosolvents/additives (butanol, pentanol, hexanol), and in some cases, swelling agents (octane), can afford SBA-15 silicas with large values of d_{100} (up to 17 nm).[43,44] The gas adsorption data reported for one of these materials with d_{100} = 14.0 nm indicated the pore diameter beyond the 12 nm limit. Recently, the use of PPO homopolymer to swell Pluronic F127 micelles afforded SBA-15 silicas with BJH pore diameters up to 13 nm.[45] The most attractive strategy for the pore size enlargement is the use of micelle swelling agents, which have been proven as a powerful pathway since the inception of ordered mesoporous materials. The swelling agents (or additives) used to increase the size of micelles of Pluronics 123 in SBA-15 synthesis included aliphatic alcohols (butanol, pentanol, hexanol),[43,44] aliphatic hydrocarbons (pentane, hexane, heptane, octane, etc.),[43,46-48] and aromatic hydrocarbons (1,3,5-triisopropylbenzene).[49] The addition of the above compounds to the synthesis mixture allowed one to synthesize SBA-15 silicas with (100) interplanar spacings up to ~17 nm and pore diameters up to ~15 nm. It should be noted that in the case of SBA-15 and MCM-41, the (100) interplanar spacing multiplied by 1.155 provides the distance between the centers of adjacent cylindrical mesopores.

An approach for the identification of swelling agents suitable for a surfactant-templated synthesis of ordered mesoporous silicas with very large pores was recently proposed by us.[50] The starting point of the reasoning was a realization that in cases of well-defined ordered mesoporous

silicas with large unit-cell sizes, such as large-pore SBA-15 (that has (100) interplanar spacing of ~14 nm) obtained in the presence of hexane, there was no evidence of any major uptake of the swelling agent by the micelles of the template.[48] On the other hand, the synthesis of less well-defined structures, such as silica mesocellular foams (MCFs) in the presence of TMB, involves a major uptake of the swelling agent.[51] On the basis of this observation, it was hypothesized that poorly ordered structures are likely to form when the uptake of the swelling agent is too high.[50] This prompted us to search for swelling agents that are more powerful than the known swelling agents suitable for the synthesis of well-ordered materials (for instance, hexane), yet less potent than those swelling agents that afford structures with very large pores devoid of ordering (for instance TMB in the case of Pluronic P123 surfactant).[50] Another important observation was that the pore diameter of SBA-15 synthesized in the presence of linear hydrocarbon swelling agents increased as the chain length of the hydrocarbon decreased, which follows the increase in the extent of solubilization of alkanes in Pluronics micelles .[46,47] This indicated that one can use the data on the extent of solubilization of substances in surfactant micelles to identify swelling agent candidates for the mesoporous silica synthesis. The whole series of linear hydrocarbons that are liquids under normal conditions, including hexane and pentane,[46-48] has already been explored, so cyclic and aromatic hydrocarbons were contemplated by us as swelling agent candidates for SBA-15.[50] In the case of aromatic hydrocarbons (benzene, toluene, xylene), the extent of solubilization in Pluronics decreases as the number and size of alkyl substituents on the benzene ring increases.[52,53] Therefore, it was predicted that 1,3,5-triethylbenzene and triisopropylbenzene (TIPB) would solubilize in Pluronics to a smaller extent than TMB does, which may allow for a lower extent of swelling and thus the retention of the SBA-15 structure with concomitant appreciable pore size enlargement. Our study carried out at low temperature conditions (11-

20 °C) confirmed that when tetraethyl orthosilicate was used as a silica source and Pluronic P123 was used as a surfactant, the addition of TIPB afforded SBA-15 with (100) interplanar spacings from 12 to as much as 26 nm, and with pore diameters from 10 to ~26 nm.[50,54] The pore diameter of these materials was controlled primarily through the selection of the initial synthesis temperature, and further adjusted through the selection of the hydrothermal treatment temperature and time, and the amount of the swelling agent. The details of this breakthrough development in SBA-15 synthesis are discussed in Chapter 2.

1.2. Ordered Mesoporous Polymer/Silica Composites

Considerable effort has been devoted to the synthesis and application of composites materials, because they can exhibit a synergistic performance in comparison to the individual components. For example, researchers found that, with only 5 wt.% of clay incorporation in the nylon matrix, the physical properties of clay/nylon composites are greatly improved in tensile strength, tensile modulus, and heat distortion temperature when compared to neat nylon.[55] Among various polymer composites, mesoporous polymer/silica composites (MPSCs) are unique as polymers can homogenously disperse within nanoporous host and at the same time nanoporous substrates can uniformly disperse in polymer matrix, meaning that two components are well blended at the nanoscale. Therefore, MPSCs are capable of providing combined advantages both of organic polymers, such as flexibility, toughness, hydrophobicity, and versatility for further functionalization, and of inorganic components, such as good mechanical and thermal stability.

Various methods have been developed to fabricate MPSCs. The mechanical mixing the polymer and mesoporous silica is one of the earliest ideas to achieve MPSC. Mesoporous silicas working as fillers can significantly improve physical properties of polymer matrix. For example,

with 5 wt.% mesoporous silica particles, PMMA composites have ~20 ^{o}C higher T_g and ~50% higher maximum stress than neat PMMA.[56,57] However, such simple mixing could randomly disperse polymers outside and inside the pores, leading to loss of materials' porosity. To selectively immobilize polymers into the pores, certain interactions must be created or enhanced between polymers and porous hosts. For example, hydrogen bonding between the silanol groups on the silica surface and the groups (such as amide moieties) in polymer chain can be applied to entrap polymers (such as poly(2-methyl-2-oxazoline), poly(N-vinylpyrrolidone), and poly(N,N-dimethylacrylamide) in the pores of mesoporous silica to form MPSC.[58] For polymers without strong hydrogen accepting groups, intentional grafting of hydrogen accepting groups onto polymer chain can help these polymers insert into the pores, such as poly (2-methoxy-5-(29-ethyl-hexyloxy)-1,4-phenylene vinylene). Polymer contents can be up to 12.9 wt.% by choosing suitable solvents and conditions.[59]

In addition to physically attaching polymers into mesoporous silicas hosts, chemical bonding is frequently used to synthesize MPSC. Surface modification strategies including "grafting-to" or "grafting-from" are applied to fabricate MPSC. In the "grafting-to" methods, highly efficient chemical coupling reactions are desired to achieve high loading and dense coverage of polymer moieties on the surface. For example, with "click" technique, the SBA-15 can turn out as a versatile nanoporous host to react with large number of molecules, including polymers.[60-63] It has been demonstrated that "click" reactions allow one to functionalize the mesoporous silicas surface by immobilizing oligomers and monosaccharides. High loadings of polymer (up to 25 wt.%) were introduced without the pore blocking, and the polymer layer thickness up to about 2 nm has been achieved.[63]

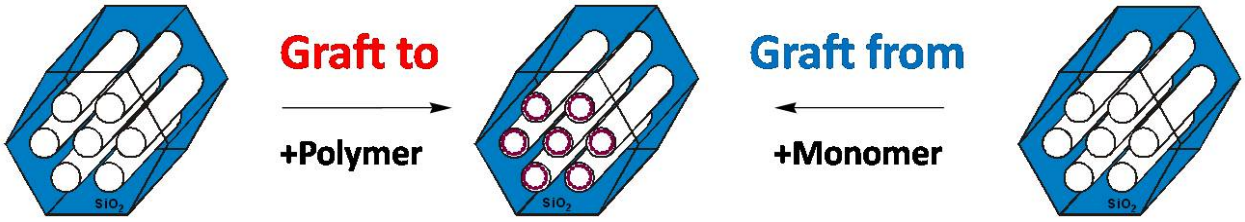

Scheme 1.2. Illustration of surface modification strategies including "Graft-to" or "Graft-from" methods.

The "grafting-from" approach, however, provides more versatile alternatives to synthesize MPSCs due to a large variety of controlled polymerization techniques.[64] For example, condensation reactions can be unitized to graft dendrimers with different generations to tailor surface properties with large number of functional groups on the surface, adjustable surface areas, pore volumes and pore diameters. [65,66] Moreover, Ryoo and coworkers successfully generated well-defined MPSC with controlled pore diameters using free radical polymerizations by adsorption of monomer (MMA and styrene) from vapor phase and following polymerizations of these surface-adsorbed monomers with monomers in solution to form controlled thin layer of polymers. [67] Similarly polyaniline can be introduced on the surface of SBA-15.[68-70] While these works do not involve "grafting-from" methodology in the strict sense, they resemble this methodology using monomers that are polymerized and immobilized on the surface.

The synthesis strategies above discussed are limited by their inherent polymerization techniques as they cannot precisely control content of polymers or need multi-step polymerizations. So polymers with designed molecular weight and narrow polydispersity are hard to produce, not to mention the formation of uniform polymer brushes or several-nanometer-thick films on the surface. To overcome the aforementioned shortcomings, the surface-initiated

polymerizations must initiate fast and proceed in the well-controlled manner; in other words, controlled polymerizations must be applied. To functionalize mesoporous materials, in most cases controlled radical polymerizations stand out in comparison to controlled cationic/anionic polymerizations[71-74] or controlled condensation polymerizations[65,66] due to their milder synthesis conditions and wider selections of monomers. One of well controlled polymerization methods is atom transfer radical polymerization (ATRP),[40] which involves a reversible halogen (Cl or Br) transfer between a dormant species (an added halogen-containing initiator or dormant propagating chain end containing halogen) and a transition metal (Cu, Fe, Ru, etc.) complex in a lower oxidation state. The halogen exchange process generates the metal complex in the higher oxidation state with a coordinated halide ligand and the propagating radical (active species), which can add monomer to grow polymer chain. In a successful ATRP reaction, all propagating species (chains) begin growth nearly at the same time and at the same rate due to its fast initiation and rapid reversible deactivation of propagating radicals to dominant species. Therefore a narrow molecular weight distribution and chain extensions can be achieved. Besides its versatility in building polymer architectures (homopolymers, block copolymers, star polymers, brush polymers, etc), ATRP is also suitable for the surface-initiated polymerization of a wide range of monomers from various substrates.[64]

However, the application of ATRP to surface-functionalize mesoporous silica has been limited so far. Fu et al.[75] grafted poly(N-isopropyl acrylamide) (PNIPAAm) from the surface of silica particles with ordered pores of diameter below 3 nm, but it is possible that the size of introduced monolayer of polymerization initiator groups already decreased the pore radius by ~1 nm, so it is hard to envision the formation of any appreciable amounts of PNIPAAm in such small ordered pores. Zhou et al.[76] synthesized similar PNIPAAm layers initiated from less

ordered silica mesocellular foam (MCF) materials with pore diameter of 22 nm, but neither molar mass nor kinetic data were given in the paper, and hence there is no clear proof of any well controlled polymerization occurring inside the pore. Kruk et al.[77] performed surface-initiated ATRP of acrylonitrile (AN) in ordered mesoporous silicas with 10-15 nm pore size to uniformly fill the pores with polyacrylonitrile and further to convert PAN to mesostructured carbons. Save et al.[78,79] for the first time studied ATRP of styrene and methyl methacrylate initiated from surface of ordered mesoporous silicas. Details concerning molar mass distribution, and grafted initiator efficiency were well described, but the information of pore accessibility was limited and did not provide any compelling evidence of well-defined polymer film formation. Recently, the work of Kruk et al.[80] has demonstrated successful grafting of polyacrylonitrile, poly(2-(dimethylamino)ethyl methacrylate) and polystyrene on concave surfaces of cylindrical mesopores of diameter 10 nm and spherical mesopores of diameter 15 nm. By adding deactivor (Cu(II)) species at the beginning of polymerizations, Kruk and coworkers have demonstrated that surface initiated ATRP was well controlled and narrow molecular weight distributions were produced with polydispersity as low as 1.06 in some cases.[80] Corresponding polymer films thicknesses were in the range up to 1−2 nm without causing any major pore blockage.

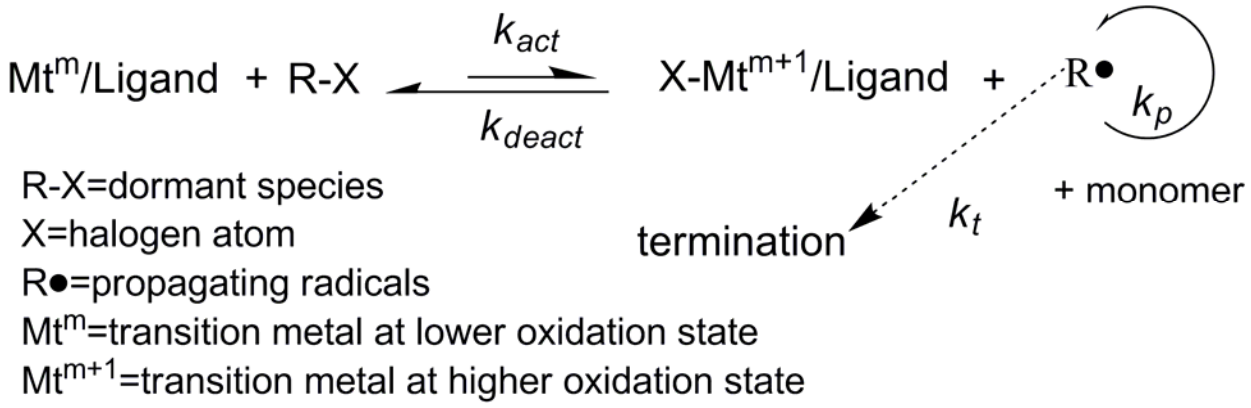

Scheme 1.3. Atom transfer radical polymerization mechanism.

However, a drawback of normal ATRP is that the polymerization needs a significant amount of catalyst, usually in the range of 1000-10000 ppm and the resulting samples may have colors indicating appreciable content of catalyst residue. Moreover, ATRP reactions require strict and time-consuming degassing procedures. Therefore, there is a need to elaborate more convenient and environmentally friendly pathways. Recently developed activators regenerated by electron transfer for ATRP (ARGET ATRP) method[81-85] provides a major improvement in both of the aforementioned areas because it effectively reduces the amount of copper catalyst to ~10-100 ppm level and can be adapted under initial presence of air without oxygen degassing steps. So ARGET ATRP, which is considered as a "green" polymerization method, can been performed without using air-tight glassware and a vacuum line to grow polymer brushes on flat surfaces,[83] convex surfaces of nanoparticles[84] and concave surfaces of OMS.[85] We reported for the first time that ARGET ATRP was used to synthesize high-surface-area MPSC.[85] The syntheses were performed in a closed vial with transparent solutions and the resulting samples were white and thus free from coloration. The ARGET ATRP method has a wide scope in the context of functionalization of nanoporous materials, as various polymers including polystyrene, poly(methyl methacrylate), polyacrylonitrile, poly(N-isopropylacrylamide) and poly(2-(dimethylamino)ethyl methacrylate) were successfully produced.[85,86] Polymer chains exhibited quite low polydispersity, and polymer loading and film thickness were well controlled.

1.3. Ordered Mesoporous Carbons

Ordered mesoporous carbons (OMCs)[87-89] constitute an important class of mesoporous materials being intensively developed in the last eleven years. They exhibit excellent properties including large surface areas and pore volumes, and high chemical and mechanical stability. Their broad potential applications are in various fields such as adsorption,[90-92] catalysis,[93] fuel cells,[94-96] and many others.[97-104]

The syntheses of mesoporous carbons mostly belong to two strategies: soft templating and hard templating. The former method utilizes self-assembled amphiphilic molecules as templates at selected conditions to direct carbon precursors to form cross-linked polymer network, which is followed by removing the template, carbonation or even graphitization in some cases. The first successful OMC sample via soft templating was prepared by Dai and coworkers.[105] Resorcinol and formaldehyde as carbon precursors were co-polymerized in the polystyrene-block-poly(4-vinylpyridine) template. The resulting OMC films had hexagonal arrangement of cylindrical mesopores with large pore diameter of ~34 nm and pore wall thickness of ~9 nm. The well-oriented mesopores were perpendicular to the substrate and this orientation prevailed across the whole film. Later, the same group[106] and Nishiyama[107] at al. independently applied the same carbon precursors and Pluronic F127 as a template in acidic solution to synthesize hexagonally ordered OMCs with well-ordered mesopores up to 9 nm in diameter. A series of excellent works in the synthesis of soft-templated OMCs were reported by Zhao and coworkers on the preparation of carbons using resols as carbon precursors and amphiliphilic block copolymer surfactants as templates.[108-113] Successful examples include C-FDU-14 carbon with 3-D bicontinuous cubic structure (*Ia3d* symmetry) and pore diameter of 2.7 nm prepared using

Pluronic P123 as a template,[108,109,111] C-FDU-15 with 2-D hexagonal structure (p6mm symmetry) and pore diameter of 5.8 nm prepared using Pluronic F127 as a template,[108-110,112] C-FDU-16 with body-centered cubic structure (Im3m symmetry) and pore diameter of 3.7 nm prepared using Pluronic F127 as a template,[108-110,112] and C-FDU-17 with cubic structure (Fd3m symmetry) and bimodal pore size distribution (diameters of 4.0 nm and 6.9 nm) prepared using $PO_{53}EO_{136}PO_{53}$ as a template. [113]

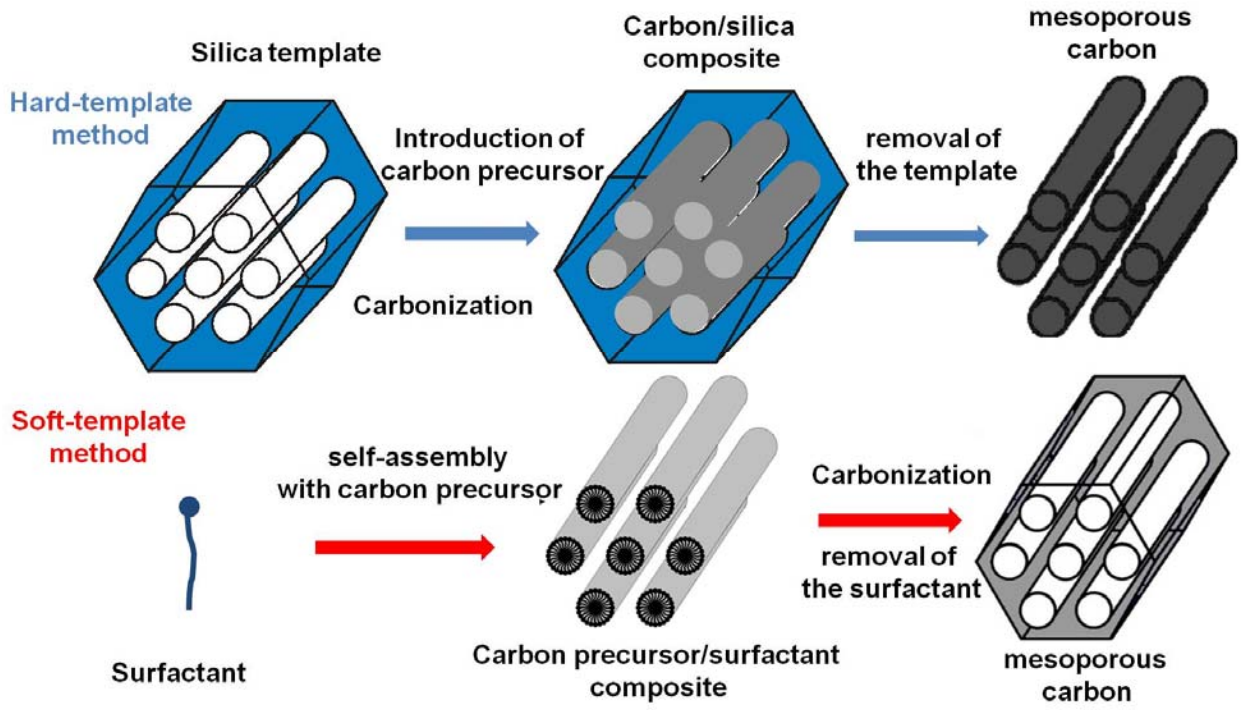

Scheme 1.4. Synthesis of ordered mesoporous carbons via "hard-template" and "soft-template" methods.

Another type of soft-template is based on nanoscale phase-separation of block copolymers with polyacrylonitrile (PAN) as a carbon precursor block and other polymer(s) as sacrificial block(s). After the block copolymer is self-assembled to form nanoscale phase-separated morphology and PAN component is converted to carbon, the sacrificial block can be removed by

pyrolysis to form empty cavities (mesopores).[114-116] Kruk et al. have synthesized PAN-PEO diblock copolymers which can afford nanoporous carbons with large pore diameter up to 40 nm in silica-assisted synthesis.[114] Ho et al. synthesized PAN-poly(caprolactone) as a precursor for nanoporous carbon, but lamellar pore structures are only confirmed by electron microscopies without detailed textural properties.[115] Peng et al. electrospun a mixture of PAN with copolymer of acrylonitrile and methyl methacrylate into fibers with mesopores of 44 nm.[116]

However, the soft-templating method has shortcoming of limited number of carbon precursors (resoles or PAN), and low carbon yield (<70 %). A more frequently used strategy is the hard-templating or nano-casting method;[117-120] that is, nano-sized or nanoporous solid particles are applied as templates to assist carbon precursors to form mesoporous structures. The strategy usually involves three major steps: (i) introduction of carbon precursor into templates, (ii) carbonation (and in some cases graphitization) of carbon precursor and (iii) removal of the template. In many cases, resulting porous carbons keep the morphology of the templates but are inverse replicas, as the framework and pores of the template will turn in the pores and framework of the produced carbon. The advantages of hard-templating method over soft-templating method are a large variety of available templates including spherical particles or ordered mesoporous materials, large selection of carbon precursors, and ease of producing ordered mesoporous carbon structures. The pioneering works on the templated synthesis of carbons were from Knox and his co-workers,[121,122] as they successfully synthesized mesoporous carbons using silica gels as templates in the 1980s. However, these materials were not ordered at nanoscale. From that time, this novel method has been used to create various mesoporous carbons

An MCM-48 OMS of cubic *Ia3d* symmetry was first applied by Ryoo et al. and Heyon et al. to fabricate OMC.[119,120] In the elaborated synthesis procedure, MCM-48 silicas was repeatedly infiltrated with sucrose as carbon precursor and sulfuric acid as an additive to promote carbonization to ensure that the pores are totally filled. Subsequent carbonization and dissolution of the silica template allowed one to obtain a mesoporous carbon, named CMK-1.[120] Ideally, the generated carbon should be a perfect inverse replica of the template, but CMK-1 was not an exact inverse replica of MCM-48 due to the peculiarity of template structure and the resulting structural change of carbon sample during the template removal. The carbon CMK-1 had rather high specific surface area of ~1700 m^2 g^{-1} and total pore volume of 1.0 cm^3 g^{-1}. The diameter of uniform pores of the carbon replica was related to the wall thickness of the MCM-48 template.

Later, MCM-41 and SBA-15 with 2-D hexagonal symmetry and cylindrical mesopores were employed as hard templates. As the mesopores in MCM-41 are isolated (disconnected), the use of MCM-41 as the template failed to produce an inverse replica with an ordered structure and the final products was found to be a disordered structure of carbon nano-rods.[100,123] In comparison, SBA-15 silica has a porous structure with ordered large primary mesopores interconnected through complementary irregular pores located in the silica walls between the primary pore channels. Therefore the inverse carbon replica of the SBA-15 silica was in array of connected carbon rods (CMK-3) with well maintained ordered structure.[120] The size of ordered mesopores located between three neighboring carbon nanorods was estimated via nitrogen adsorption as 4.5 nm.

Another breakthrough in the history of OMC was the development of CMK-5 carbon,[94] which is an array of carbon nanopipes interconnected through small bridges. The synthesis

started with incorporation of $AlCl_3$ catalyst on the surface of the SBA-15 mesopores to introduce acidic sites. Subsequently, furfuryl alcohol (carbon source) was polymerized at elevated temperature on the SBA-15 pore surface. The carbonization of the polymer and the silica template dissolution allowed one to obtain well-defined OMC revealing two types of mesopores of the size of 5.9 nm corresponding to the space between the nanopipes and of 4.2 nm for tubular pores in the nanopipes.

Besides the synthesis methods, the selection of carbon precursor is another important factor as it may significantly affect the carbon properties. For example, sucrose as the most commonly applied carbon precursor can generate extremely high specific surface area because of resulting samples' amorphous carbon framework with irregular micropores in the walls.[120] Synthetic polymers are also frequently employed as their polymerizations in situ within the pores of the template can lead to high and/or controlled loading of carbon precursors. Successfully used polymers include phenolic resin,[94,119] poly(furfuryl alcohol),[124-127] poly(divinylbenzene),[128,129] polyacrylonitrile,[114,130,131] and poly(vinyl chloride).[132] Another category is aromatic compounds as acenaphthene,[133] benzene, naphthalene, antracene, and pyrene,[134] and polyaromatic hydrocarbons including petroleum pitch[135,136] and mesophase pitch.[135,137,138] Mesophase pitches[135,137,138] are special as their well-stacked layers of aromatic rings in the liquid crystalline domains are beneficial in providing of high graphitization tendency and formation of low amount of microporocity. Besides, their anisotropic property makes them less viscous above the softening point. The mesophase-pitch-based OMC was proven as excellent semi-graphitic carbon which was further graphitized at high temperature. Li and Jaroniec have proposed the imprinting process as simple and reproducible method to fabricate OMC using silica templates.[139-142]

OMCs with hetero atoms other than carbon and hydrogen are expected to bring new properties and have been synthesized by different methods. For example, polyacrylonitrile, synthesized via free radical or controlled radical polymerizations inside the OMS, afforded N-doped OMS after carbonization and silica dissolution.[77,131,137] Carboxyl groups can be introduced onto CMK-3 carbons after nitric acid treatment to change the surface to moderately hydrophilic.[143] The fluorinated mesoporous carbons were synthesized via reaction of CMK-1 carbon with fluorine and can be utilized in electrochemistry, for instance, as the material for highly efficient batteries.[138] Similarly, chlorine-, ester-, and alkyl-containing diazonium compounds were attached to the carbon surface by the reaction of 4-substituted anilines with isoamyl nitrite inside OMC mesopores.[144]

OMC with semi-graphitic and graphitic framework have attracted a lot of research interest because of their good electrical conductivity and high surface homogeneity. The general method to synthesize graphitic frameworks is to heat the carbon at high temperature (above 2000 ^{o}C) and under inert atmosphere. Depending on the type of carbon precursor, graphitization temperatures are different as aromatic and polyaromatic compounds (divinylbenzene, pyrrole, polyacrylonitrile and mesophase pitch) can provide semi-graphitic structure at ~900 ºC,[133-135,138,140,145-147] but further heat treatment is needed to obtain better defined graphitic carbons at ~2300 ºC.[130] However, under such conditions, the disappearance of most micropores and in many cases, collapse of carbon framework were observed and led to a significant drop of the specific surface area and the total pore volume of OMC, or even the loss of porosity. The other approach is catalytic graphitization, which allows one to produce (partial) graphitization at considerably lower temperature, typically of 800 – 900 ºC.[131,148-152] However, during the removal

of the catalyst from the pores, an undesired secondary porosity in the framework might be formed.

In the graphitized carbons, the directionality of alignment of graphene sheets attracted research focus as it may significantly change samples' conducting properties or mechanical strength. For example, when polyaromatic hydrocarbon (acenaphthene) was carbonized at 1173 K, wide-angle XRD pattern and TEM images conformed that short graphene sheets were stacked perpendicular to the surface of the material.[133] On the other hand, graphene sheets parallel to the surface was observed for OMCs synthesized from polypyrrole and PAN.[130,146]

Chapter 2.

Synthesis of Ordered Mesoporous Silica SBA-15 with Two-Dimensional Hexagonal Structure and Large Pores

2.1. Introduction

From the time of its disclosure twelve years ago, [21,22] SBA-15 silica with two-dimensional (2-D) hexagonal arrays of cylindrical mesopores (typically with connections much narrower than the main cylindrical mesopores) [118,153,154] has attracted significant attention in the scientific and engineering community. SBA-15 is suitable as an adsorbent, a catalyst support, an immobilization medium for biomolecules, a host or template for nanostructures and so forth [9,87,155-158]. SBA-15 is typically templated by surfactants from commercially available Pluronic family of poly(ethylene oxide)-poly(propylene oxide)-poly(ethylene oxide) triblock copolymers, out of which Pluronic P123 ($EO_{20}PO_{70}EO_{20}$) is particularly suitable to template the formation of cylindrical mesopores.[21,22] Originally, it appeared that SBA-15 with a pore diameter anywhere in 5-30 nm range can be synthesized by selecting appropriate conditions of the hydrothermal treatment and/or the relative amount of the micelle swelling agent, 1,3,5-trimethylbenzene (TMB).[21,22] However, a subsequent study [28] indicated that the pore diameter of cylindrical mesopores of SBA-15 can be increased up to 12 nm by increasing the amount of TMB. On the other hand, a further increase in the amount of TMB leads to the formation of a different structure, called a mesocellular foam (MCF),[29] which is weakly ordered or disordered and features spherical mesopores of large diameter (20-40 nm). A subsequent effort in increasing the pore diameter of SBA-15 went in two directions: the use of custom-made block-copolymer surfactants[32,33,41,42] and the identification of suitable swelling agents for Pluronic block copolymer templates. The swelling agents (or additives) used to increase the size of micelles of Pluronics in SBA-15 synthesis included aliphatic alcohols (butanol, pentanol and hexanol) [43], aliphatic hydrocarbons, such as hexane, and octane,[43,46,47] cyclohexane,[50] and 1,3,5-

triisopropylbenzene (TIPB).[159] The addition of the above compounds to the synthesis mixture allowed one to synthesize SBA-15 silicas with (100) interplanar spacings up to ~17 nm and pore diameters up to ~15 nm. Although the strategy of adding micelle expanders is very promising, there had been lack of successful reports of preparing ultra-large-pore SBA-15 materials (pore diameter above ~20 nm), until our study was reported.[50]

In this chapter, the discussion will focus on study of pore size expansion in the presence of micelle expanders. Several micelle expanders were carefully chosen and tested to enlarge the pore size without losing ordered structures. The chapter includes:

1. The use of hexane to synthesize highly ordered SBA-15 silicas with BJH (nominal) pore diameters readily adjustable in the range from 10 to 18 nm (and the actual pore diameters up to 15 nm);

2. Extensive investigation of 1,3,5-triisopropylbenzene (TIPB) to tailor SBA-15 pore diameter up to 30 nm while maintaining periodic pore structures.

3. The comparison of the silica precursor tetramethyl orthosilicate (TMOS) with TEOS in the attempt to improve the quality of large-pore SBA-15 prepared in the presence of TIPB;

4. The development of a facile and rapid method to synthesize SBA-15 in a few hours instead of originally reported 2 days or more. The method was further extended to other mesoporous silicas, such as large pore FDU-12 with face-centered cubic structure.

5. The selection of short stirring time followed by static conditions to induce the formation of SBA-15 with platelet morphology, in which highly ordered mesopores are arranged in very large domains and pore lengths are on the order of half a micrometer.

2.2. Pore Size Tailoring in Large-Pore SBA-15 Silica Synthesized in The Presence Of Hexane[48]

2.2.1. Experimental section

2.2.1.1. Materials

$EO_{20}PO_{70}EO_{20}$ block copolymer Pluronic P123 was provided by BASF. SBA-15 silica samples were synthesized using hexane as a micelle expander, as reported by Sun et al.[46] with some modifications. The molar composition of the synthesis mixture was TEOS : P123 : C_6H_{14} : NH_4F : HCl : H_2O = 1 : 0.0168 : 4.02 : 0.0295 : 4.42 : 186,[46] where TEOS stands for tetraethyl orthosilicate and C_6H_{14} stands for hexanes (a mixture of hexanes, with n-hexane as a major component). The synthesis procedure was as follows. 2.4 g P123 and 0.027 g NH_4F were dissolved in 84.0 mL of 1.30 M aqueous HCl solution at room temperature. Subsequently, the solution was transferred to a water bath (nominal temperature accuracy of 0.01 °C) set at 15.00 °C and after at least one hour, a mixture of 5.5 mL TEOS and 13.0 mL hexanes was added. The solution was stirred for 24 hours at 15 °C in an open container using a mechanical stirrer. Then, the product was either isolated (see below) or heated at different temperatures (from 40 to 130 °C) in a closed container for periods of time from 3 hours to 5 days. The heating at 40 °C (and in one case, at 60 °C) was performed in polypropylene bottles, whereas the heating at higher temperatures was carried out in Teflon-lined autoclaves. The resulting as-synthesized products were isolated by filtering, washing with water and drying at ~60 °C in a vacuum oven. Finally, the samples were calcined under air at 550 °C for 5 hours (heating ramp 2 °C min^{-1}). The calcined samples are denoted by specifying the initial temperature and time and (if applicable)

the heating temperature and time, e.g., "15C1d+40C1d" (or simply "+40C1d") denotes a sample synthesized initially at 15 °C and heated at 40 °C for 1 day and "15C1d" denotes a sample synthesized initially at 15 °C with no heating. The as-synthesized (uncalcined) samples are denoted in the same way, but "UC" is added at the end of the name. For two samples prepared at the same conditions, the second one is denoted #2. The sample hydrothermally treated at 60 °C in PP container is denoted 15C1d+60C5d PP.

2.2.1.2. Characterization

Small-angle X-ray scattering (SAXS) measurements were performed at Station D1 of CHESS (synchrotron facility) at Cornell University. The samples were placed in a hole in an aluminum sample holder and secured from both sides using a Kapton tape. Nitrogen adsorption measurements were performed at -196 °C on a Micromeritics ASAP 2020 volumetric adsorption analyzer. Before the analysis, calcined samples were outgassed under vacuum at 200 °C in the port of the adsorption analyzer.

2.2.1.3. Calculations

The specific surface area, S_{BET}, was evaluated from nitrogen adsorption data in the relative pressure range from 0.04 to 0.2 using the Brunauer-Emmett-Teller (BET) method.[1] The total pore volume, V_t, was determined from the amount adsorbed at a relative pressure of 0.99.[1] The micropore volume, V_{mi}, was evaluated using the α_s plot method[1,160] in the standard reduced adsorption (α_s) range from 0.9 to 1.2. The external surface area, S_{ext}, and the sum of the primary (ordered) mesopore volume, V_p, and the micropore volume, V_{mi}, were calculated using the α_s plot method in α_s range selected within 2.0-2.55 interval. The reference adsorption isotherm for macroporous silica was used in the α_s plot analysis.[160] For samples with pore diameter above ~18 nm, it was not possible to assess $V_p + V_{mi}$ using the α_s plot method, because it would require the

calculations from adsorption data at pressures very close to the saturation vapor pressure ($p/p_0 > 0.95$), for which fully reliable reference adsorption data are not available. Moreover, any contribution from secondary (interparticle) porosity would have a detrimental effect on the accuracy of the results. Therefore, $V_p + V_{mi}$ (which is used to evaluate V_p, which in turn is needed in pore size calculations using eq 1) was estimated as $0.783 \times V_t$, the constant 0.783 being determined on the basis of data for samples for which $(V_p + V_{mi})/V_t$ ratio could be determined with acceptable confidence. Pore size distributions (PSDs) were determined from adsorption branches of isotherms[161] using the Barrett-Joyner-Halenda (BJH) method[162] with the Kelvin equation for hemispherical meniscus and the statistical film thickness curve for macroporous silica.[160] The BJH pore diameter, w_{BJH}, is defined as a position of the maximum on the pore size distribution. For 2-D hexagonally ordered samples, the diameter of ordered mesopores, w_d, was calculated using a geometrical equation for materials with 2-D hexagonal structure of cylindrical pores that are separated by microporous walls:[163]

$$w_d = 1.213\, d_{100} \sqrt{\frac{V_p}{\frac{1}{\rho} + V_p + V_{mi}}} \qquad (1)$$

where d_{100} is (100) interplanar spacing obtained from SAXS, and ρ is the density of silica framework (assumed to be 2.2 g cm^{-3}). It should be noted that while V_p for some of the samples was indirectly estimated as described above, even 10% error in V_p would result in less than 2% error in the pore diameter estimation (assuming that V_p = ~1.0 cm^3 g^{-1} and V_{mi} = 0.02 cm^3 g^{-1}, which is a good approximation for the samples under study), due to the nature of eq 1.[164]

2.2.2. Results and discussion

2.2.2.1. Small-angle X-ray scattering

Sun et al.[46] reported that SBA-15 forms in the presence of hexane in the temperature range from 10 to 17 °C, so the initial synthesis temperature of 15 °C was employed in our studies. The as-synthesized material isolated after 1 day at 15 °C exhibited a SAXS pattern (Figure 2.1) with three peaks that can be indexed as (100), (200) and (210) reflections of 2-D hexagonal structure. There was also a shoulder at q value at which (110) reflection of the 2-D hexagonal structure would be expected. After calcination, the (110) peak became clearly pronounced for the 15C1d sample. The low intensity of the (110) reflection observed in case of the 15C1d sample is consistent with earlier studies of SBA-15 prepared without the hydrothermal treatment.[154] The patterns for as-synthesized and calcined samples that were subjected to the hydrothermal treatments at 100 and 130 °C were all very similar and featured peaks that can be identified as (100), (110), (200), and (210) reflections of 2-D hexagonal structure. There was also a peak or shoulder at a position characteristic of (300) reflection. The widths of the (100) peak are similar for all the considered samples, suggesting a comparable degree of structural ordering. On the basis of SAXS patterns, the samples both without and with the hydrothermal treatment for up to 5 days at 130 °C are highly ordered SBA-15 materials. This finding suggests that temperature of the hydrothermal treatment can be adjusted from 15 to 130 °C and the treatment can be prolonged for at least five days while maintaining the SBA-15 structure of the material.

The unit-cell parameters were calculated from the positions of the peaks on SAXS patterns (see Table 2.1). The unit-cell parameters for as-synthesized samples prepared either without or with hydrothermal treatment at 100 or 130 °C were very similar, being the largest (17.1 nm) for the sample treated at 100 °C. The latter value is similar to that reported by Sun et al.[46] (16.4 nm)

for the sample prepared at 100 °C. It can be concluded that the hydrothermal treatment does not lead to any appreciable change in the unit-cell parameter for as-synthesized SBA-15. However, the sample 15C1d prepared without the hydrothermal treatment exhibited 14% decrease in its unit-cell size upon calcination (see Table 2.1), whereas the hydrothermally treated samples shrank much less (2-5%), which is consistent with earlier reports on the reduction of structural shrinkage as a result of a hydrothermal treatment.[19,22,165] The shrinkage accounts for the appreciably smaller unit-cell size of the sample 15C1d (14.0 nm vs. ~16.3 nm for the hydrothermally treated samples).

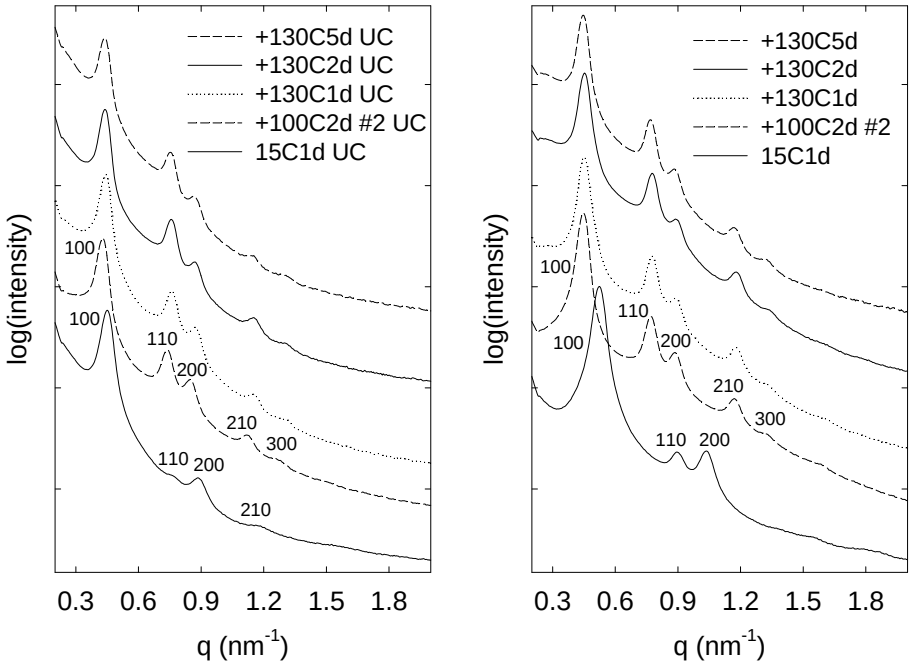

Figure 2.1. Small-angle X-ray scattering patterns for as-synthesized (uncalcined, UC) and calcined SBA-15 silicas.[48]

2.2.2.2. Nitrogen adsorption

To assess the influence of the synthesis conditions on the pore structure of calcined SBA-15 silicas, nitrogen adsorption isotherms were acquired for the sample synthesized at 15 °C, as well as for several series of samples that were additionally hydrothermally treated at temperatures from 40 to 130 °C for time periods of 1, 2 and 5 days. For 100 °C treatments, time periods of 3, 6 and 12 hours were also studied. Nitrogen adsorption isotherms for selected samples are shown in Figures 2.2 and 2.3, in which all the isotherms featured sharp steps of capillary condensation in the relative pressure interval from 0.7 to 0.95, indicating the presence of uniform large mesopores. The isotherm for the sample prepared without the hydrothermal treatment had a broad hysteresis loop that closed at a lower limit of adsorption-desorption hysteresis,[1,22,166] indicating the presence of constrictions of diameter below about 5 nm[36,167] in its mesopores. Similar isotherms have been reported for SBA-15 silicas prepared with excess of silica source.[36,168] These samples exhibited constrictions or "plugs" in their cylindrical mesopores and were first described by Van der Voort et al. as plugged hexagonal templated silicas (PHTSs).[35] The formation of PHTSs was suggested to be related with the solubilization of the excess TEOS silica source (or products of its incomplete hydrolysis) in the hydrophobic poly(propylene oxide) (PPO) cores of the micelles that template mesopores of SBA-15.[36] The hydrolysis of the PPO-solubilized TEOS was suggested to be relatively slow and to lead to the formation of the constrictions or plugs inside the uniform mesopores of SBA-15. A similar mechanism may be operative in the present case. At 15 °C, some amount of TEOS (or products of its incomplete hydrolysis) solubilized in the PPO cores of the templating micelles may remain unhydrolyzed or incompletely hydrolyzed even after one day. This silica source solubilized in the copolymer-filled voids of the siliceous framework may cross-link and convert to silica during calcination,

forming constrictions inside the mesopores. Further studies are required to fully explain this interesting phenomenon.

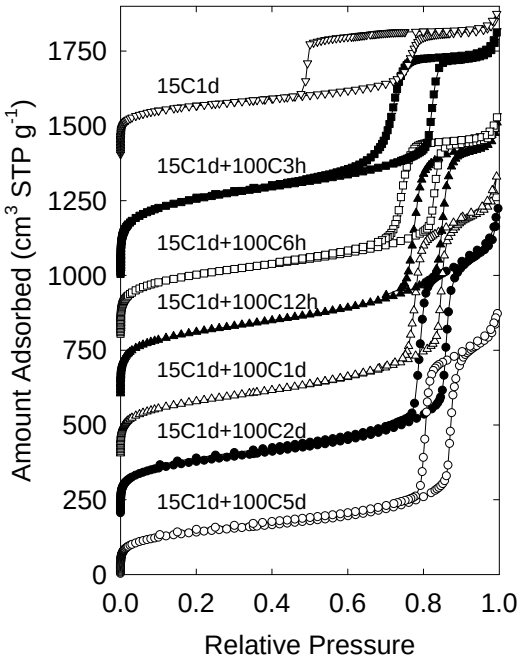

Figure 2.2. Nitrogen adsorption isotherms for calcined SBA-15 silicas synthesized at 15 °C and hydrothermally treated at 100 °C for periods of time from 3 hours to 5 days. . The isotherms for samples +100C2d, +100C1d, +100C12h, +100C6h, +100C3h and 15C1d are offset vertically by 200, 400, 600, 800, 1000 and 1400 cm^3 STP g^{-1}.[48]

Table 2.1. Structural properties of materials synthesized under different initial synthesis and hydrothermal treatment temperatures [a]

Sample	$d_{100\ UC}$	d_{100}	S_{BET}	V_t	V_{mi}	V_p	S_{ext}	w_{BJH}	w_d
15C1d	13.96	12.01	594	0.70	0.12	0.46	54	10.0	9.8
+40C1d	14.82	12.98	642	0.96	0.10	0.68	105	12.5	11.7
+40C2d	14.85	13.20	910	1.21	0.18	0.87	90	12.8	12.2
+40C5d	14.82	13.66	727	1.10	0.13	0.76	132	14.4	12.5
+60C1d	14.82	13.37	761	1.15	0.13	0.84	98	13.2	12.5
+60C2d	14.82	13.78	784	1.28	0.12	0.94	133	14.7	13.2
+60C5d	14.82	14.34	848	1.53	0.14	b	b	15.7	c
+60C5d PP	14.65	14.25	867	1.52	0.11	b	b	15.4	c
+80C1d	14.51	13.57	733	1.35	0.08	0.96	176	14.1	13.2
+80C2d	14.48	13.75	658	1.34	0.06	b	b	14.9	c
+80C5d	14.51	13.96	573	1.31	0.06	b	b	15.5	c
+100C3h	14.41	13.26	918	1.20	0.19	0.83	94	12.7	12.1
+100C6h	14.41	13.42	728	1.07	0.12	0.78	86	13.2	12.3
+100C12h	14.45	13.87	758	1.35	0.11	0.99	144	14.8	13.4
+100C1d	14.21	13.48	647	1.36	0.06	b	b	14.5	c
+100C2d	14.21	13.75	640	1.49	0.08	b	b	15.8	c
+100C2d #2	14.68	14.02	552	1.36	0.04	b	b	15.6	c
+100C5d	14.25	13.90	510	1.29	0.07	b	b	17.0	c
+120C1d	14.61	14.34	482	1.31	0.06	b	b	17.1	c
+120C2d	14.61	14.19	416	1.28	0.04	b	b	17.7	c
+120C5d	14.61	14.28	374	1.31	0.06	b	b	18.4	c
+130C1d	14.22	13.96	434	1.36	0.04	b	b	17.3	c
+130C2d	14.31	13.90	386	1.39	0.03	b	b	18.1	c
+130C5d	14.35	14.09	312	1.17	0.04	b	b	18.8	c

[a] Notation: $d_{100\ UC}$, (100) interplanar spacing for uncalcined sample; d_{100}, (100) interplanar spacing for calcined sample; S_{BET}, BET specific surface area; V_t, total pore volume; V_{mi}, micropore volume; V_p, primary mesopore volume; S_{ext}, external surface area; w_{BJH}, BJH pore diameter. w_d, pore diameter calculated using eq 1. [b] External surface area was unrealistically high, which implies a significant underestimation of the primary mesopore volume. [c] Could not be calculated using eq 1 because of the lack of V_p and S_{ext}.

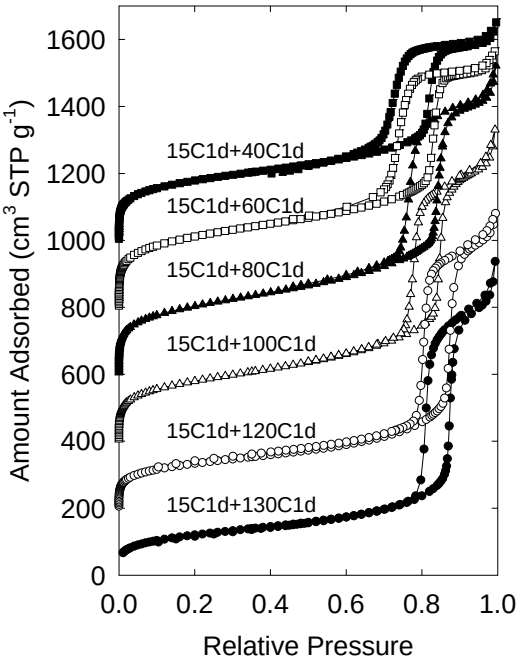

Figure 2.3. Nitrogen adsorption isotherms for calcined SBA-15 silicas synthesized at 15 °C and hydrothermally treated for one day at temperatures from 40 to 130 °C. The isotherms for samples +120C1d, +100C1d, +80C1d, +60C1d, and +40C1d are offset vertically by 200, 400, 600, 800, and 1000 cm^3 STP g^{-1}.[48]

Even a mild hydrothermal treatment (3 hours at 100 °C or 1 day at 40 °C) results in a dramatic change in shape of the adsorption isotherm. Namely, rather narrow hysteresis loops with two approximately parallel branches were observed for all the hydrothermally treated samples (see Figures 2.2 and 2.3). It should be noted that a slight broadening of hysteresis loops and some deviations from parallel arrangement of adsorption and desorption branches of hysteresis loops were observed for samples prepared at lower temperatures (40 °C) or shorter times (up to 6 hours at 100 °C). In any case, the shapes of the hysteresis loops provided evidence of the lack of any major constrictions in the mesopores of hydrothermally treated samples, unlike in the case of the sample that was prepared at low temperature only. The observed disappearance of constrictions as a result of the hydrothermal treatment can be understood when one assumes that TEOS (or products of its incomplete hydrolysis) solubilized in the micelles of the copolymer template may be expelled toward the surface of the templated siliceous framework and subsequently incorporated in it as the temperature is increased. The adsorption isotherms for the hydrothermally treated samples resembled those commonly reported for SBA-15 silicas,[22,154] although the latter usually exhibit capillary condensation steps centered at lower relative pressures (below ~0.82 vs. 0.82-0.89 for the present samples).

The structural parameters determined on the basis of the nitrogen adsorption data are listed in Table 2.1. The BET specific surface area was 590 m^2 g^{-1} for sample prepared without the hydrothermal treatment and ranged from 310 to 920 m^2 g^{-1} for the hydrothermally treated samples. In particular, the specific surface areas of two samples prepared with the treatment for two days at 100 °C, as in the work of Sun et al.,[46] were about 600 m^2 g^{-1}, being close to the value of 614 m^2 g^{-1} reported by these authors. For the samples hydrothermally treated at or above 80 °C, the specific surface area tended to decrease with time of the treatment. On the other hand, for

samples treated at lower temperature, the opposite tendency was observed. The specific surface area was typically correlated with the micropore volume that was in the range from 0.03 to 0.19 $cm^3\ g^{-1}$, and tended to decrease with the temperature and time of the hydrothermal treatment, being the lowest for the samples synthesized at 130 °C, and the highest for some samples hydrothermally treated at short times or at low temperatures. The micropores and perhaps some mesopores are likely to provide connectivity between adjacent cylindrical mesopores of the considered SBA-15 samples, which was verified through the successful synthesis of inverse carbon replicas[118] using a method similar to that proposed by Li and Jaroniec[141] (data discussed in Chapter 4).

The total pore volume was only 0.70 $cm^3\ g^{-1}$ for the sample synthesized at low-temperature only, whereas the hydrothermally treated samples exhibited total pore volumes from 0.96 to 1.53 $cm^3\ g^{-1}$, with lowest values observed primarily for samples treated at low temperature (40 °C) or for short time (3-6 h). The external surface area was quite low (50 $m^2\ g^{-1}$) for the sample synthesized at 15 °C and exhibited a clear tendency to increase with the hydrothermal treatment temperature and time. An adsorption measurement on as-synthesized sample 15C1d+100C2d #2 UC indicated that the development of secondary mesoporosity may be primarily responsible for the aforementioned behavior. In fact, unrealistically high values of the external surface area calculated using α_s plot method were observed for some samples, which stem from the capillary condensation in secondary mesopores (these unrealistic values and the related inaccurate primary pore volume values were not listed in Table 2.1).

The pore size distributions for selected samples are shown in Figures 2.4 and 2.5. The positions of the maxima on PSDs are listed in Table 2.1 and plotted as a function time for

particular temperatures in Figure 2.6. The BJH (nominal) pore diameter for the sample synthesized without a hydrothermal treatment was 9.4 nm. A similar pore size estimate (9.8 nm) was obtained using Equation 1. The pore wall thickness for this sample, estimated as a difference between the unit-cell parameter and the pore diameter was above 4 nm.

A clear tendency for the pore size enlargement as a function of time of the hydrothermal treatment was observed (see Figures 2.4 and 2.6). For instance, the BJH (nominal) pore diameter increased to 12.1 nm after 3 hours of treatment at 100 °C and reached 16.4 nm after 5 days. It should be noted that the irregularity observed for times of 12 hours and 1 day is related to a slight difference in pore diameters for samples prepared from two different initial synthesis mixtures prepared at 15 °C, whereas samples obtained from the same initial synthesis mixture always exhibited the pore size increase over time. The increase of the pore diameter of copolymer-templated silicas as a function of the hydrothermal treatment time was hinted by the results for two SBA-15 samples reported in the original work of Zhao et al.[22] and then documented[169-173] for FDU-1 silica[34] (primarily cubic close-packed structure),[169] SBA-16 silica (body-centered cubic, Im3m, structure)[22] and large-pore silica with Ia3d structure. The mesopore size increase as a function of hydrothermal treatment time for SBA-15 was investigated in more depth only recently.[174] It is important to note that the work of Morishige et al.[173] is perhaps the only prior example of this adjustment capability demonstrated for ordered block-copolymer-templated silicas synthesized in the presence of micelle expanders. Earlier studies of synthesis of alkylammonium-surfactant-templated silica in the presence of a micelle expander (decane) did not show any consistent trends regarding the pore size changes over time.[175] On the other hand, disordered block-copolymer-templated silicas (MCFs) synthesized in the presence of mesitylene exhibited the pore size increase as the hydrothermal treatment was prolonged.[176]

PSDs for the hexane-expanded SBA-15 silicas were in most cases the narrowest for the synthesis times of one day or less. Most of PSDs exhibited more or less pronounced tailing towards larger pore sizes, which became particularly pronounced for samples prepared with longer hydrothermal treatment times and at temperatures of 120 °C or larger. The occurrence of the tailing will be discussed later.

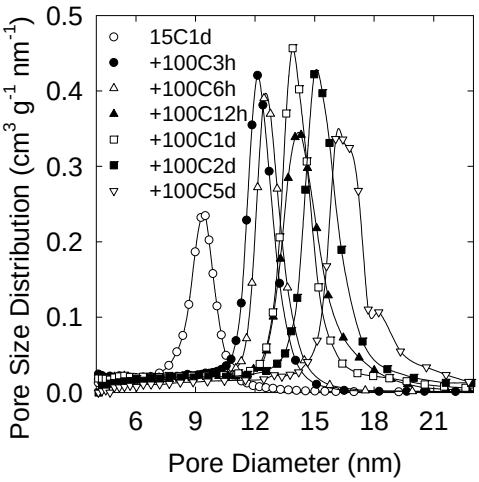

Figure 2.4. BJH pore size distributions for calcined SBA-15 silicas synthesized at 15 °C and hydrothermally treated at 100 °C for periods of time from 3 hours to 5 days.[48]

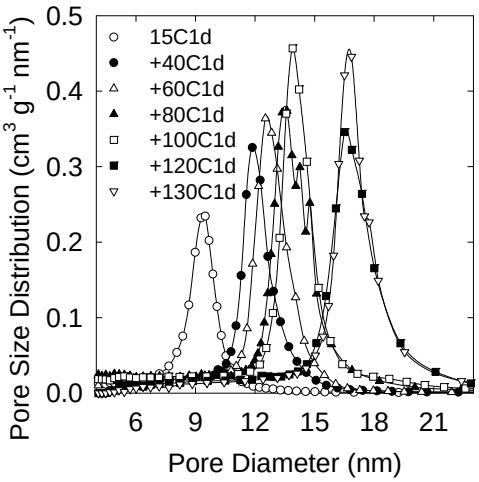

Figure 2.5. BJH pore size distributions for calcined SBA-15 silicas synthesized at 15 °C and hydrothermally treated for one day at temperatures from 40 to 130 °C.[48]

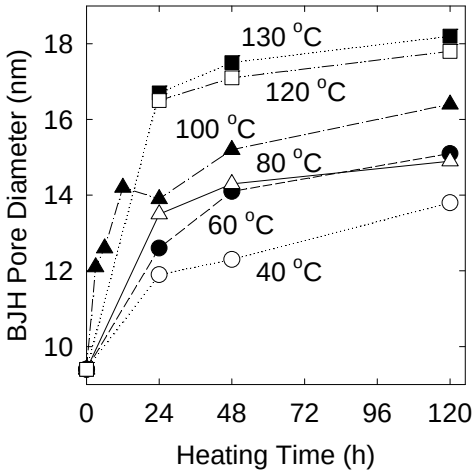

Figure 2.6. BJH pore diameter for calcined SBA-15 silicas synthesized at 15 °C and hydrothermally treated for different periods of time at temperatures from 40 to 130 °C. The lines are included to guide the eye.[48]

It is important to note that the pore diameters for two samples prepared with the hydrothermal treatment at 100C for 2 days, following conditions employed by Sun et al.,[46] were 15.2 and 15.6 nm, which is nearly the same as 15.7 nm value originally reported. In general, different pore size calculation methods may afford widely different pore size estimates from the same gas adsorption isotherm. However, the present comparison is valid because the same general method of calculation (BJH) was used, and more importantly, the nitrogen capillary condensation pressures for the samples discussed herein were nearly identical, proving the similarity in the pore size. These results show a remarkably good reproducibility of the synthesis reported by Sun et al.[46]

The pore diameter of the large-pore SBA-15 prepared in the presence of hexane can also be adjusted by the selection of temperature of the hydrothermal treatment. For instance, one-day treatments afforded BJH (nominal) pore diameters increasing from 11.9 to 16.7 nm as the treatment temperature was increased from 40 to 130 °C (see Figure 2.5 and 2.6). The increase in

pore size of SBA-15 with the increase in the hydrothermal treatment temperature was first reported by Zhao et al.[22] and confirmed by others,[154,177] and them demonstrated for FDU-1,[169] SBA-16,[170] FDU-12 silica with face-centered cubic structure,[178] and large-pore silica (KIT-6) with Ia3d structure.[179] FDU-12 appears to be the only case where this method of the pore size control was demonstrated in the presence of a micelle expander, as in the case of SBA-15 discussed herein.

In the case of some hydrothermally treated samples, it was clear that the BJH pore diameter was close to or even larger than the distance between the pore centers (which is equal to the unit-cell parameter). For isolated cylindrical pores, their diameter must be equal to or smaller than the distance between pore centers. These apparent inconsistencies for the considered SBA-15 samples can be understood as follows. First, the cylindrical mesopores of SBA-15, especially synthesized at about 130 °C in the presence of a micelle expander, may be connected through large mesoporous gaps in the pore walls,[180] leading to some degree of coalescence of adjacent mesopores. Therefore, for the 15C1d+130Cxd samples (x = 1, 2 and 5), BJH PSD may reflect the diameter of cylindrical mesopores as well as the size of voids formed as a result of partial coalescence of the adjacent cylindrical mesopores. This contention is additionally supported by the fact that the PSD for 15C1d+130C1d sample exhibited a pronounced tailing toward larger pore sizes, and moreover, PSDs for samples treated at 130 °C for more than one day broadened and developed even stronger tailing. Therefore, the pore sizes inferred from PSDs for these samples may inherently overestimate the actual diameter of the cylindrical pores in these materials. The partial coalescence of adjacent pores may be operative even at lower temperatures, e.g., 100 °C, because PSDs for some samples, especially those hydrothermally treated for longer periods of time, also exhibit noticeable tailing. However, the tailing may also

reflect the increasing contribution of the secondary mesoporosity, as seen from adsorption characterization of as-synthesized SBA-15.

2.2.2.3. Synthesis of large-pore SBA-15 in PP bottle

When hexane is used as a micelle expander, the hydrothermal treatment at temperatures of 80 °C or above needs to be carried out in a Teflon-lined autoclave, otherwise hexane (boiling point of 69 °C) can readily escape from containers that are not suitable for heating under pressure (including PP bottles). To make the synthesis of large-pore SBA-15 more readily achievable and more suitable for larger-quantity synthesis, it is demonstrated herein that materials with pore diameter of about 15 nm can be synthesized in PP bottles at 60 °C by extending the hydrothermal treatment time to 5 days (see structural parameters in Table 2.1). The specific surface area and PSD were essentially the same for samples prepared in autoclave and PP bottle under these conditions.

2.2.2.4. Pore size adjustment process

Micelle expanders, such as mesitylene and neutral amines, typically significantly increase the volume of the micelles, leading to a marked pore volume increase for the resulting templated silicas, which often scales with the amount of the micelle expander added.[51,181] In the case of hexane, the pore volumes of the SBA-15 silicas with significantly enlarged pores (see Table 2.1) were comparable to those typically reported for SBA-15 synthesized in the absence of the micelle expander.[22,154] This finding suggests that hexane solubilizes in the PEO-PPO-PEO block copolymer micelles only to a small extent, as already shown by Nagarajan and Ruckenstein,[52] and Nagarajan[53] in their work on solubilization of hydrocarbons in micellar solutions. Therefore,

in the case of SBA-15 synthesis, hexane appears to act not as a typical micelle swelling agent, but as an additive that modifies the size of the micelles, that is, as a "non-swelling" micelle expander. It is clear that most of hexane added to the synthesis mixture does not solubilize in the micelles and is needed perhaps to ensure the saturation of PEO-PPO-PEO micelles with hexane, which may account for the observed good reproducibility of pore size in the resulting SBA-15 materials.

The ability to easily control the pore diameter of large-pore SBA-15 in the range from 12 to 15 or more nanometers through the selection of an appropriate hydrothermal treatment temperature and time appears to stem from two properties of block-copolymer-templated silica systems. First, the shrinkage upon calcination was substantially reduced (from 14% to 2-5%) for our SBA-15 samples when the hydrothermal treatment was employed. The data shown in Table 2.1 suggest that the shrinkage is a function of the treatment temperature, as the samples treated at 130 °C exhibited a smaller shrinkage (2-3%) than the typical samples treated at 100 °C. This behavior follows the pattern that was evident from the data reported in the original paper of Zhao et al.[21] on the synthesis of SBA-15. The decrease in shrinkage for hydrothermally treated samples, combined with the approximate constancy in the unit-cell size of as-synthesized materials prepared without and with the treatment, is expected to account for larger pore dimensions for materials that underwent a lower degree of shrinkage (that is, those hydrothermally treated at higher temperatures or longer time). Second, the penetration of PEO blocks in the silica framework of silica/PEO-PPO-PEO composites[182] creates another general mechanism for the pore size enlargement.[22,153,154] Namely, the increase in temperature reduces the hydrophilicity of the PEO blocks, which is considered as a driving force for their partial withdrawal toward the PPO cores of the micelles. This phenomenon increases the dimensions of the hydrophobic

(silica-free) parts of the copolymer template, thus leading to the enlargement of size of voids in the silica framework (with concomitant pore wall thickness reduction), [21,153,154] which progresses with temperature and time.[21,153,154,169] These two mechanisms are postulated to account for the observed pore size adjustability in large-pore SBA-15 prepared in the presence of hexane. The present study is perhaps the first demonstration that the synthesis of block-copolymer-templated ordered mesoporous materials with a micelle expander is amenable to both of the convenient pore size adjustment techniques known for the syntheses without micelle expanders: the hydrothermal treatment time and temperature control.

2.2.3. Conclusions

The use of low-temperature initial synthesis conditions and hexane as a micelle expander allows one to synthesize highly ordered SBA-15 silicas with BJH (nominal) pore diameters readily adjustable in the range from 12 to 18 nm (actual diameter of cylindrical pores up to about 15 nm). SBA-15 prepared at 15 °C was highly ordered and exhibited a narrow pore size distribution centered at about 9.5 nm, but most of its mesopores featured constrictions of size below about 5 nm. The constrictions are essentially fully eliminated even by a mild hydrothermal treatment. The mesopores can be gradually enlarged by extending the time of the hydrothermal treatment at fixed temperature or by applying the hydrothermal treatment at higher temperatures. The studies of samples prepared at the lowest and the highest hydrothermal treatment temperatures suggest that the unit-cell size of as-synthesized SBA-15 is nearly constant (16.3-17.1 nm) for samples obtained at different synthesis conditions. It appears that the pore diameter enlargement with the increase of the hydrothermal treatment temperature or time is primarily related to: (i) the decrease in the shrinkage of the framework upon calcination, and (ii) the

decrease in the pore wall thickness. The upper limit of the achievable pore diameter of cylindrical pores in these SBA-15 structures is imposed at about 16 nm by the unit-cell size (that is, the distance between pore centers) of about 17 nm for the as-synthesized samples. Therefore, the BJH (nominal) pore diameters appear to overestimate the pore size range achievable for the considered materials. SBA-15 samples with BJH pore diameters up to 15 nm can be conveniently synthesized at 60 °C in PP bottles.

2.3. Synthesis of Ultra-Large-Pore SBA-15 Silica Using Triisopropylbenzene as Micelle Expander[50]

2.3.1. Experimental section

2.3.1.1. Materials

SBA-15 silicas were synthesized using triblock copolymer Pluronic P123 (BASF) as a template and TIPB as a micelle expander. In most cases, the molar composition of the synthesis mixture was: TEOS: P123 : TIPB : NH_4F : HCl : H_2O = 1 : 0.0168 : 0.199 : 0.0295 : 4.42 : 186, where TEOS stands for tetraethyl orthosilicate. A typical synthesis procedure was as follows. 2.4 g P123 and 0.027 g NH_4F were dissolved in 84.0 mL of 1.30 M aqueous HCl solution at room temperature. Subsequently, the solution was transferred to a water bath (nominal temperature accuracy of 0.01 °C) set at a temperature between 12.00 and 20.00 °C and after at least one hour, a mixture of 5.5 mL TEOS and 1.2 mL (1.0 g) TIPB was added. The solution was stirred for 24 hours at the selected initial temperature in an open container using a mechanical stirrer. Then, the product was either isolated (see below) or heated at 100 or 130 °C in a closed container for periods of time from 3 hours to 5 days (usually 2 days). As-synthesized material was isolated by filtering, washing with water and drying at ~60 °C in a vacuum oven. Finally, the sample was calcined under air at 550 °C for 5 hours (heating ramp 2 °C min^{-1}). The synthesis was also performed in a similar way with cyclohexane and 1,3,5-triethylbenzene as micelle expanders.

2.3.1.2. Characterization

Small-angle X-ray scattering (SAXS) patterns were either acquired at Station D1 of Cornell High Energy Synchrotron Source (CHESS) at Cornell University or recorded using a Bruker Nanostar U SAXS/wide-angle X-ray scattering (WAXS) system with a rotating anode X-ray source and Vantec-2000 area detector. The Nanostar U system had a sample-to-detector distance of 72 cm and was in high-flux configuration. The powder samples were placed in a hole in a sample holder and secured from both sides using a Kapton or Scotch tape. Nitrogen adsorption isotherms were measured at -196 °C on a Micromeritics ASAP 2020 volumetric adsorption analyzer. Before the adsorption analysis, calcined samples were outgassed under vacuum at 200 °C in the port of the adsorption analyzer. Transmission electron microscopy (TEM) images were recorded on a Philips CM 100 microscope operated at 80 kV or a FEI Tecnai G2 Twin microscope operated at 120 kV. Before the imaging, the samples were dispersed in ethanol through sonication and subsequently deposited on a carbon-coated copper grid.

2.3.1.3. Calculations

See the **section 2.2.1.3.**

2.3.2. Results and discussion

2.3.2.1. Effect of initial synthesis temperature

Shown in Figure 2.7 are SAXS patterns for calcined silicas synthesized with surfactant (Pluronic P123) to micelle expander (TIPB) mass ratio of 2.4 to 1 at initial temperatures from 13 to 20 °C. In the case of these samples, TIPB was mixed with the silica source (TEOS) and

simultaneously added to the surfactant solution under mechanical stirring. The initial synthesis temperature was maintained for one day under stirring, and then the synthesis mixture was transferred to an oven and heated in a closed container for two days at 100 °C. Relative positions of SAXS peaks for the samples prepared at 13.5-20 °C corresponded to the 2-D hexagonal structure characteristic of SBA-15. The patterns were somewhat less well resolved for the samples prepared at 14 and 13.5 °C. In the case of the sample synthesized at 13 °C, there was only one well-pronounced peak, and a shoulder at a position where (110) reflection of 2-D hexagonal structure would be expected. The peaks on the SAXS patterns shifted to lower q values as the initial synthesis temperature was lowered, indicating the increase in the unit-cell size. The position of the main peak on the SAXS pattern corresponded to (100) interplanar spacings of 12.6 to 20.7 nm for 2-D hexagonal structures (see Table 2.2), the latter being exceptionally large. The less well-defined sample obtained at 13 °C had d_{100} of 22.6 nm. As discussed above, commercially available Pluronic block copolymers[43,46-48,159] and purposefully synthesized PMA-PEO-PMA block copolymers[33] are suitable for the synthesis of SBA-15 with (100) interplanar spacings up to ~17 nm (for calcined samples). The synthesis procedure described herein extends the achievable d_{100} range for 2-D hexagonal structure to 21 nm. For a sample prepared at initial temperature of 12 °C, the SAXS pattern (not shown) was featureless. The 2-D hexagonal structure of samples prepared at 13.5-20 °C was confirmed by TEM (see Figure 2.8 for images for selected samples). In the case of the sample prepared at 13 °C, TEM indicated that the pores were channel-like and their arrangement was similar to that for 2-D hexagonal (honeycomb) structure, but with some imperfections. Finally, TEM images for the sample prepared at 12 °C showed channel-like, spherical and irregularly-shaped pores with a wide distribution of sizes. It should be noted that MCF impurity was observed in some samples

of well-ordered 2-D hexagonal materials (see for instance the upper right corner of Figure 2.8 (middle)). The occurrence of MCF domains was not correlated with the initial synthesis temperature. Perhaps the MCF impurity formed sporadically as a result of less effective local mixing in the reaction mixture.

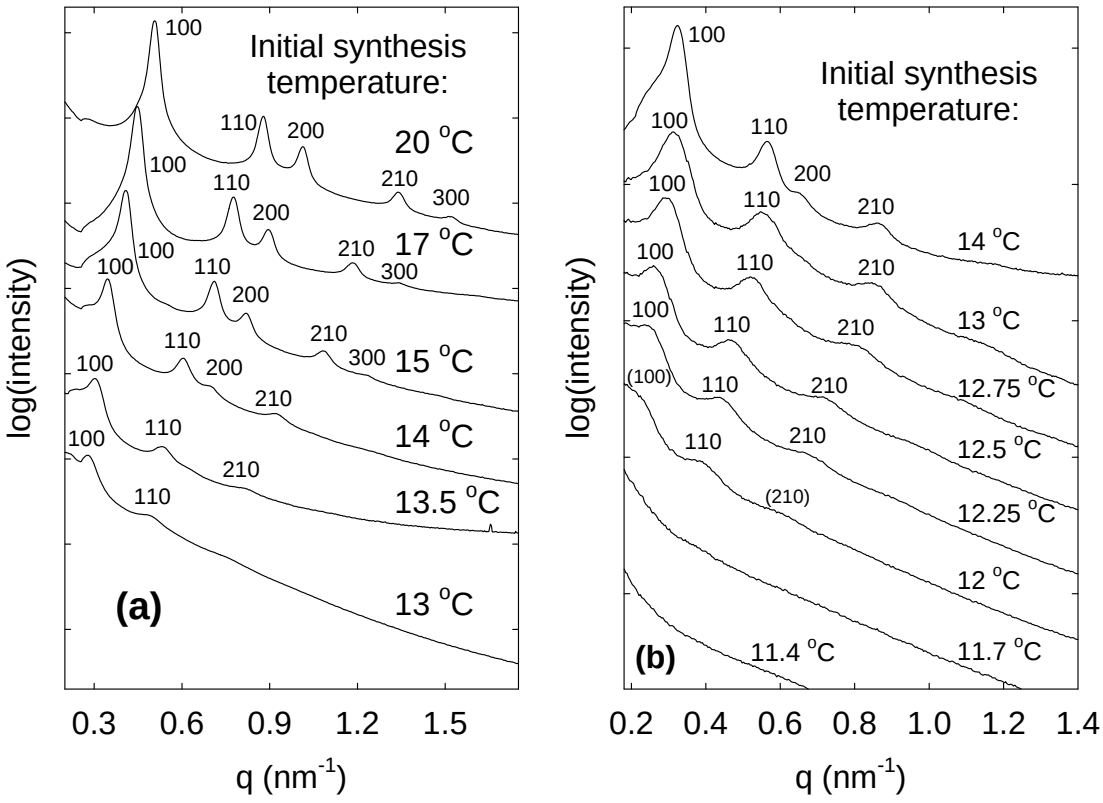

Figure 2.7. Small-angle X-ray scattering patterns for calcined silica samples synthesized at different initial temperatures with surfactant (P123) : swelling agent (TIPB) mass ratio of: (a) 2.4 to 1 (with hydrothermal treatment at 100 °C for 2 day); (b) 2.4 to 2 (except for samples synthesized at 12.25 and 12 °C, for which ratios of 2.4 : 2.5 and 2.4 : 3 were employed) (with hydrothermal treatment at 130 °C for 1 day). Data in (a) and the uppermost pattern in (b) were collected using SAXS with synchrotron X-ray source. Other data shown in (b) were collected using a laboratory SAXS setup.[50]

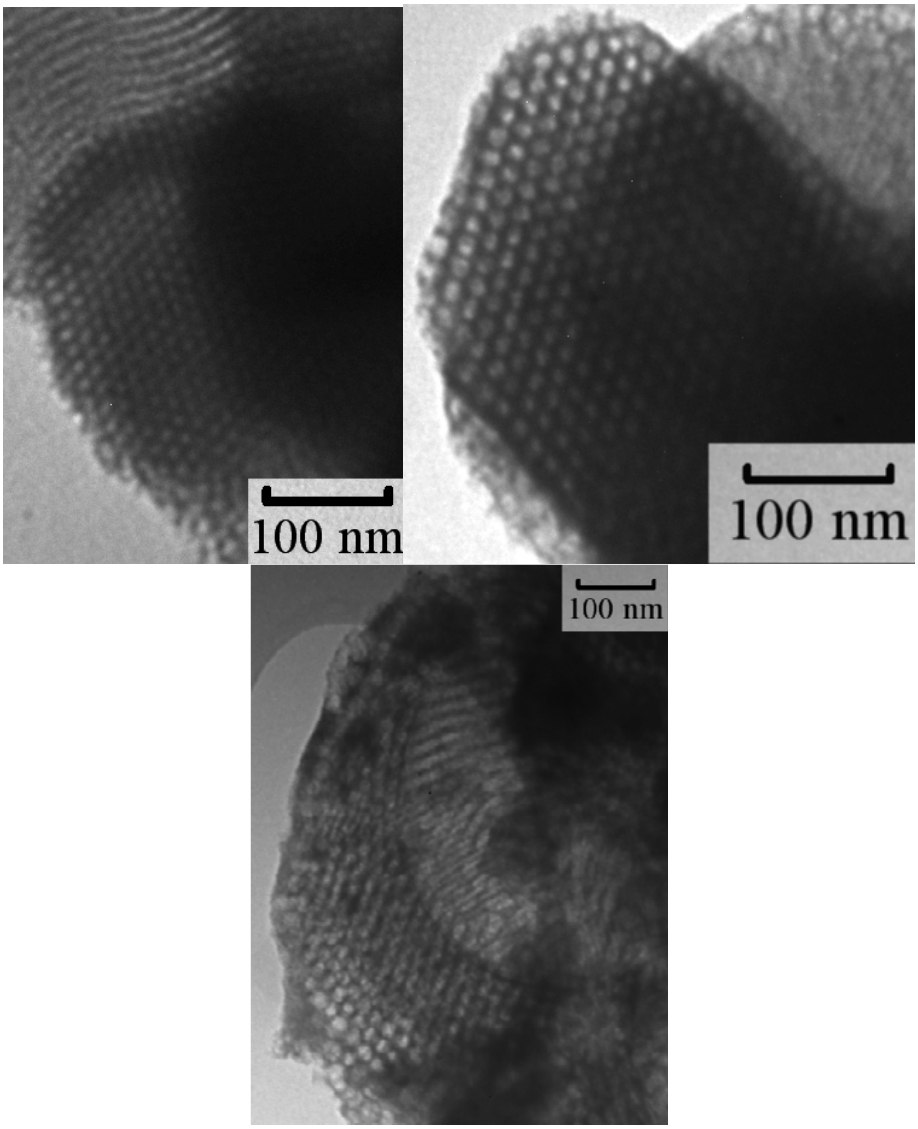

Figure 2.8. TEM images of calcined silica samples synthesized at: (top left) 17 °C, (top right) 15 °C and (bottom) 13.5 °C with surfactant (P123) : swelling agent (TIPB) mass ratio of 2.4 to 1.[50]

Table 2.2. Structural properties of materials synthesized under different conditions.[a]

Sample	$d_{100\ UC}$ (nm)	d_{100} (nm)	S_{BET} ($m^2\ g^{-1}$)	V_t ($cm^3\ g^{-1}$)	V_{mi} ($cm^3\ g^{-1}$)	V_p ($cm^3\ g^{-1}$)	w_{BJH} (nm)	w_d (nm)
20 °C, 100 °C 2d, 2.4 : 1	13.0	12.6	620	1.38	0.05	(1.03)[b]	13.9	12.5[c]
17 °C, 100 °C 2d, 2.4 : 1	14.4	14.1	680	1.40	0.08	1.01	15.0	13.8
17 °C, 100 °C 2d, 2.4 : 1.5	15.8	15.4	570	1.49	0.02	1.10	16.3	15.6
17 °C, 100 °C 2d, 2.4 : 2	16.8	16.3	530	1.48	0.03	(1.13)[b]	17.4	16.5[c]
17 °C, 100 °C 2d, 2.4 : 3	17.8	17.2	580	1.85	0.07	b	18.4	d
15 °C, 100 °C 2d, 2.4 : 1	15.8	15.4	590	1.28	0.08	0.90	15.7	14.8
14 °C, 100 °C 2d, 2.4 : 1	19.4	18.6	570	1.13	0.05	0.81	20.4	17.7
13.5 °C, 100 °C 2d, 2.4 : 1	21.3	20.7	520	1.05	0.07	(0.75)[b]	24.6	19.3[c]
13 °C, 100 °C 2d, 2.4 : 1	23.3	22.6	520	1.04	0.02	b	30	e
12 °C, 100 °C 2d, 2.4 : 1	f	f	520	0.95	0.04	b	~50	e
14 °C, 130 °C 1d, 2.4 : 2	19.9	19.4	350	1.30	0.04	(0.98)[b]	22.6	19.2[c]
13 °C, 130 °C 1d, 2.4 : 2	20.8	20.1	350	1.34	0.02	(1.03)[b]	25.5	20.2[c]
12.75°C, 130°C 1d, 2.4 : 2	22.6	21.6	330	1.29	0.02	(0.98)[b]	27.8	21.4[c]
12.5 °C, 130 °C 1d, 2.4 : 2	24.5	24.2	330	1.33	0.03	(1.01)[b]	29.8	24.2[c]
12.25°C,130°C 1d, 2.4:2.5	26.0[g]	25.8[g]	360	1.50	0.02	(1.15)[b]	33.9	26.3[c]
12 °C, 130 °C 1d, 2.4 : 3	h	h	300	1.40	0.01	b	42	i
11.7 °C, 130 °C 1d, 2.4 : 2	f	f	300	1.21	0.00	b	52	e
11.4 °C, 130 °C 1d, 2.4 : 2	f	f	290	1.09	0.00	b	71	e

[a] Notation: $d_{100\ UC}$, (100) interplanar spacing for uncalcined sample; d_{100}, (100) interplanar spacing for calcined sample; S_{BET}, BET specific surface area; V_t, total pore volume; V_{mi}, micropore volume; V_p, primary mesopore volume; S_{ext}, external surface area; w_{BJH}, BJH pore diameter; w_d, pore diameter calculated using eq 1. [b] Could not be calculated with acceptable accuracy using α_s plot method. Values in parentheses are estimates based on V_t and V_{mi} values for the particular sample (see Calculations section). [c] Value based on the estimated value of V_p. [d] Could not be estimated with acceptable accuracy due to a significant uncertainty in the value of V_p. [e] Could not be calculated using eq 1 because the lack of clear evidence of 2-D hexagonal symmetry. [f] No observable peaks on SAXS pattern. [g] Estimated on the basis of position of (100) and (110) peaks. [h] (100) peak not fully resolved. [i] Could not be estimated because (100) peak was not fully resolved.

Nitrogen adsorption isotherms for the samples synthesized at initial temperatures from 12 to 20 °C (Figure 2.9(a)) featured capillary condensation steps whose relative pressure at midpoint systematically shifted from 0.85 to 0.96. In particular, the sample synthesized at 13.5 °C exhibited capillary condensation at relative pressure of 0.917. The highest relative pressure of capillary condensation of nitrogen at -196 °C observed for well-defined SBA-15 silica with cylindrical mesopores was ~0.87 for materials templated by Pluronic block copolymers,[46,48] and ~0.90 for silicas templated by PEO-PMA or PMA-PEO-PMA block copolymers,[32,33,41] which is much lower than that observed for our aforementioned sample. This provides strong evidence that our material exhibited higher pore diameter than other silicas with 2-D hexagonal pore structure documented to date. It should be noted that SBA-15 silicas with large-mesopore connections between ordered mesopores[48,180] are not taken into account, because in such cases, the adjacent mesopores are merged to a significant extent and thus the pore shape deviates significantly from cylindrical. It appears that such materials can readily be generated using the present synthesis method when extended hydrothermal treatments (2 days or more) at high temperature (130 °C) are applied. For regular SBA-15 materials, the capillary condensation pressure is correlated with the pore diameter determined using eq 1 or simulations of XRD/SAXS patterns,[183] following the behavior observed earlier for MCM-41 silicas.[161] In the cases of SBA-15 suspected of the merging of adjacent mesopores, the capillary condensation pressure was much higher than that for similar samples hydrothermally treated for shorter time at 130 °C or treated at lower temperatures.

It should be noted that the samples prepared with P123 : TIPB ratio of 2.4 : 1 at an initial temperature of 13 °C or lower clearly exhibited an additional hysteresis loop in a relative pressure range ca. 0.45-0.7 (see Figure 2.9(a)), which is indicative of the presence of mesopores

of size 5-8 nm, which is much smaller than the size of the main mesopores. SBA-15 prepared at 13.5 °C also exhibited such a feature on its isotherm, although its relative magnitude was much smaller. TEM images did not provide any clear indication as to the nature of this additional porosity. As this porosity is fully or largely eliminated by increasing the copolymer: swelling agent ratio (such samples are discussed below), it is suggested that these additional pores might be present in disordered domains that were micelle-expander-depleted.

Pore size distributions (PSDs) for the discussed samples, calculated from the nitrogen adsorption isotherms using the BJH method, are shown in Figure 2.10a. To better show the full range of relevant pore diameters, the logarithmic scale was used. The pore diameter increased as an initial synthesis temperature decreased. PSDs for samples prepared at 13.5-20 °C were narrow, but as the temperature decreased further, a significant broadening of PSD was observed. The BJH pore diameter for samples that exhibited 2-D hexagonal ordering, as inferred from SAXS and TEM, reached 25 nm. This BJH pore size is significantly larger than that of ~16 nm reported for SBA-15 templated by Pluronic block copolymers[46,48] (except for those in which the adjacent mesopores were shown to be, or are likely to be, merged with one another) and that of 21 nm reported for SBA-15 templated by PEO-PMA or PMA-PEO-PMA.[32,33,41] While the BJH PSDs calculated from adsorption branches of isotherms allow one to compare a relative magnitude of size of pores of a particular geometry, they overestimate the diameter of large cylindrical mesopores (above 10 nm).[183,184] Such an overestimation is caused by an inaccuracy in the relation between the pore diameter and the capillary condensation pressure (in the considered case, this relation is the Kelvin equation), which is a crucial component in PSD calculations. Therefore, eq 1 was used herein to obtain reliable estimates of actual pore diameters for samples

for which the 2-D hexagonal ordering was confirmed. As can be seen in Table 2.2, the actual pore diameters for the 2-D hexagonally ordered samples were 12 to ~19 nm.

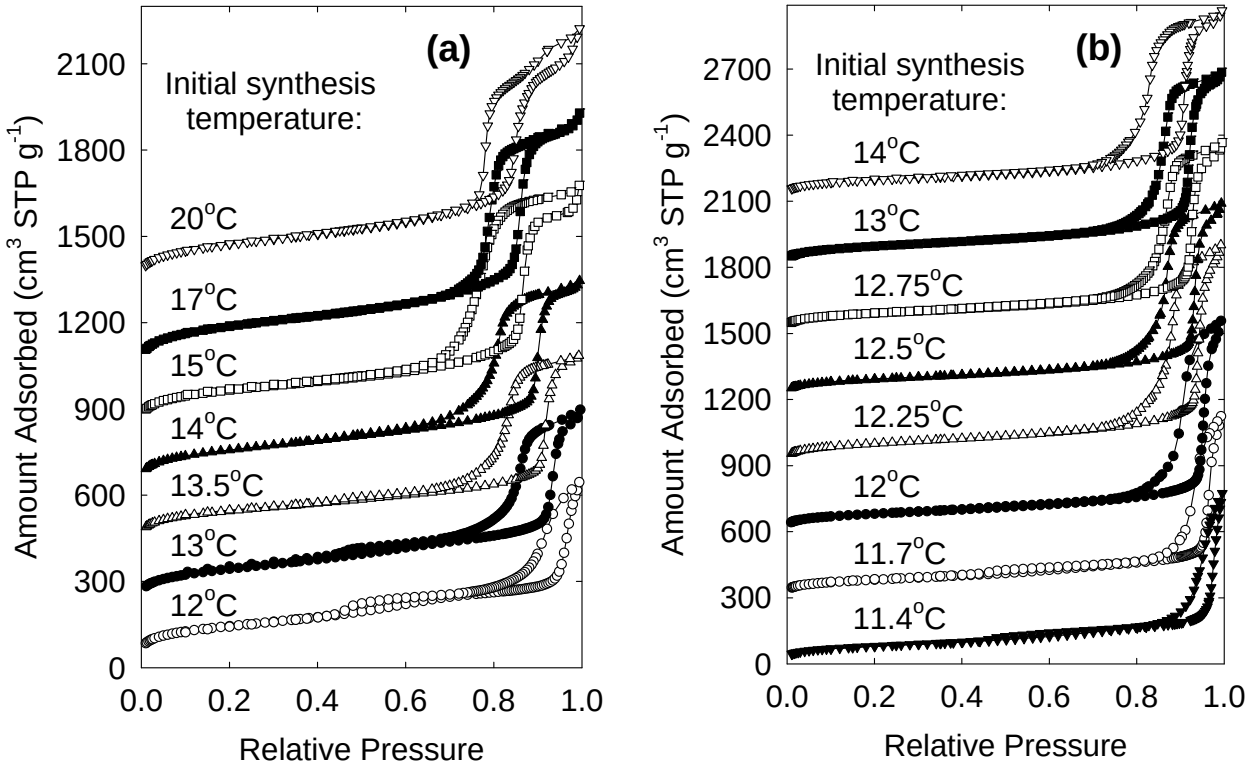

Figure 2.9. Nitrogen adsorption isotherms for calcined silica samples synthesized at different initial temperatures with surfactant (P123) : swelling agent (TIPB) mass ratio of: (a) 2.4 to 1 (with hydrothermal treatment at 100 °C for 2 day); (b) 2.4 to 2 (except for samples synthesized at 12.25 and 12 °C, for which ratios of 2.4 : 2.5 and 2.4 : 3 were employed) (with hydrothermal treatment at 130 °C for 1 day). For clarity, in (a) the isotherms for samples prepared at 13, 13.5, 14, 15, 17 and 20 °C were offset vertically by 200, 400, 600, 800, 1000 and 1300 cm^3 STP g^{-1}) and in (b), the isotherms for samples prepared at 11.7, 12, 12.25, 12.5, 12.75, 13 and 14 °C were offset vertically by 300, 600, 900, 1200, 1500 and 1800 cm^3 STP g^{-1}.[50]

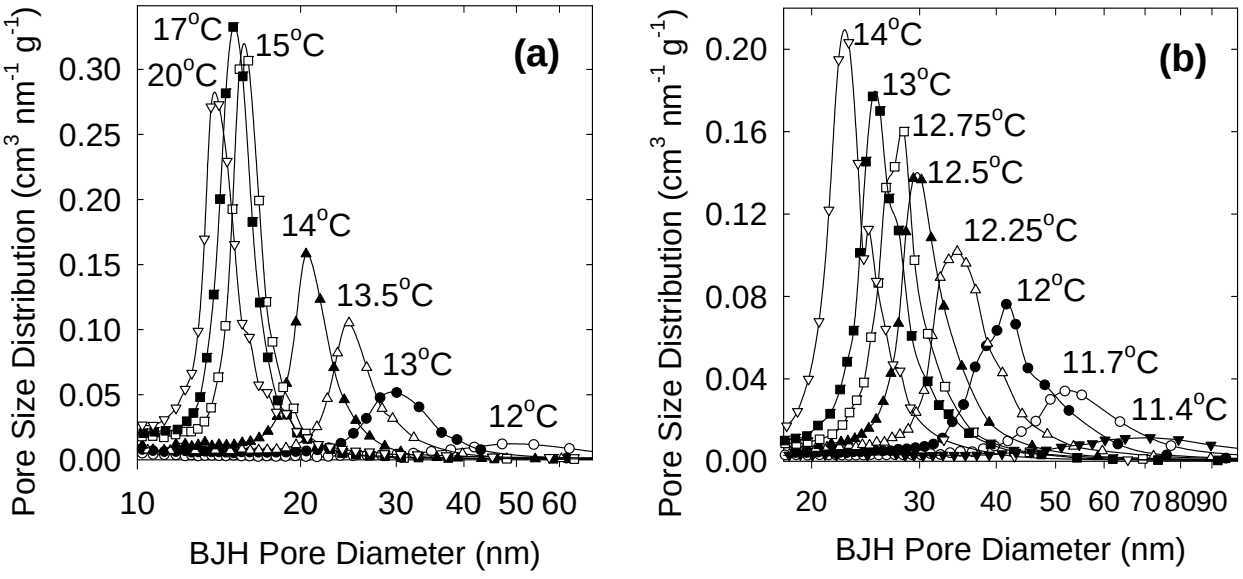

Figure 2.10. Pore size distributions for calcined silica samples synthesized at different initial temperatures with surfactant (P123) : swelling agent (TIPB) mass ratio of: (a) 2.4 to 1; (b) 2.4 to 2 (except for samples synthesized at 12.25 and 12 °C, for which ratios of 2.4 : 2.5 and 2.4 : 3 were employed) (with hydrothermal treatment at 130 °C for 1 day).[50]

2.3.2.2. Effect of amount of the swelling agent

In typical syntheses with micelle expanders, the pore diameter can be adjusted in a wide range by changing the amount of the micelle expander.[7,22,181] In the case of the low-temperature synthesis with TIPB, the behavior was more complicated. At 20 °C, the material exhibited a significant secondary mesoporosity even when P123 : TIPB mass ratio was 2.4 to 1 and the increase in this ratio to 2.4 to 2 enhanced the secondary mesoporosity even further. Thus, the increase in the amount of the swelling agent was not beneficial. At somewhat lower temperatures (14-17 °C), the pore diameter can be tailored to some extent by changing the amount of TIPB. For instance, when the initial synthesis temperature was 17 °C, highly ordered SBA-15 silicas

with (100) interplanar spacings up to 16.3 nm were obtained when the mass of TIPB was increased to 1.5 and 2 g per 2.4 g P123 (see Table 2.2). Five pronounced reflections and two additional less well-resolved reflections were observed on SAXS patterns for these samples. Although the increase in the amount of TIPB to 3 g per 2.4 g P123 resulted in further increase in d_{100}, the degree of structural ordering was significantly diminished. Moreover, the shape of the nitrogen adsorption isotherm for the considered sample differed from the shape of adsorption isotherms for the other samples, as the amount adsorbed continued to significantly increase after the completion of the capillary condensation in ordered mesopores. This behavior suggests a major population of secondary (disordered) mesopores with broad size distribution overlapping with the size distribution of the ordered mesopores. At 14 °C, it was possible to reduce the amount of TIPB to 0.5 g per 2.4 g of P123 while still achieving a BJH pore diameter of ~16.5 nm, thus achieving for a micelle-expander/copolymer mass ratio as low as ca. 1 : 5 the pore diameter comparable to the highest reported earlier for Pluronic-templated synthesis of SBA-15. On the other hand, the increase in the amount of TIPB at 14 °C or lower allowed us to achieve a major improvement of quality of materials and to achieve much higher unit-cell sizes and pore diameters with retention of 2-D hexagonal ordering.

2.3.2.3. Further extension of pore size range for SBA-15 via adjustment of the amount of swelling agent

At 14 °C, the change in P123 : TIPB mass ratio to 2.4 : 2 resulted in a slight pore diameter enlargement, but more importantly, it led to a major improvement of the quality of the material. For the resulting SBA-15, the SAXS pattern was very well resolved featuring a strong (210) peak, which was a clear improvement over the sample prepared with P123 : TIPB mass ratio to

2.4 : 1 (Figure 2.7), while d_{100} was somewhat larger for the former. The mesopore volume was also increased. It should be noted that a broadening of the hysteresis loop on nitrogen adsorption isotherms was observed for the samples prepared at 14 °C or lower with 2 g or more of TIPB per 2.4 g P123, indicating the development of minor constrictions in the mesopores. When the hydrothermal treatment at 100 °C was prolonged to 5 d, or its temperature was increased to 130 °C, the hysteresis loops became narrower, indicating the elimination of these constrictions.

Shown in Figures 2.7(b), 2.9(b), 2.10(b) and 2.11 are SAXS patterns, nitrogen adsorption isotherms, PSDs and TEM for SBA-15 silicas synthesized with increased relative amount of TIPB (P123 : TIPB = 2.4 : 2, 2.4 : 2.5 and 2.4 : 3) at initial temperatures decreasing from 14 to 11.4 °C and subsequently hydrothermally treated at 130 °C for 1 day. SAXS patterns indicated that 2-D hexagonal structure formed at temperatures from 14 to 12.25 °C and d_{100} interplanar spacing for calcined materials increased from 19.4 to 25.8 nm as the temperature decreased, but the patterns became less well resolved as the temperature decreased, indicating a gradual decrease of degree of structural ordering. All the considered materials exhibited (100), (110) and (210) peaks on SAXS patterns (Figure 2.7(b)). It should be noted that while the silica synthesized at 12.25 °C with the P123 : TIPB ratio of 2.4 to 2 also exhibited three reflections on SAXS pattern, the increase in the ratio to 2.4 : 2.5 made the pattern better resolved. TEM images (Figure 2.11) provided further corroboration of 2-D hexagonal structures of the materials, as patterns of parallel stripes (which are known to be a side projection of the honeycomb)[185] and honeycomb patterns were observed. SAXS pattern of the sample synthesized at initial temperature of 12 °C was less well resolved, but on the basis of the SAXS patterns of the samples discussed above, it appears that the shoulder at q = ~0.23 was a residual (100) peak, and the feature observed at q = ~0.39 was (110) reflection, which would correspond to d_{100} = ~28

nm. TEM confirmed the presence of honeycomb domains in the aforementioned material (see Figure 2.11), but these domains were accompanied by a significant fraction of less well-defined domains with appreciably larger pores, some of which being apparently cylindrical in shape. The silicas formed at 11.7 and 11.4 °C, whose SAXS patterns were featureless (see Figure 2.7(b)), were also comprised of similar domains.

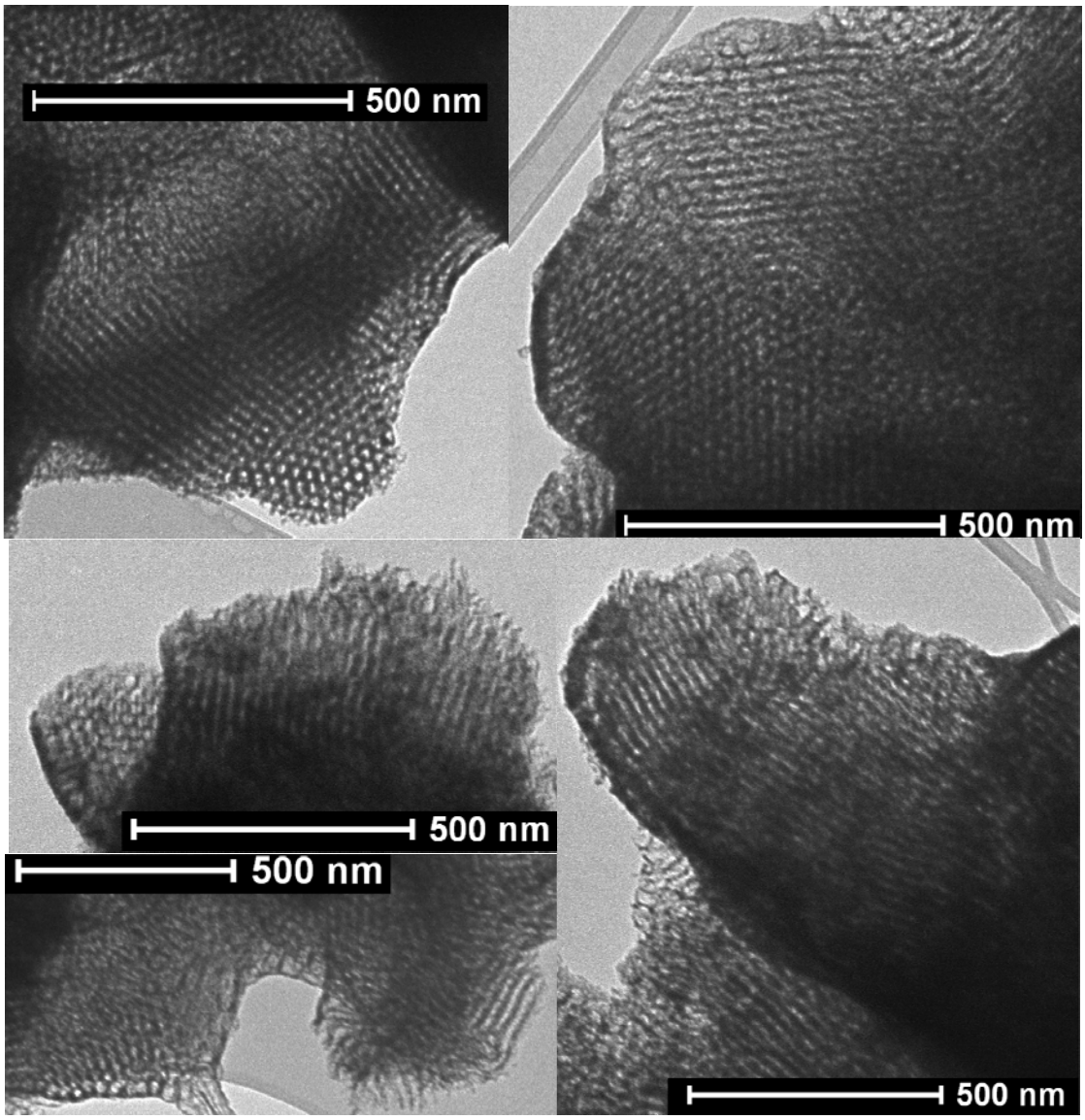

Figure 2.11. TEM images of calcined silica samples synthesized at: 14 °C (top, left), 12.75 °C (top, right) and 12.5 °C (middle, left) with surfactant (P123) : swelling agent (TIPB) mass ratio of 2.4 to 2; 12.25 °C (bottom, right) with P123 : TIPB mass ratio of 2.4 to 2.5; and 12 °C (bottom, left) with P123 : TIPB mass ratio of 2.4 to 3.[50]

Nitrogen adsorption isotherms of the obtained SBA-15 silicas with ultra-large unit-cell sizes are shown in Figure 2.9(a). It can be seen that the capillary condensation step shifted from the relative pressure of ~0.91 to 0.94 as the initial synthesis temperature was lowered from 14 to 12.25 °C. As noted above, the highest relative pressure of capillary condensation (for nitrogen adsorption at -196 °C) observed for previously reported and well-documented silicas with 2-D hexagonal structures was ~0.90, which is well below the range observed for our samples considered here. This clearly indicates that the latter samples had larger pore diameters than their literature counterparts. Even if the TMB-expanded material reported in the first disclosure of SBA-15[21,22] had been 2-D hexagonally ordered, which is unlikely based on the subsequent report on the mesocellular foam nature of large-pore TMB-expanded silicas,[28] its capillary condensation pressure was ~0.92, which is in the lower range of values observed for our 2-D hexagonal samples whose isotherms are shown in Figure 2.9(b). Further insight regarding the magnitude of pore diameters of the present silicas relative to the diameter of cylindrical pores of 2-D hexagonal silicas reported earlier can be gained by comparing nominal pore diameters assessed from adsorption branches of isotherms using the BJH method.[162] The BJH pore diameter of our samples ranged from 21 to as high as 34 nm (see PSDs in Figure 2.10(b)). The BJH pore diameters of well-documented SBA-15-type silicas reported to date were up to ~21 nm.[32,33,41] The BJH pore diameters initially reported for SBA-15[21,22] ranged to 30 nm, although it was later reported that the 2-D hexagonal structure persists only up to 12 nm.[28] In any case, the BJH pore diameter for our SBA-15 silicas was beyond that reported earlier for SBA-15. It is interesting to note that even at temperatures of 12 °C or lower, in which case the 2-D hexagonal structure was partially or fully lost, the pore diameter still systematically increased as the initial synthesis temperature decreased and the BJH pore diameter reached 70 nm. One can conclude

that the initial temperature adjustment in the present synthesis affords materials with pore diameters in the entire upper part of the mesopore range. While the adjustability of the pore size over most of the mesopore range using swelling agents has been demonstrated earlier,[186] our synthesis gives an unprecedented range of diameters for cylindrical pores. It should be noted that the improvement in quality of the sample prepared at 12 °C was reached through further increase of the P123 to TIPB mass ratio to 2.4 : 3. Clearly, larger relative amounts of TIPB are beneficial in the synthesis of silicas with very large mesopores at initial temperatures of ~12 °C.

The BJH pore size calculations from adsorption branches of isotherms provided the information about the shape of pore size distribution and allowed for a reliable comparison of pore diameters for different samples. However, a more accurate pore diameter evaluation is desirable, and can be achieved using eq 1, which allows one to assess the diameter of cylindrical pores on the basis of (100) interplanar spacing, primary mesopore volume and micropore volume. As can be seen in Table 2.2, the resulting pore diameters ranged from 19 to 26 nm, the latter being exceptionally large. It can be inferred from Table 1 that the nominal BJH pore diameter of ~21nm corresponds to the actual pore diameter of 18 nm (see Table 2.2). Therefore, one can conclude that our work extended the pore size range achievable for silicas with ordered cylindrical pores from 18 nm to 26 nm.

2.3.2.4. Effect of the hydrothermal treatment time and temperature

A pore diameter adjustment was also achievable through the change in the duration of the hydrothermal treatment, which is a known feature of SBA-15 synthesis.[22,48,174] For instance, in the case of the initial synthesis temperature of 17 °C , the BJH pore diameter could be adjusted from 10 to 15 nm by extending the hydrothermal treatment time from 0 hours to 2 days. It should

be noted that adsorption/desorption hysteresis loops on adsorption isotherms for the samples prepared without a hydrothermal treatment, or with short treatments, exhibited broadening and/or tailing to lower pressures, which was similar to the behavior of SBA-15 synthesized using hexane as a swelling agent.[48] Such an adsorption behavior indicates that the ordered mesopores exhibited constrictions, which were gradually diminished during the hydrothermal treatment.[48]

The increase in the hydrothermal treatment temperature allows one to achieve larger pore sizes[22] in a shorter period of time.[48] For instance, the heating at 130 °C for one day afforded a larger pore size than the heating at 100 °C for two days. As noted above, long hydrothermal treatment times at high temperatures (e.g., two days at 130 °C) appear to lead to the merging of adjacent cylindrical mesopores.

2.3.2.5. Influence of the order of addition of silica source and TIPB

The pore size increase was also achieved in case where TIPB was added 3 hours before the addition of TEOS instead of adding both at the same time, as in our standard procedure. For initial synthesis temperature of 17 °C, d_{100} interplanar spacing of the obtained SBA-15 was 15.6 nm, which is 1.5 nm larger than d_{100} obtained in our standard procedure. The pore diameter was also increased. In case of the synthesis at an initial temperature of 14 °C, the pore size was also increased when TIPB was added prior to TEOS, but SAXS pattern featured only one broad peak, indicating a low degree of structural ordering, unlike in the case of the standard procedure.

2.3.2.6. Cyclohexane and triethylbenzene as swelling agents

As noted in the introduction, our expectation was that swelling agents of moderate tendency of solubilization in Pluronics are suitable as micelle expanders in the synthesis of large-pore SBA-15. In addition to TIPB, which was found to be an excellent swelling agent, 1,3,5-triethylbenzene (TEB) was evaluated, but with TEB substituted for TIPB with the same mass ratio. A large-pore material with disordered structure (as inferred from featureless SAXS pattern in Figure 2.12) was obtained, showing that TEB is indeed a powerful swelling agent, but it leads to uncontrolled swelling under the considered conditions . It should be noted that silica synthesized under similar conditions using the common swelling agent TMB (2 g per 2.4 g P123) did not feature any uniform mesopores, thus showing that TIPB, which is expected on the basis of its structure to solubilize in Pluronics to the least extent among TIPB, TEB and TMB, is by far the most suitable for the synthesis of ultra-large-pore SBA-15. It was also conjectured that cyclohexane is likely to be a potent swelling agent in SBA-15 synthesis. The synthesis at an initial temperature of 15 °C using 1 g of cyclohexane per 2.4 g P123 indeed afforded a large-pore SBA-15 (BJH pore diameter of ~13 nm; see Figure 2.12), while the use of 8.5 g of cyclohexane per 2.4 g P123 (this is the mass ratio analogous to that used in the synthesis of Sun et al. involving hexane[46,48] that affords SBA-15 with pore diameter of ~15 nm) afforded a material with a broad PSD centered at ~20 nm and with a quite featureless SAXS pattern (data not shown). Clearly, cyclohexane is a powerful swelling agent that is useful in the synthesis of large-pore SBA-15.

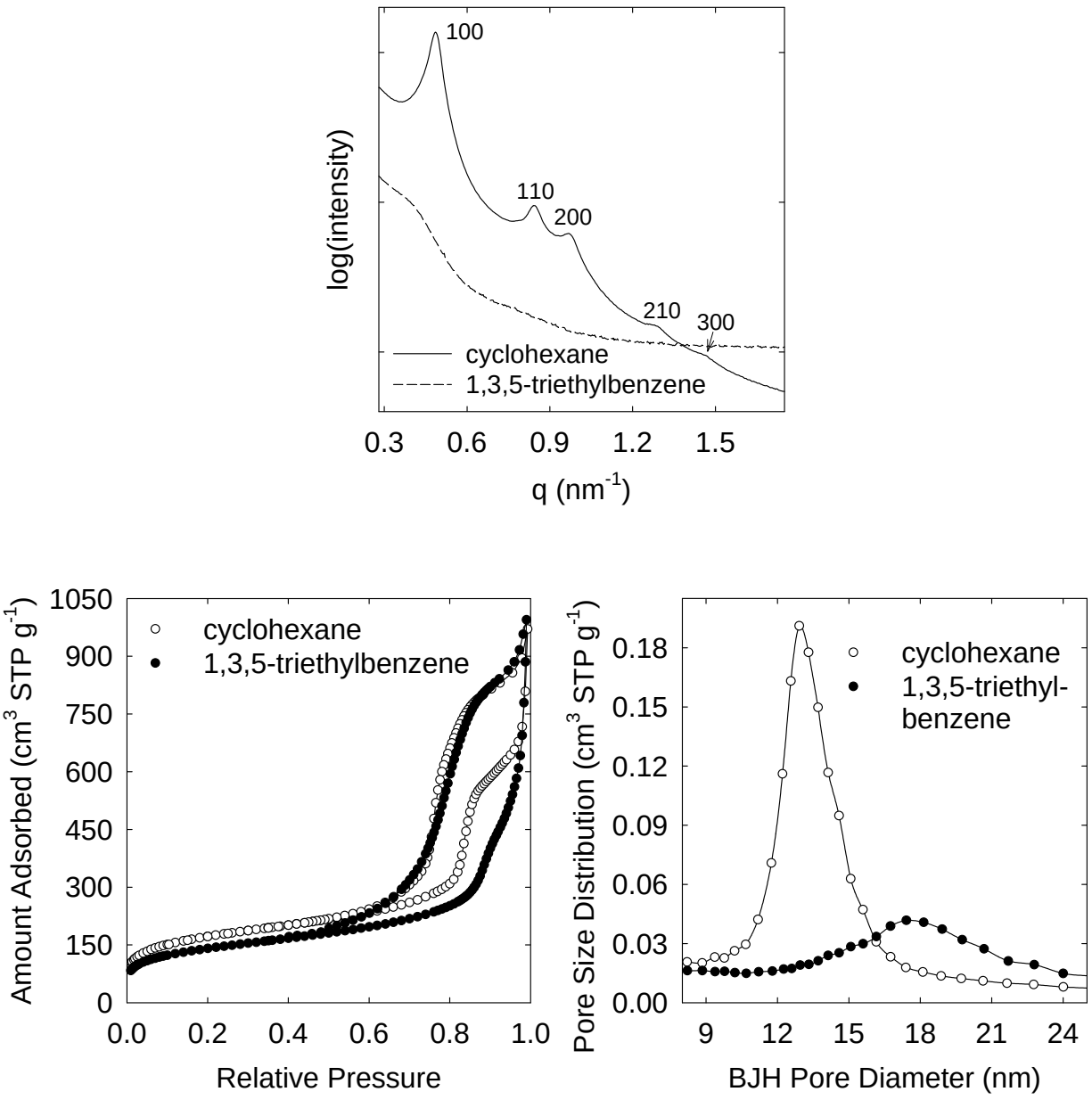

Figure 2.12. (top) SAXS patterns, (bottom left) nitrogen adsorption isotherms and (bottom right) pore size distributions for silicas prepared at: (i) initial temperature of 15 °C using cyclohexane as a swelling agent, and (ii) initial temperature of 17 °C using 1,3,5-triethylbenzene as a swelling agent.[50]

2.3.2.7. Proposed pore size expansion mechanism

It was reported that in the synthesis of SBA-15, the use of TMB as a swelling agent allows one to expand the diameter of cylindrical pores only to a limited extent, while mesocellular foams with spherical mesopores form when higher relative amounts of TMB are used [28] If the micelle expander solubilizes in the hydrophobic core of the micelle (which in the present case consists of poly(propylene oxide) blocks of the triblock copolymer), the volume ratio of the hydrophilic domains to the hydrophobic domains decrease, promoting lower-surface-curvature micellar structures (cylindrical, gyroid, lamellar) rather than high-surface-curvature spherical micelles (spherical).[28] Therefore, the formation of MCFs templated by high-surface-curvature domains can be understood as a result of templating by oil-in-water microemulsions, in which oil (TMB) droplets are stabilized by the block copolymer surfactant.[28,51] In contrast, TIPB is shown herein to promote the formation of silicas with cylindrical mesopores with a wide range of sizes (10-26 nm), thus indicating the templating by TIPB-swollen micelles (rather than microemulsions), whose sizes can be adjusted in a wide range by changing the initial synthesis temperature and the amount of micelle expander.

The temperature-dependent gradual pore size enlargement in the SBA-15 synthesis in the presence of TIPB is an exceptional behavior. While the influence of the initial synthesis temperature was studied for aliphatic hydrocarbons used as micelle expanders, the change from SBA-15 to vesicular phase or MCF was observed.[187] Our study of SBA-15 synthesis with hexane swelling agent in the temperature range of 12-17 °C revealed essentially no variation in the pore diameter. Moreover, changes of initial synthesis temperature from 10 to 15 and 20 °C had little effect on the pore size for cyclohexane used as a swelling agent. In the case of the synthesis of

LP-FDU-12 with spherical mesopores arranged in fcc structure templated by Pluronic F127 ($EO_{106}PO_{70}EO_{106}$) block copolymer, the pore diameter increased as the temperature was lowered to 15 °C, but then stabilized until the temperature was lowered so much that the ordered material no longer formed.[188,189] On the basis of this survey, the temperature behavior observed in the synthesis involving TIPB does not seem to have any reported counterpart, although it bears some resemblance of the behavior observed in the synthesis of LP-FDU-12. Perhaps the interactions between TIPB and $EO_{20}PO_{70}EO_{20}$ change significantly as the temperature is lowered in the 11-20 °C range. It is notable that at lower temperatures, a larger relative amount of TIPB is needed to achieve a higher degree of structural ordering and to suppress the formation of disordered domains, whose presence is indicated by the occurrence of additional mesopores of size below 10 nm with concomitant lowering of the total pore volume. At the same time, the diameter of the uniform mesopores does not vary much as the amount of the swelling agent is increased, and the extent of the pore volume increase is smaller than the extent of increase in the sum of volumes of the block copolymer template and the micelle expander (unlike in some other cases, where there is a proportional increase[181]). These findings suggest that only a part of available TIPB is solubilized in the micelles, similarly to the case of the use of hexane as a swelling agent, wherein hexane is supplied in large excess.[48] The micelle diameter in the presence of TIPB is primarily temperature-dependent, being much less dependent on the relative amount of TIPB. This suggests that the temperature modifies the extent of stretching of the PPO block in the micelles in the presence of TIPB, while it affects the extent of solubilization of TIPB to a lesser extent. In this context, the fact that the increase in the relative amount of TIPB leads to improvement in quality of samples synthesized at lower temperatures might suggest that a significant excess of

TIPB promotes the homogeneity of the material, suppressing the separation into more uniform, TIPB-rich domains and disordered, TIPB-depleted domains.

2.3.3 Conclusions

Considerations of the extent of solubilization of hydrophobic molecules in micelles of Pluronic block copolymers allowed us to identify TIPB, TEB and cyclohexane as potentially suitable for the synthesis of large-pore SBA-15. Following this identification, the synthesis of ultra-large-pore SBA-15 (ULP-SBA-15) with pore diameter up to 26 nm (BJH pore diameter up to 34 nm) was accomplished using commercially available Pluronic P123 triblock copolymer as a template and TIPB as a micelle expander. In comparison to other micelle expanders, TIPB appears to exhibit a moderate extent of solubilization in PEO-PPO-PEO copolymer, which is likely to be a key factor in avoiding an uncontrolled swelling and loss of structural uniformity of the micelles. In the case of the synthesis involving TIPB, the pore diameter of SBA-15 was adjusted primarily by the selection of the initial synthesis temperature. However, the pore diameter fine-tuning was achieved through the change in the amount of the micelle expander (relative to the copolymer surfactant), or the change in the duration of the hydrothermal treatment or its temperature. Cyclohexane and TEB were also verified as swelling agents for the synthesis of large-pore silicas and the former was demonstrated to be suitable for synthesis of large-pore SBA-15.

2.4. Synthesis of Large-Pore SBA-15 Silica from Tetramethyl Orthosilicate[56]

2.4.1 Experimental section

2.4.1.1. Materials

SBA-15 silicas were synthesized using Pluronic P123 triblock copolymer $EO_{20}PO_{70}EO_{20}$ (BASF) as a template and TIPB as a micelle expander. In most cases, the molar composition of the synthesis mixture was: TMOS : P123 : TIPB : NH_4F : HCl : H2O = 1 : 0.0165 : 0.196 : 0.0290 : 4.35 : 183. This composition follows that used in our earlier study,[50] but TEOS was replaced with an equal number of moles of TMOS. A synthesis was carried out as follows. 2.4 g Pluronic P123 and 0.027 g NH_4F were dissolved in 84.0 mL of 1.30 M aqueous HCl solution at room temperature. Then, the solution was transferred to a water bath (nominal temperature accuracy of 0.01 °C) set at a temperature between 12.50 and 15.00 °C and after at least one hour, a mixture of 3.7 mL TMOS and 1.2 mL (1.0 g) TIPB was added. The solution was stirred for 24 hours at the initial temperature in an open container using a mechanical stirrer. Subsequently, the synthesis mixture was heated at 100 °C in a closed container for periods of time from 2 to 5 days. A sample was also synthesized at an initial temperature of 12.5 °C or similar using two times larger amount of TIPB (2.4 mL per 3.75 mL TMOS). In this case, the hydrothermal treatment was performed at 130 °C for 1 day. As-synthesized products were isolated by filtration with water washing, and were dried at ~60 °C in a vacuum oven. Finally, the materials were calcined under air at 550 °C for 5 hours with a heating ramp 2 °C/min to remove the surfactant template.

2.4.1.2. Characterizations

See the **section 2.3.1.2.**

2.4.1.3. Calculations

See the **section 2.2.1.3.**

2.4.2. Results and discussion

Our motivations to perform this study was based on the results that in the synthesis of large-pore SBA-15 using PEO-PMA surfactants,[41] some improvements in degree of structural ordering and pore size uniformity were observed when TEOS was replaced by a faster-hydrolyzing tetramethyl orthosilicate (TMOS) as a silica source. The present work explores the use of TMOS instead of most commonly used TEOS for the synthesis of large-pore SBA-15 in the presence of Pluronic P123 template and TIPB swelling agent.

2.4.2.1. Small-angle X-ray scattering

SAXS patterns for calcined samples synthesized at initial temperature of 12.75 to 15 °C featured three or more peaks (Figure 2.13) that can be indexed as reflections of a 2-D hexagonal structure (p6mm symmetry). The (100) interplanar spacing for calcined samples spanned a range from 15.4 to 21.0 nm (see Table 2.3), the latter value being very large and comparable only with that of the SBA-15 silicas synthesized using TIPB and TEOS.[50] The decrease in the unit-cell size upon calcination was 2-4 %. The sample synthesized at 12.5 °C exhibited an interplanar spacing of ~24 nm, which is close to the highest unit-cell parameters documented for SBA-15 (which is 26 nm, see ref.[50]). However, the SAXS pattern for this material had a broad peak at q = 0.26 nm^{-1}

and a broad feature located in a position where the corresponding (110) and (200) peaks can be expected. Therefore, the identification of this pattern as the one for a 2-D hexagonal structure is uncertain. Nonetheless, TEM of the considered material strongly indicated that it was indeed a 2-D hexagonal structure (see Figure 2.14). It should be noted that in the case of the TEM imaging of a 2-D hexagonal structure, the honeycomb features arise when the electron beam is parallel to the axis of the pores. However, when the electron beam is perpendicular to the pore axis, series of stripes can result.[185] In particular, if the beam is parallel to the plane that contains the axes of nearest-neighbor pores, the TEM image consists of stripes with the spacing of d_{100}.[185] In this case, the contrast in TEM images arises because the electrons that go along the aforementioned planes encounter less silica framework and more pore void space than the electrons that go in between these planes.[185] One can also envision that if the 2-D hexagonal structure arranged in a way discussed above is tilted by 30° degrees about the pore axis, then the beam goes parallel to planes that contain axes of second-nearest-neighbor pores. In such a case, the spacing between the lines would be $d_{110} = d_{100}/3^{1/2}$. This explains why one of the images shown in Figure 2.14 features series of lines with two different spacings.

For the samples synthesized at 12.75-13 °C, the SAXS patters collected at the synchrotron source featured shoulders at the left side of the (100) peaks and the samples prepared at 13 °C also exhibited noticeable, although weak, shoulders between (100) and (110) peaks. The occurrence of shoulders on the left side of the main peak was not confirmed on our laboratory SAXS setup that was suitable for measurements down to somewhat lower q values (that is, in somewhat wider range of interplanar spacings) than the setup used at the synchrotron source. On the other hand, the occurrence of features between (100) and (110) peaks was confirmed. Therefore, the presence of an ordered (or weakly ordered, for instance MCF)

impurity phase cannot be ruled out for the considered materials prepared at 12.5 - 13 °C, although an impurity phase was not apparent in TEM.

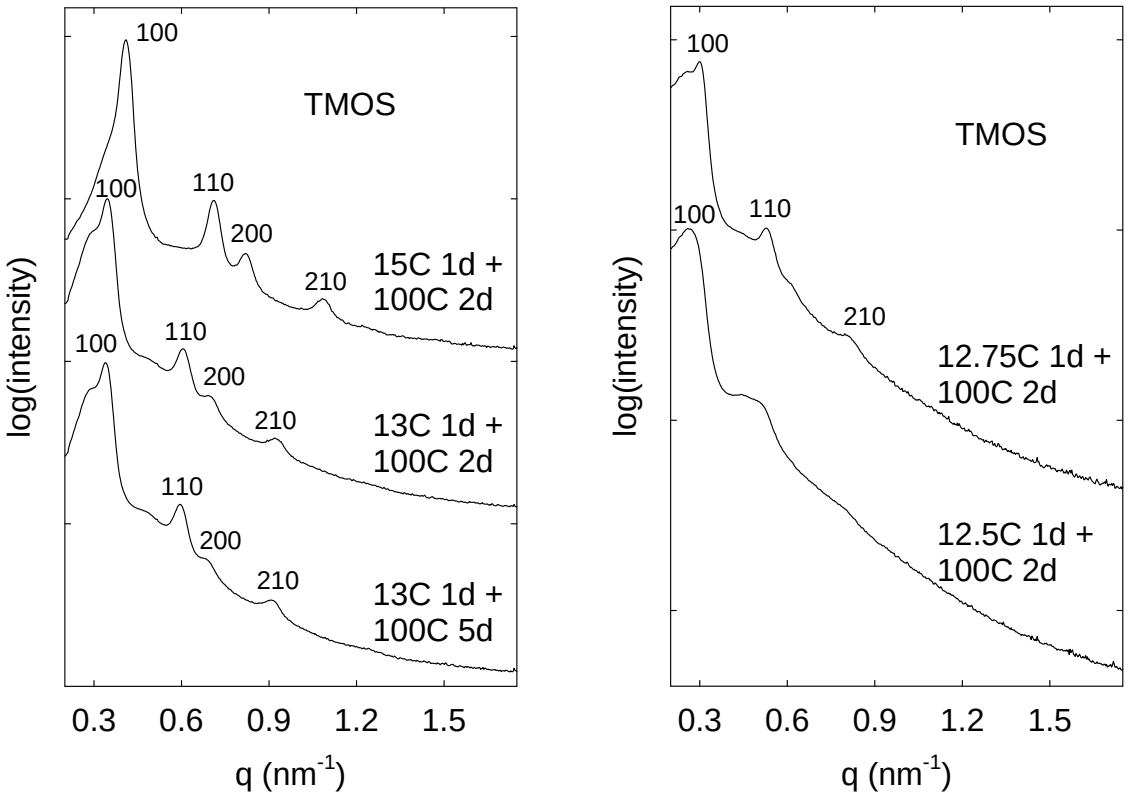

Figure 2.13. SAXS patterns acquired using a synchrotron X-ray source for calcined SBA-15 silicas prepared at different initial temperatures or different times of hydrothermal treatment.[56]

Table 2.3. Structural properties of silicas.[a]

Conditions[b]	$d_{100,UC}$ (nm)	d_{100} (nm)	S_{BET} (m^2/g)	V_t (cm^3/g)	V_{mi} (cm^3/g)	V_p (cm^3/g)	w_{BJH} (nm)	w_d (nm)	b_d (nm)
15°C, 100°C 2d	15.9	15.4	580	1.32	0.07	1.03	16.3	15.0	2.7
13°C, 100°C 2d	19.0	18.2	540	1.24	0.06	0.96	20.0	17.5	3.5
13°C, 100°C 5d	18.9	18.5	460	1.23	0.05	0.91[c]	21.7	18.0[d]	3.3
12.75°C,100°C 2d	21.8	21.0	540	1.18	0.04	0.88[c]	23.0	20.5[d]	3.9
12.5°C,100°C 2d	24.7[e]	23.7[e]	510	1.11	0.04	0.83[c]	24.8	22.8[f]	4.6
12.5°C,130°C 1d 2x TIPB	23.0	21.6	360	1.27	0.03	0.96[c]	26.1	21.3[d]	3.6

[a] Notation: $d_{100\ UC}$, (100) interplanar spacing for uncalcined sample; d_{100}, (100) interplanar spacing for calcined sample; S_{BET}, BET specific surface area; V_t, total pore volume; V_{mi}, micropore volume; V_p, primary mesopore volume; w_{BJH}, BJH pore diameter; w_d, pore diameter calculated using Equation 1; b_d, pore wall thickness; [b] Initial synthesis temperature followed by the hydrothermal treatment temperature and time; for the last sample, two times higher relative amount of TIPB was used. [c] Could not be calculated with acceptable accuracy using α_s plot method. Values in parentheses are estimates based on V_t and V_{mi} values for the particular sample (see Calculations section). [d] Value based on the estimated value of V_p. [e] Tentative assignment of peak on the basis of TEM observation of 2-D hexagonal structure. [f] Approximate value based on the assumption of 2-D hexagonal symmetry that was indicated by TEM.

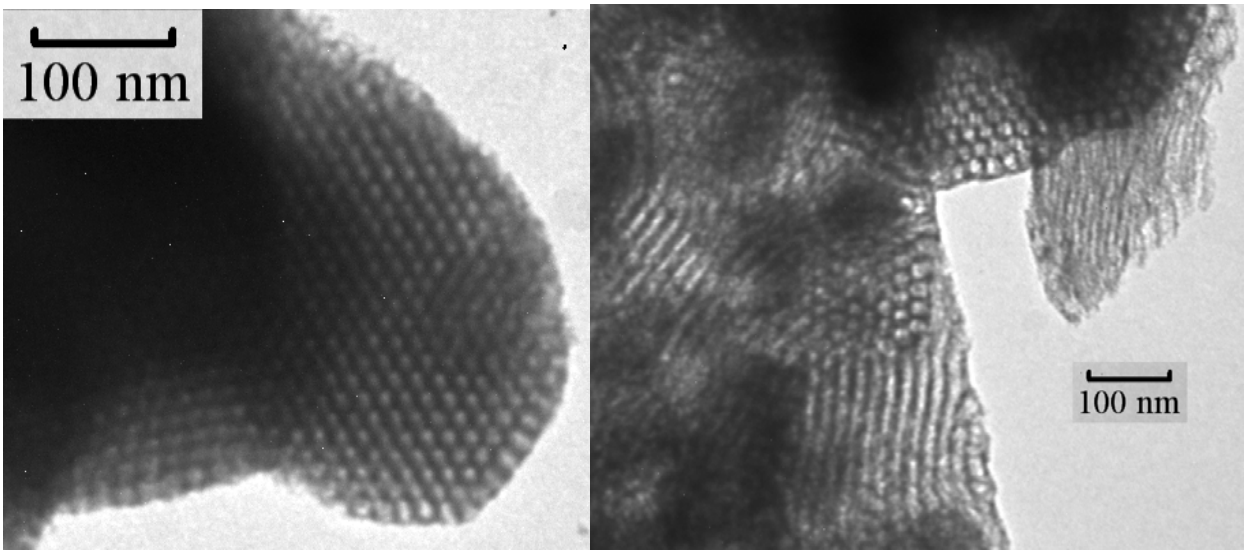

Figure 2.14. TEM images of calcined silicas synthesized at: 15 °C (left) and 12.5 °C (right).[56]

2.4.2.2. Nitrogen adsorption

As can be seen in Figure 2.15, nitrogen adsorption isotherms for the samples exhibited steep capillary condensation steps at relative pressures above 0.85, suggesting the presence of large mesopores of narrowly defined size. The adsorption isotherms were used to calculate the specific surface area, micropore volume, mesopore volume, the diameter of primary (ordered) mesopores (through Equation 1) and PSD (shown in Figure 2.16). The specific surface areas were 460-580 $m^2\ g^{-1}$, and the total pore volumes were 1.11-1.32 $cm^3\ g^{-1}$, while the micropore volume was ~0.05 $cm^3\ g^{-1}$ (see Table 2.3). The pore diameters for 2-D hexagonal samples (as confirmed by SAXS) were from 15 to 20.5 nm, as determined using Equation 1. The pore wall thickness was estimated to be 2.7-4.6 nm and it tended to increase as the (100) interplanar spacing increased. The BJH pore diameters ranged from 16 to 23 nm for the aforementioned samples, and the BJH pore diameter was 25 nm for the sample whose 2-D hexagonal ordering was indicated primarily

by TEM. It should be noted that the application of the BJH algorithm to perform PSD calculation from adsorption branches of isotherms using the Kelvin equation for the hemispherical meniscus leads to an overestimation of diameter of cylindrical mesopores in the range above ~10 nm.[48,50] On the other hand, PSDs calculated as described above are expected to reflect reasonably well the shape and breadth of the size distribution for large mesopores, and they allow one to compare pore diameters for different samples (as long as the pore geometry is the same, which is a good approximation in the present work).

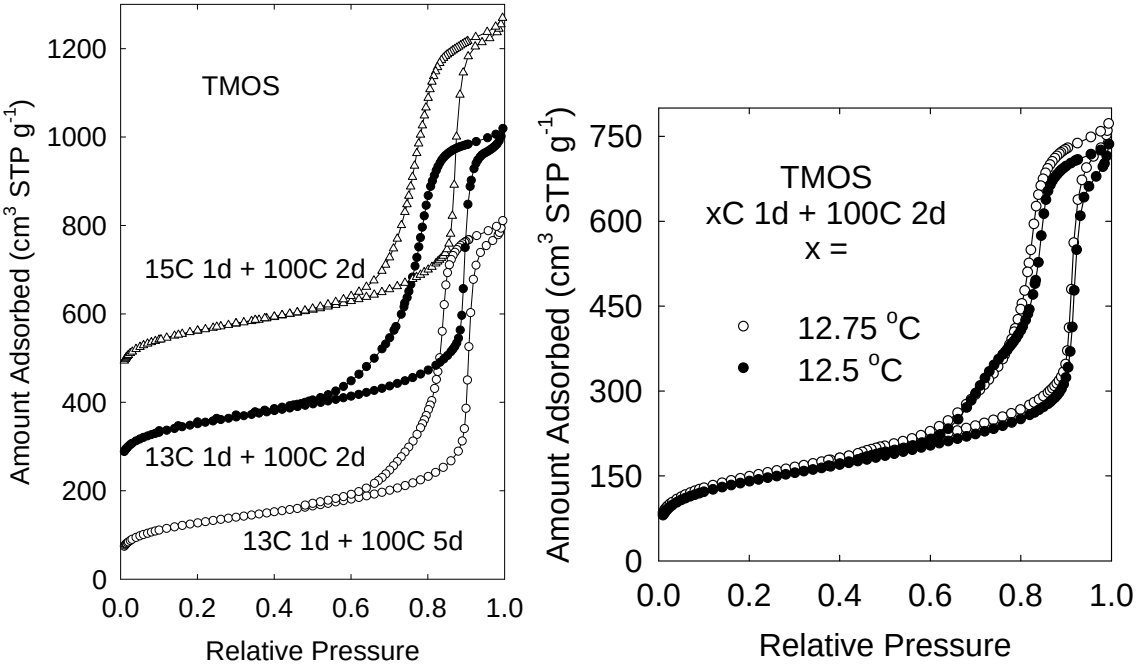

Figure 2.15. Nitrogen adsorption isotherms for calcined SBA-15 silicas prepared at different initial temperatures or different times of hydrothermal treatment (for clarity, the isotherms for samples 13C1d+100C2d and 15C1d+100C2d were offset vertically by 200 and 400 cm^3 STP g^{-1}, respectively).[56]

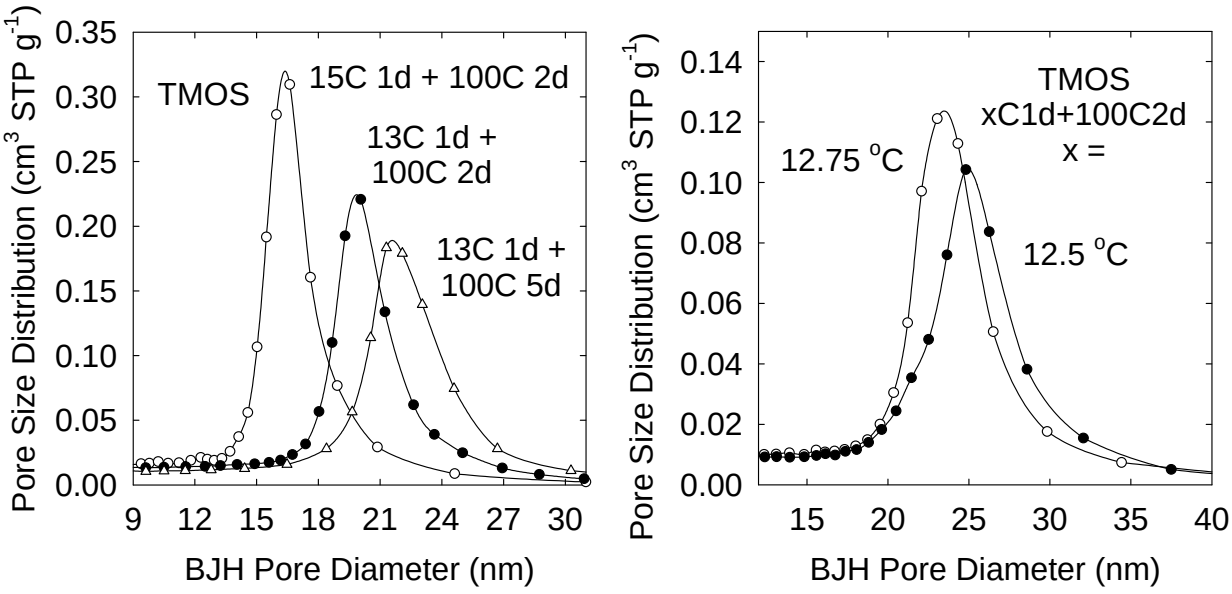

Figure 2.16. Pore size distributions for calcined SBA-15 silicas prepared at different initial temperatures or different times of hydrothermal treatment.[56]

2.4.2.3. Effect of amount of the swelling agent and initial synthesis temperature

It can be seen that as the initial synthesis temperature decreased, the pore diameter increased, as observed earlier for samples synthesized using TEOS as a silica source.[50] In fact, there was a close resemblance in the temperature range at which a particular pore size was attained in both cases. Perhaps the most significant difference between the synthesis with TMOS and TEOS was that for P123 : TIPB mass ratio of 2.4 to 1, the samples synthesized with TEOS at 13.5 °C or below featured additional mesoporosity of diameter 5-8 nm.[50] The volume of these mesopores was correlated with the loss in the volume of the ordered mesopores. The increase in the relative amount of TIPB in the synthesis mixture allowed us to eliminate the considered undesirable feature, so the additional 5-8 nm porosity observed in the case of TEOS precursor could be due

to the existence of swelling-agent-depleted domains in the material.[50] It is interesting to note that the occurrence of the considered structural feature was never observed when TMOS was used as a silica source. Moreover, PSDs for the samples synthesized using TMOS were narrow, and in some cases even more narrow than those for SBA-15 synthesized from TEOS. A common feature of the two considered synthesis procedures for large-pore SBA-15, as well as that for many other polymer-templated syntheses of ordered mesoporous silicas [22,169-171] is that the pore diameter can be enlarged to some extent by increasing the duration of the hydrothermal treatment (see data for samples synthesized at 13 °C). This process is accompanied by the narrowing of the hysteresis loop (see Figure 2.15). The sample prepared at 12.5 °C exhibited a two-step desorption behavior. This additionally supports an expectation that the material is contaminated with another phase, whose structure remains unclear at present.

A beneficial effect of the addition of a larger relative amount of TIPB at low temperatures (14 °C or below) observed in the TEOS-based synthesis of SBA-15 [50] prompted us to examine whether similar benefits can be achieved when TMOS is used as a silica source. Indeed, for P123 : TIPB mass ratio of 2.4 to 2, SBA-15 samples with SAXS patterns without the shoulders between the (100) and (110) peaks were obtained (see Figure 2.17). In particular, SBA-15 samples with (100) interplanar spacing ~22 nm were synthesized at 12.5-12.75 °C, and the (100) peak on their patterns was better separated from the background (see Figure 2.17) than in the case of the comparable sample from the synthesis at 12.75 °C with lower P123 : TIPB ratio (2.4 to 1). It should be noted that at higher P123 : TIPB ratio, the hydrothermal treatment at 130 °C for 1 day was employed in order to obtain a narrower hysteresis loop (see adsorption data in Figure 2.18), while the hydrothermal treatment at 100 °C for 2 days may afford samples with wider or tailing hysteresis loops (see Figure 2.15 and Ref.[50]). The geometrical pore diameter for

the considered SBA-15 sample was 21.3 nm, while the nominal (BJH) pore diameter was 26 nm (see Figure 2.18), which is the largest among the samples reported herein. However, the reproducibility of this synthesis was not as good as in the case of the use of TEOS as a silica source.

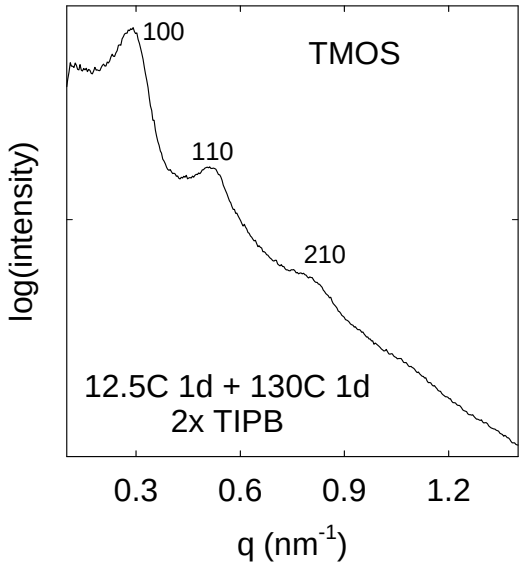

Figure 2.17. SAXS pattern recorded using Nanostar U SAXS/WAXS system for calcined SBA-15 silica prepared with the amount of TIPB increased two times with respect to the original synthesis procedure.[56]

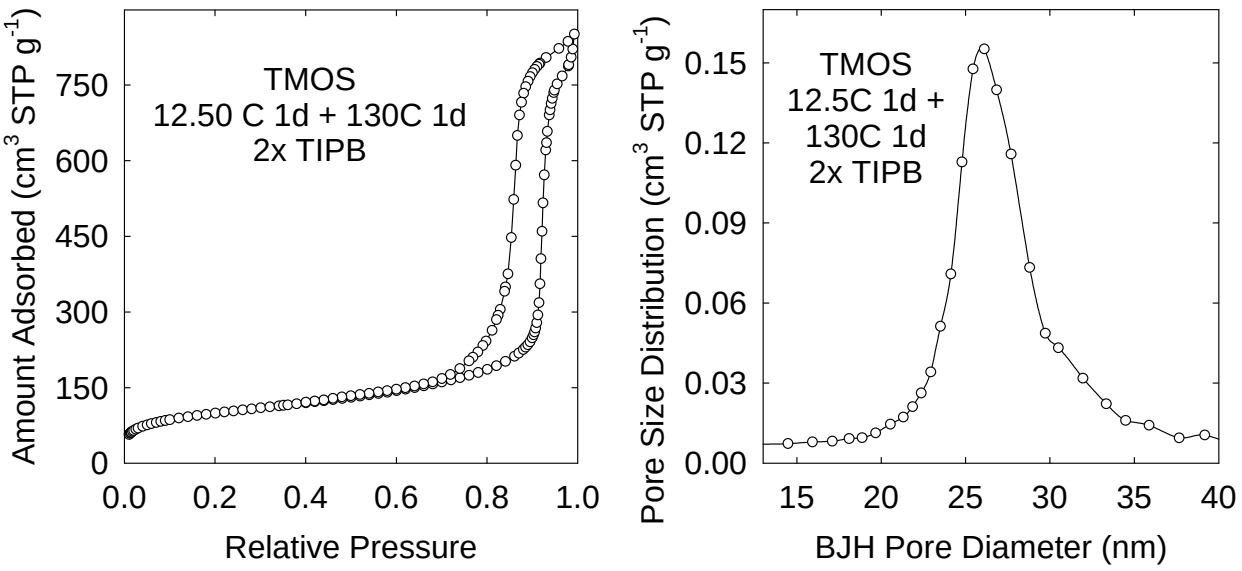

Figure 2.18. Nitrogen adsorption isotherm (left) and pore size distribution (right) for calcined SBA-15 silica prepared with the amount of TIPB increased two times with respect to the original synthesis procedure.[56]

2.4.3 Conclusions

TMOS is suitable as a silica source for the synthesis of SBA-15 with (100) interplanar spacings up to 22 nm, mesopore diameters up to 21 nm and with BJH (nominal) pore diameters up to 26 nm. While the ordering of 2-D hexagonal structure of these materials and narrowness of PSD is comparable (in some cases even better) than in the case of SBA-15 synthesized from TEOS, the range of the achievable pore diameters appears to be more restricted and the reproducibility of the synthesis of materials with the largest achievable pore diameters is inferior. The initial temperature at which a particular pore diameter can be achieved is similar for both silica sources, indicating that the nature of hydrolizable groups on the silicon atom of the silica precursor has a small effect on the formation of the ordered mesostructure.

2.5. Rapid Synthesis of Ordered Mesoporous Silicas with Ultra Large Pores

The results discussed earlier demonstrated that 2-D hexagonally ordered cylindrical pores of SBA-15 can be readily adjusted from 10 nm to 26 nm in diameter by changing the amount of TIPB and the initial temperature.[50,54] The syntheses were based on "surfactant-templating" and normally took at least 2 days, which is relatively long. The required time included the time in which (i) the block polymers must be fully dissolved, (ii) the condensation of silica precursor, such as TEOS, takes place to avoid the structure collapse upon template removal, (iii) the hydrothermal treatment is performed to increase the mesopore diameter and volume, and (iv) the template is totally removed by either calcination or solvent extraction. From the point of view of conservation of energy and time, rapid and efficient methodologies are in demand, but so far limited reports were published such as using highly acidic conditions to accelerate dissolution of block copolymers,[190] or adding heteropolyacids as catalysts to accelerate hydrolysis of silica precursors,[191,192] or applying microwave heating[193-195] and so forth.[196-199] However, these syntheses are often limited by using special instrumentation and chemicals while most of them afforded OMSs with pore diameters below 10 nm, which may greatly hinder OMSs application in the areas of catalysts and polymer composites. Herein, we proposed a facile and rapid method to synthesize high quality OMSs with ultra-large pores using micelle expanders, such as TIPB or TMB. These methods allow one with common instrumentation setup to obtain OMSs with pore diameters up to ~30 nm in two dimensional (2-D) hexagonal structures (SBA-15) and ~22 nm in cubic structures (FDU-12) in a few hours.

2.5.1. Materials and synthesis

A typical synthesis of LP-SBA-15 was as follows: 2.4 g of P123 and 0.027 g of NH_4F were dissolved using a mechanical stirrer in 84.0 mL of 1.30 M aqueous HCl solution at required initial temperature for 30 minutes, then a mixture of 5.5 mL TEOS and a selected amount of TIPB was added and stirred for 1 hour at the same temperature in an open polypropylene container. Afterwards, the product was moved into a closed Teflon-lined autoclave and heated at 170 ^{o}C for periods of time from 1 hour to 1 day. As-synthesized silicas were isolated by filtering, and calcined under air at 400 °C for 2 hours (heating ramp 20 °C min^{-1}).

A typical synthesis of LP-FDU-12 was as follows: 1.0 g of F127 copolymer and 2.5 g of KCl were dissolved using a mechanical stirrer in 64 mL of 2.0 M aqueous HCl solution at 14°C for 30 minutes. Then, 2.3 mL of TMB was introduced. After 10 minutes of constant stirring, 4.35 mL (4.1 g) of TEOS was added and the mixture was stirred for 3 hours in an open container at the same temperature in an open polypropylene container. Afterwards, the product was moved into in a closed Teflon-lined autoclave heated at 170 ^{o}C for periods from 1 to 6 hours. As-synthesized silicas were isolated by filtering, and calcined under air at 500 °C for 2 hours (heating ramp 20 °C min^{-1}).

2.5.2. Characterization and calculations

See the ***section 2.3.1.2*** and ***section 2.2.1.3***

For cubic *Fm3m* ordered samples, the diameter of ordered mesopores, w_d, was calculated using a geometrical equation for materials with face-centered cubic (fcc) arrangement of spherical mesopores that are separated by microporous walls:[200]

$$w_d = a\left(\frac{6}{\pi v}\frac{V_p\rho}{1+V_p\rho+V_{mi}\rho}\right)^{1/3} \quad (2)$$

where α is the unit-cell parameter for the fcc structure determined from the position of (111) peak on SAXS pattern and υ is 4, the number of spherical pores in the unit cell.

2.5.3. Results and discussions

Ultra-large-pore SBA-15 (ULP-SBA-15) was synthesized using triblock copolymer $EO_{20}PO_{70}EO_{20}$ (Pluronic P123, BASF) as a template, TIPB as a swelling agent and ammonium fluoride (NH_4F) as an additive. A typical synthesis time was as short as 6 hours. The copolymer quickly dissolved in an acidic solution and formed a clear solution in 30 minutes, then the mixture of TEOS and TIPB was added and stirring was continued for an hour. The precipitation was observed after ~20 minutes. After short hydrothermal treatment at high temperature and fast calcination, samples were obtained and are denoted as Xg+Y^{o}C/Y'H+Z^{o}C/Z'H, which means samples were synthesized with X grams of TIPB (per 2.4 g P123) at initial temperature Y for Y' hours and at the hydrothermal temperature Z for Z' hours. Samples prepared with rapid synthesis show highly ordered structures as it is the case for samples with standard synthesis procedure which takes about 2 days or more.[50] Small-angle X-ray scattering (SAXS) patterns (Figure 2.19 (a)) show three or more obvious (100), (110) and (210) peaks, the characteristic of 2-D hexagonal structure (except for samples with 3.0 g TIPB). SAXS peak positions continually shifted to lower 2θ values and corresponding (100) interplanar spacing (d_{100}) increased to 29 nm as the initial temperature was lowered and the TIPB amount was adjusted. At the same time, very low shrinkage upon calcination (<3 wt.%) of all samples suggested good thermal stability of the products (Table

2.4). In nitrogen adsorption isotherms (Figure 2.19(b)) the capillary condensation steps gradually shifted to the relative pressure of ~0.95 for sample 3.0g+12.5C/1H+170C/4.5H, which to our best knowledge is higher than the highest relative pressure of well-documented surfactant-templated silicas with 2-D hexagonal structure of cylindrical mesopores reported in scientific literature. The corresponding BJH pore diameters (Figure 2.19(c)) increased from ~17 nm to ~39 nm with narrow pore size distributions as the temperature decreased. More reliable pore diameters are calculated using the geometrical equation 1 because the BJH method overestimates pore diameters of large cylindrical mesopores.[48,50] Transmission electron microscopy (TEM) images (Figure 2.19(d)) confirmed the 2-D hexagonal structures, as honeycombs and parallel stripes were clearly observed.

After the appearance of precipitates, which is an indication of formation of surfactant-templated silica particles, further solidification (in other words, the complete hydrolysis of silica precursor) and structural adjustment (increased pore diameter and decreased pore wall thickness) can be accelerated by applying high temperature hydrothermal treatment. To fully investigate the hydrothermal conditions that lead to high-quality products, a series of control experiments with 1.0 g TIPB and temperature of 17 ^{o}C maintained for 1 hour were performed, but hydrothermal temperatures were varied from 100 ^{o}C to 190 ^{o}C and the time periods were varied from 1 hour to 3 hours. The resulting d_{100} for calcined samples tended to slightly increase with temperature of hydrothermal treatment, but were almost the same (Figure 2.20(a)). Concomitantly, the mesopore size increase (Figure 2.20(e)) was observed in nitrogen adsorption analysis (Figure 2.20(b)), as the relative pressure of capillary condensation steps systematically shifted to higher relative pressures when the temperature increased to 170 ^{o}C. Moreover, the higher hydrothermal treatment temperature (above 150

^{o}C) and longer time (above 2 hours) effectively eliminated the tails on the desorption branch of the isotherm appearing at lower hydrothermal treatment temperatures or shorter treatment times, which indicate that some constrictions existed inside cylindrical mesopores.[48,50] BJH nominal pore diameters gradually increased with hydrothermal treatment temperature and time to 17.2 nm at 170 ^{o}C for 3 hours (Figure 2.20(c) and (d)). The preferred hydrothermal temperature is 150 ^{o}C or at most 170 ^{o}C (not higher temperature) because Pluronic P123 may start to decompose above 180 ^{o}C and lead to partial collapse of the framework.[201] TEM images clearly showed honeycomb and channel-like structures, which confirmed that our materials were 2-D hexagonal structures (Figure 2.20e and f).

The applied rapid calcination (400 ^{o}C for 2 hours, ramp 20 ^{o}C min^{-1}) was proven to be as efficient as the normal calcination procedure (550 ^{o}C for 5 hours, ramp ~5 ^{o}C min^{-1}).[48,50] The thermal gravimetric analysis (TGA) results indicated complete removal of the block copolymer template. The comparison of SAXS and nitrogen adsorption data further supports that OMSs free of surfactant have similar d_{100} and pore diameters, specific surface area and pore volumes as OMSs prepared at commonly used calcination conditions (Figure 2.21).

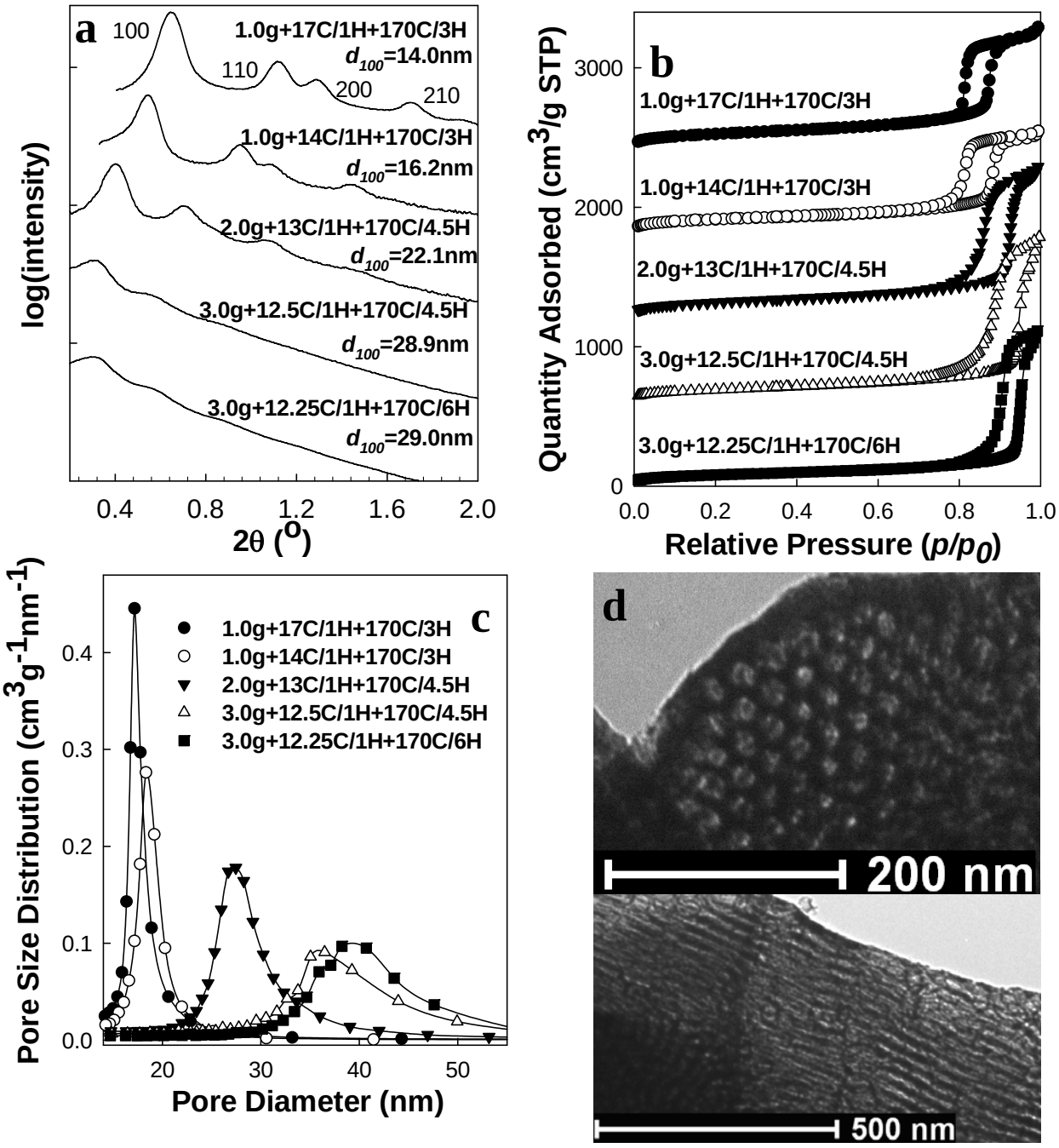

Figure 2.19. (a) SAXS patterns, (b) nitrogen adsorption isotherms and (c) pore diameter distributions of calcined samples with various amounts of TIPB and at different initial temperature and hydrothermal treatment conditions. (d) TEM images of calcined samples with 3.0g+12.5C/1H+170C/4.5H. The SAXS patterns were offset vertically to facilitate comparison; The isotherm for samples 3.0g+12.5C/1H+170C/4.5H, 2.0g+13C/1H+ 170C/4.5H, 1.0g+14C/1H+170C/3H and 1.0g+17C/1H+170C/3H were shifted vertically 600, 1200, 1800 and 2400 cm^3 STP g^{-1}, respectively.

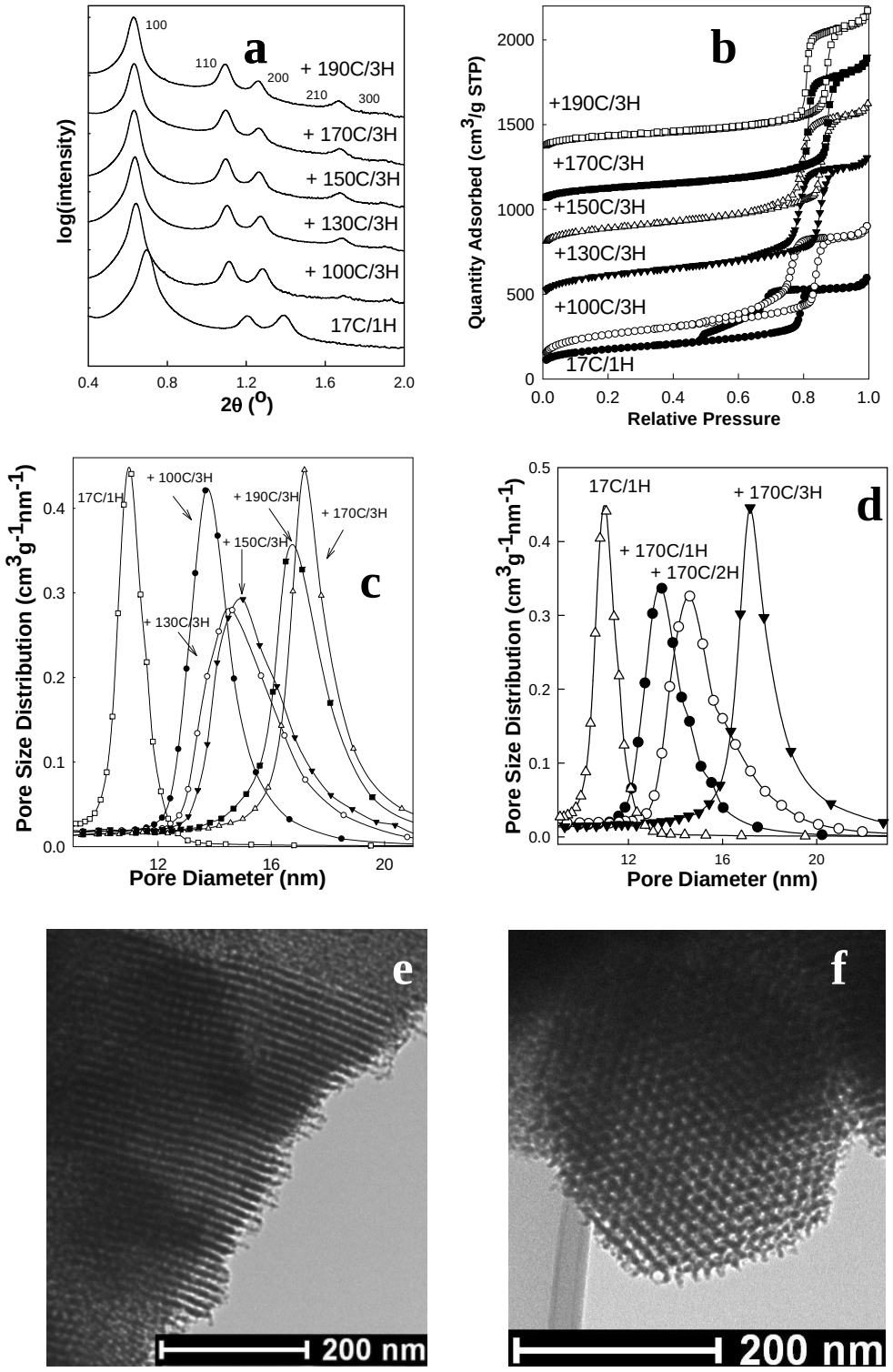

Figure 2.20 (a) SAXS patterns of calcined samples with hydrothermal temperature from 100 ^{o}C to 190 ^{o}C. The patterns were offset vertically to facilitate comparison; (b) and (c) nitrogen adsorption isotherm and pore diameter distribution of samples with hydrothermal temperature from 100 ^{o}C and 190 ^{o}C for 3 hours. The isotherm for samples +130C/3H, +150C/3H,

+170C/3H, +190C/3H were shifted vertically 400, 700, 1000, and 1300 cm^3 STP g^{-1}, respectively; (d) pore diameter distribution of samples aged at 170 ^oC from 0 to 3 hours; (e) and (f) TEM images of calcined samples hydrothermally treated at 170 ^oC for 3 hours.

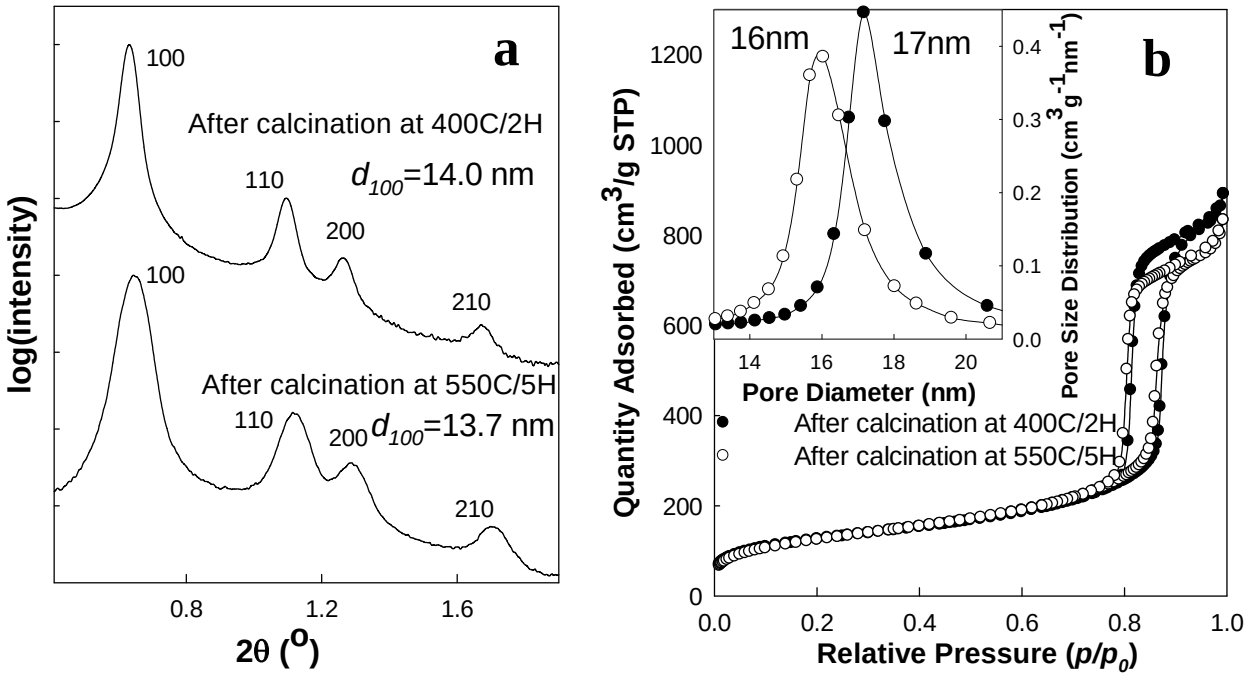

Figure 2.21. (a) SAXS patterns and (b) Nitrogen adsorption isotherm and insert pore diameter distributions of LP-SBA-15 after rapid and standard calcination. LP-SBA-15 samples were synthesized with the condition of 17C/1H+170C/3H, 2.4:1. SAXS patterns were offset vertically to facilitate comparison.

To verify the generality of the proposed rapid synthesis strategy, we extended it to the standard SBA-15 synthesis, which does not need TIPB and NH_4F and in which the initial step is above room temperature.[21] The control experiment was performed at initial temperature of 40 ^oC for 2 hour and hydrothermal treatment at 170 ^oC for 3 hours. The synthesized sample had similar pore diameter (~11 nm), surface area (850 m^2g^{-1}) and pore volume (1.26 cm^3g^{-1}) as normal SBA-15,[21] but the required synthesis time was reduced from 3 days to 6 hours (Figure 2.22).

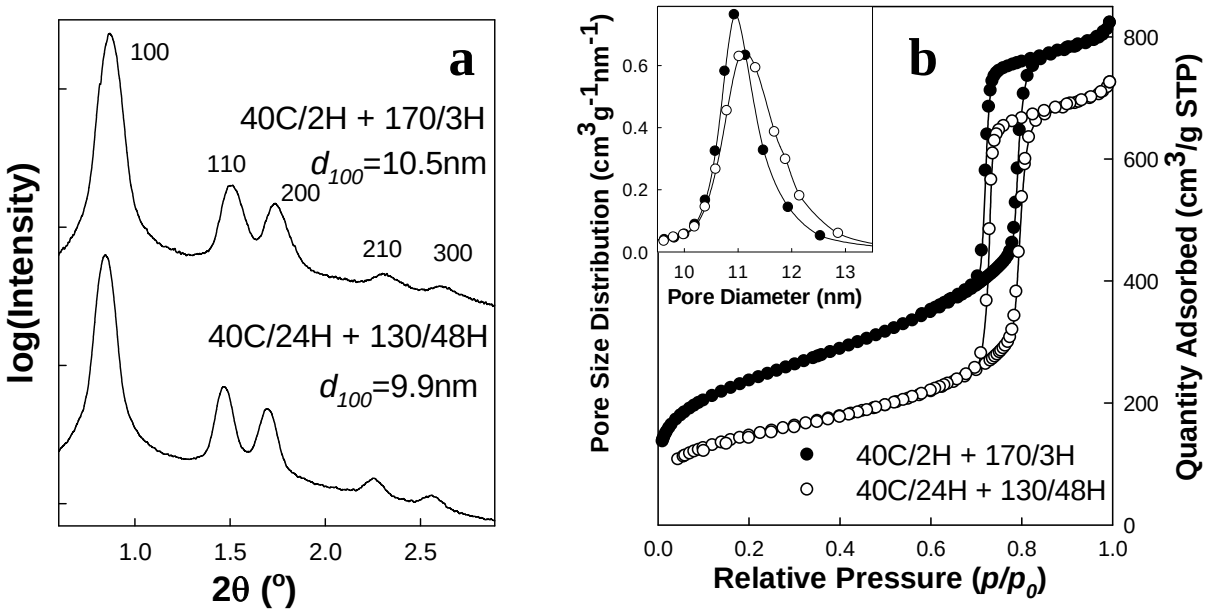

Figure 2.22. (a) SAXS patterns of calcined SBA-15 under rapid and standard synthesis conditions. The patterns were offset vertically to facilitate comparison; (b) Nitrogen isotherm and (inset) pore diameter distribution of SBA-15 under rapid and standard synthesis conditions.

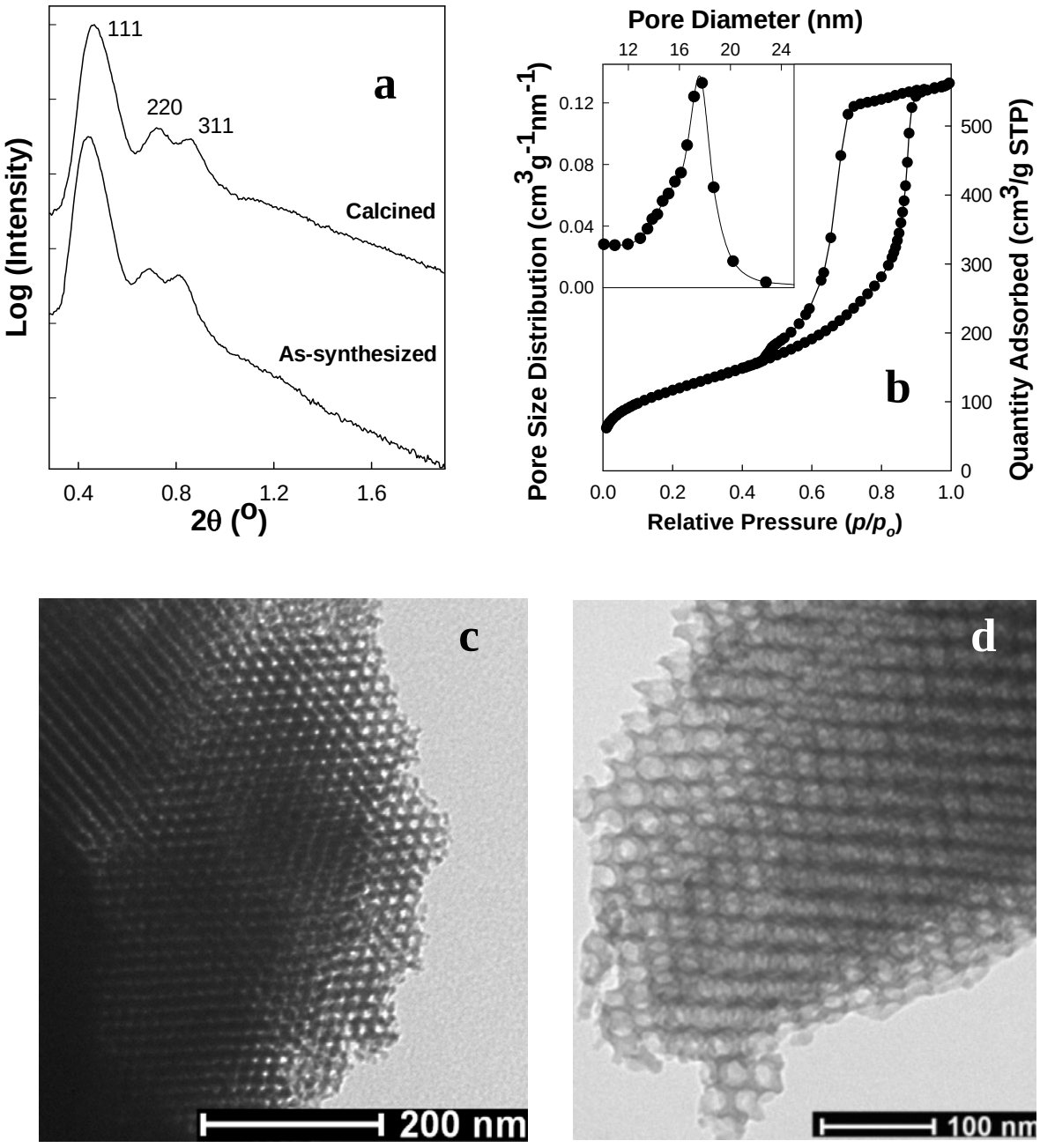

Figure 2.23 (a) SAXS patterns of as-synthesized and calcined LP-FDU-12, (b) Nitrogen adsorption isotherm with (inset) pore diameter distribution and (c) TEM images of calcined LP-FDU-12 from rapid synthesis; and (d) TEM images of calcined LP-FDU-12 prepared using xylene as a micelle expander.

Table 2.4 Synthesis conditions and structural parameters for selected samples[a]

synthesis conditions	$d_{100\ UC}$ (nm)	d_{100} (nm)	shrinkage	S_{BET} ($m^2\ g^{-1}$)	V_t ($cm^3\ g^{-1}$)	V_{mi} ($cm^3\ g^{-1}$)	V_p ($cm^3\ g^{-1}$)	w_{BJH} (nm)	w_d (nm)
0g+40C/1H+170C/3H	10.5	10.2	3%	850	1.26	0.05	1.04	11.0	10.2
1.0g+17C/1H+170C/0H	14.5	12.7	12%	622	0.88	0.08	0.66	10.9	11.4
1.0g+17C/1H+100C/3H	14.3	13.8	3%	903	1.31	0.16	0.99	13.7	13.1
1.0g+17C/1H+130C/3H	14.3	13.9	3%	764	1.37	0.10	1.08	14.9	13.7
1.0g+17C/1H+150C/3H	14.3	14.0	2%	674	1.34	0.07	1.03	14.9	13.8
1.0g+17C/1H+170C/3H	14.2	14.0	1%	456	1.34	0.02	0.95	17.2	13.9
1.0g+17C/1H+190C/3H	14.1	14.1	0%	449	1.22	0.06	0.82	16.7	13.4
1.0g+17C/1H+170C/1H	14.5	13.6	6%	978	1.26	0.21	0.90	13.3	12.5
1.0g+17C/1H+170C/2H	14.3	14.1	1%	725	1.37	0.07	1.09	14.5	14.1
1.0g+14C/1H+170C/3H	16.4	16.2	1%	405	1.12	0.04	0.77	18.4	15.3
2.0g+13C/1H+170C/4.5H	22.7	22.1	3%	425	1.63	0.02	(1.28)[c]	27.3	22.9
3.0g+12.5C/1H+170C/4.5H	28.9	28.9	0%	330	1.76	0	(1.38)[c]	36.1	30.5
3.0g+12.25C/1H+170C/6H	29.0	29.0	0%	290	1.65	0	(1.29)[c]	39.2	30.2
[b]14C/3H+170C/4.5H	[d]19.6	[d]19.0	3%	426	0.87	0	0.84	17.4	22.3

[a] Sample Notation: Xg+Y°C/Y'H+Z°C/Z'H, which means samples were synthesized with X grams of micelle expander per 2.4 g P123 at initial temperature Y for Y' hours and at the hydrothermal temperature Z for Z' hours. $d_{100\ UC}$ or d_{100}, (100) interplanar spacing for uncalcined sample or calcined sample; shrinkage was calculated as 1- d_{100}/ $d_{100\ UC}$ for SBA-15 or 1- d_{111}/ d_{111UC} for LP-FDU-12; S_{BET}, BET specific surface area; V_t, total pore volume; V_{mi}, micropore volume; V_p, primary mesopore volume; w_{BJH}, BJH pore diameter; w_d, pore diameter calculated using geometrical equation 1or 2. [b] Synthesis conditions for LP-FDU-12.[c] Could not be calculated with acceptable accuracy using α_s plot method. Values in parentheses are estimates based on V_t values for the particular sample. [d] d_{111} for sample LP-FDU-12

Large pore FDU-12 (LP-FDU-12) with face-centered cubic structure was also successfully synthesized within hours. Its synthesis involved block copolymer $EO_{106}PO_{70}EO_{106}$ (Pluronic F127, BASF) as a template, TEOS as a silica precursor and TMB as a micelle expander. Both as-synthesized and calcined samples exhibited three peaks in SAXS patterns indexed as (111), (220) and (311) (Figure 2.23a), reflecting cubic *Fm3m* structure with d_{111} of ~19.0 nm. Nitrogen adsorption (Figure 2.23b) showed that calcined LP-FDU-12 had a pore volume of 0.87 cm^3g^{-1}, specific surface area of 426 m^2g^{-1}, accessible spherical mesopores of diameter ~18 nm (BJH method) and entrance size ~8 nm (based on capillary evaporation pressure). All of these parameters are comparable to LP-FDU-12 from standard synthesis that lasts 2-5 days.[188,189] Besides using TMB as the micelle expander, xylene was also proven to be suitable in achieving LP-FDU-12 with cubic structure and mesopores up to 22 nm.[202] TEM images (Figure 2.23c and d) confirmed well-organized spherical mesopores for the resulting material.

2.5.4. Conclusions

We have demonstrated a facile and rapid method to obtain SBA-15 with large or ultra-large ordered mesopores (10-30 nm) as well as large pore FDU-12 in hours instead of days. The whole synthesis time was dramatically shortened because of the quick block copolymers dissolution, fast hydrolysis of TEOS and formation of silicate/surfactant composites, and short high-temperature hydrothermal treatment. The rapid calcination step supplements the rapid synthesis. Our method is compatible with tailoring the pore diameter by adjusting the initial synthesis temperature with additional adjustment of the amount of micelle expander, and hydrothermal temperature and time.

2.6. A Facile Method to Synthesize Platelet SBA-15 with Highly Ordered Large Mesopores

In most of SBA-15 samples, cylindrical mesopores with diameters below 10 nm are organized as rod-like/fiber-like bundles of the length of several tens of micrometers.[21,22] However, it was realized that such long parallel nano-tunnels limit efficient diffusion and loading of molecules, especially those with high molecular weight architectures, such as synthetic polymers, [21,22] enzymes,[203-205] catalysts,[206] etc.

The tuning of mesopore length of SBA-15 is usually related to controlling the particle morphology. [203-216] Successful examples include smaller particle size of the rod-like SBA-15 particles with less than 200 nm in width,[204,207,210,211] or parallel mesoporous tunnels with the direction of the short axis of the particles, that is, platelet with thickness on the order of 200 nm.[203,206,210-214] In these cases, unusual conditions, such as no stirring[207-209,212,215] or/and diluted surfactant solutions[209] were used, or special chemicals, such as inorganic salts[207,212,213], or organic additives[203,211] were added, although the formation mechanism is not fully understood so far.

Herein, we propose a facile method to synthesize platelet SBA-15 particles with thickness of half of micrometer which also reflects the length of cylindrical pores with BJH nominal pore size up to 22 nm, which is unusually large. The highly reproducible synthesis was performed with a micelle expander TIPB under the static condition without other special equipment or reagents.

2.6.1. Materials and synthesis

A typical synthesis of platelet SBA-15 (P-SBA-15) was as follows: 2.4 g of P123 was dissolved in 84.0 ml of 1.30 M aqueous HCl solution at 17 ^{o}C under mechanical stirrer for 3 hours, then a mixture of 5.5 ml TEOS and 1.0 g of TIPB was added and stirring was continued for 10 minutes at the same temperature in an open polypropylene container. Afterwards, the stirring was discontinued and solution was kept without stirring for 1 day. Later, the solution was hydrothermally treated in a closed Teflon-lined autoclave at 130 ^{o}C for 2 days and then the product was isolated by filtering and calcined under air at 550 °C for 5 hours (heating ramp 5 °C min^{-1}). The normal SBA-15 (N-SBA-15) is prepared under the same conditions as the P-SBA-15, except that the mechanical stirring was applied continuously before the solution was subjected to the hydrothermal treatment.

2.6.2. Characterization and calculations.

See the **section 2.3.1.2** and **section 2.2.1.3.**

2.6.3 Results and discussions

The successful fabrication of platelet P-SBA-15 is first evident from the SEM images (Figure 2.24a), in which platelet-like particles have relatively uniform flat surface, diameters in the range of 3-5 micrometers and thickness less than half of micrometer. Such structures are further confirmed by TEM images. The uniform mesopores were nearly perfectly arranged as the hexagonal structures within a large domain of the size around 3 micrometers (Figure 2.25 (a)), and these mesopores were perpendicular to the flat surface of platelet particles and extended

throughout the whole particles (Figure 2.25 (b)). The length of pores was around 500 nm, close to the particle thickness seen from SEM.

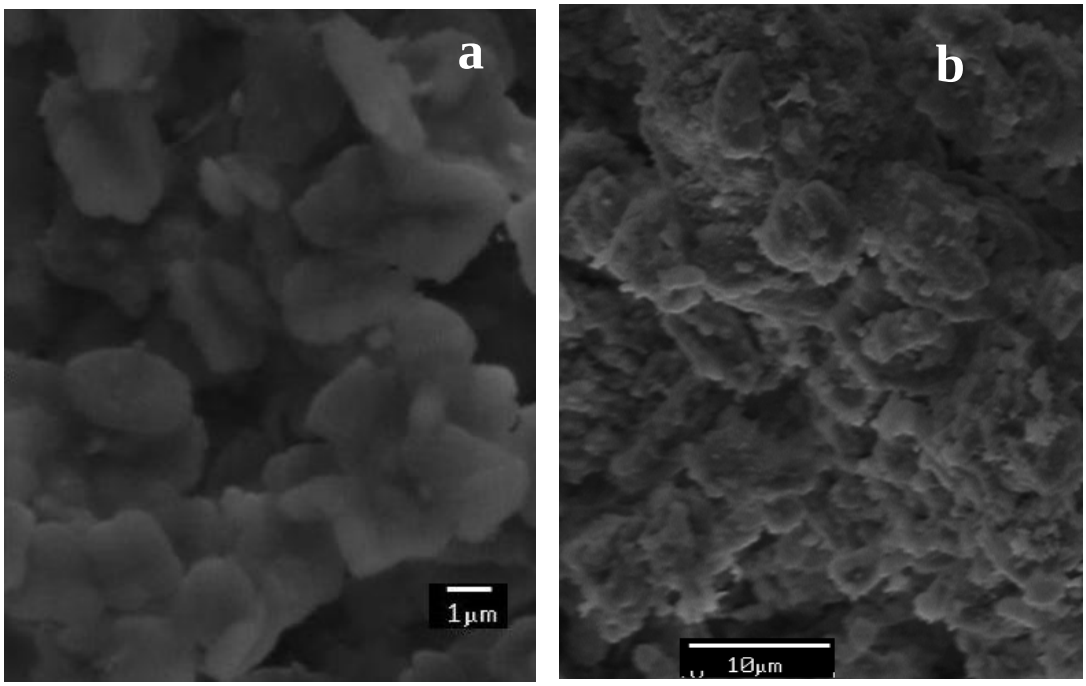

Figure 2.24. SEM of P-SBA-15 (a) and N-SBA-15 (b).

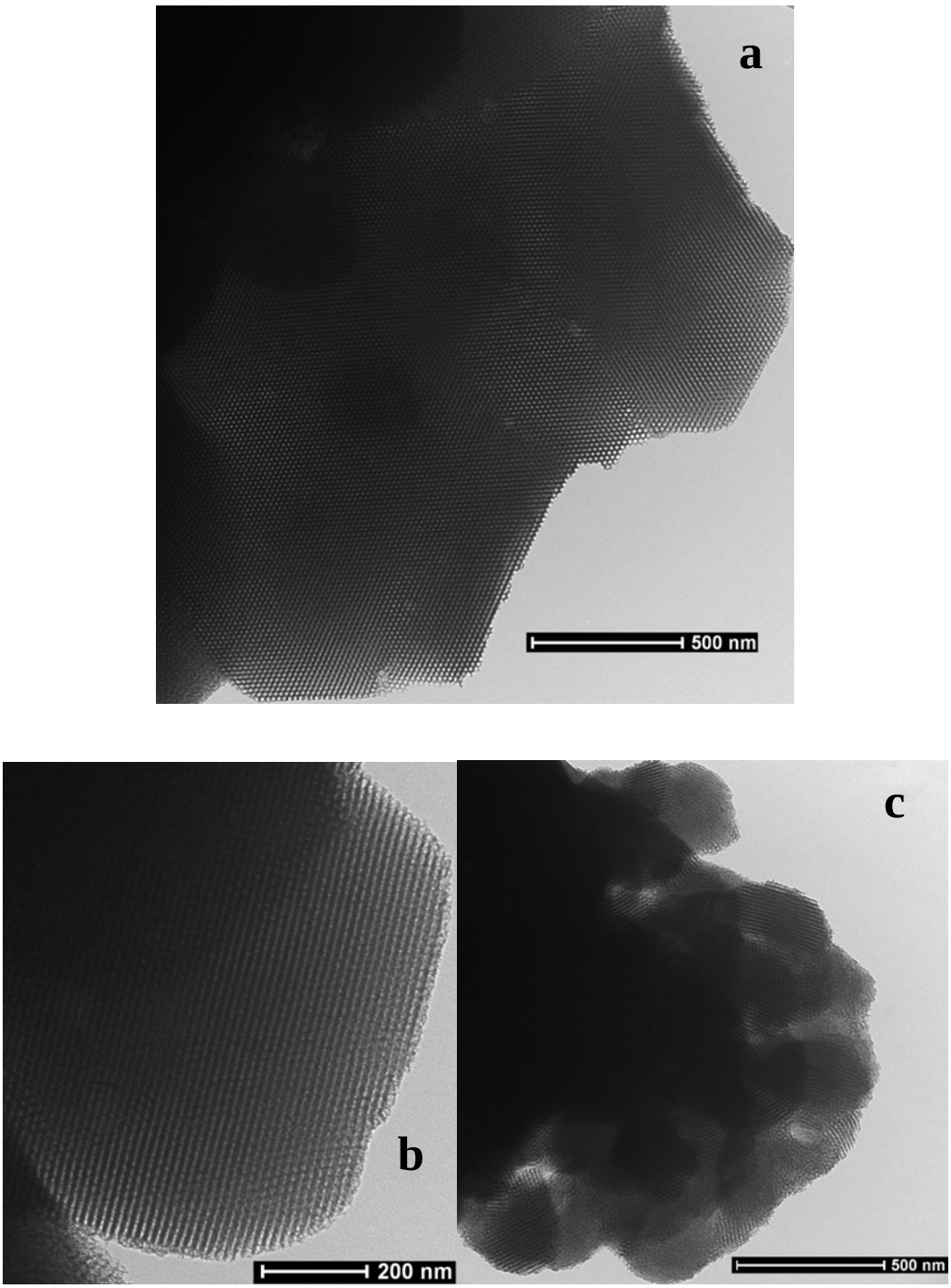

Figure 2.25. TEM of P-SBA-15 (a) (b) and N-SBA-15 (c).

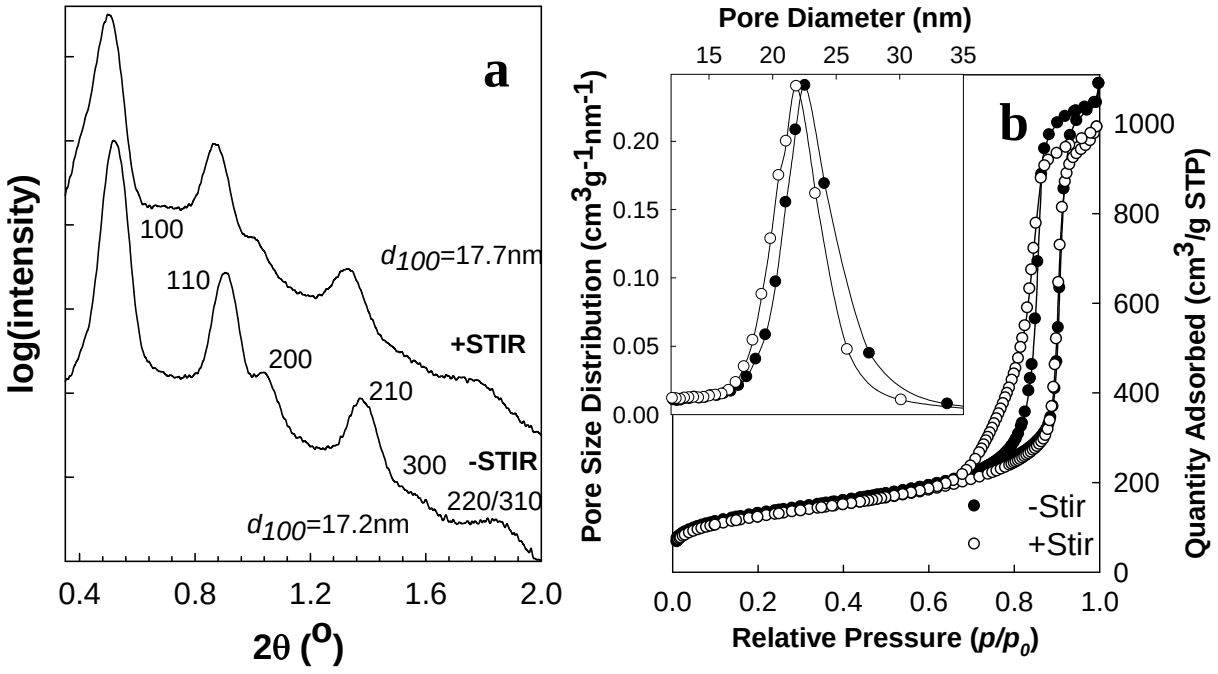

Figure 2.26. (a) SAXS patterns, (b) nitrogen adsorption isotherms with inset pore size distributions of P-SBA-15 and N-SBA-15.

The 2-D hexagonal structure of P-SBA-15 is also proven on the basis of the SAXS pattern (Figure 2.26a) in which six peaks (or shoulders) can be indexed as (100), (110), (200), (210), (300), (220) and/or (310). The corresponding (100) interplanar spacing (d_{100}) was 17.2 nm and unit cell parameter was 19.9 nm. The nitrogen adsorption isotherm (Figure 2.26b) for the sample showed type IV adsorption-desorption isotherm with well-defined capillary condensation step at ~0.90 p/p_o. The BET specific surface area and total pore volume were 470 m^2 g^{-1} and 1.6 cm^3 g^{-1}, respectively. The pore size distribution was relatively narrow and had a maximum around 22 nm, although a more accurate pore diameter was calculated as 18 nm using the geometrical equation (eq 1) because the BJH method overestimates pore diameters of large cylindrical mesopores.

To verify the stirring effect, we performed a control experiment to keep the stirring at 17 ^{o}C for 1 day before the solution was transferred to the hydrothermal treatment. The SEM image (Figure 2.24 (b)) showed that the resulting N-SBA-15 exhibited less uniform particles and varied shapes. TEM image (Figure 2.25 (c)) revealed that ordered domains were significantly smaller (half a micrometer) and some mesopores were curved. On the other hand, the SAXS experiment (Figure 2.26 (a)) showed that N-SBA-15 had a similar scattering pattern and similar d_{100} (17.7 nm) as P-SBA-15. Moreover, nitrogen adsorption (Figure 2.26b) showed the N-SBA-15 had BET specific surface area of 450 m^2 g^{-1}, pore volume of 1.5 cm^3 g^{-1}, and BJH pore diameter of 21 nm, which are similar to those of P-SBA-15. These comparable structural properties and different particle morphologies for the two samples indicate that the stirring significantly affected the particle morphology, but has negligible influence on the mesopores. The large ordered mesostructured domains and the platelet morphology might be due to slow rate of precipitation under static conditions.

2.6.4. Conclusions

We have demonstrated a facile method to synthesize platelet SBA-15 particles with highly ordered mesopores, large specific surface area and pore volume, large pore diameter and short pore length (half of micrometer). The unique properties make the material more promising for loading or transferring large molecules when we compare the new material to convictional SBA-15 which has pore size below 10 nm and large pore length (micrometers).

Chapter 3.

Synthesis of Mesoporous Polymer/Silica Composites via Surface-Initiated Atom Transfer Radical Polymerization

3.1. Introduction

Surface-initiated controlled polymerization methods[64,217,218] have been demonstrated as powerful strategies to achieve polymeric composites with substrates of various geometries, including planar surfaces (such as wafers),[71,72,219-229] convex surfaces (such as spherical nanoparticles[73,230-235] or nanotubes[236-238]), and concave surfaces (such as inner pores of nanoporous materials).[65,66,74-78,80,85,239-250] Among various controlled radical polymerizations, atom transfer radical polymerization (ATRP)[40] is perhaps the most robust and convenient method providing polymers with expected molecular weight and low polydispersity. The applications of ATRP for surface grafting of nanoporous materials include macroporous hosts (pore size above 50 nm), such as silica gels,[239,243] silicon scaffold,[240] or membranes,[242] etched polymer films,[241,244] etc., as well as mesoporous silicas.[75-78,80,85,246-249] The mesoporous supports included two-dimensional hexagonal arrays of cylindrical pores, such as SBA-15,[41,77,80,85,248,249] MCM-41[75,250] and MSU,[78,248] face-centered cubic arrays of spherical pores of FDU-1 silica,[77] and disordered spherical pores of a mesocellular foam.[76] Polymerized monomers include styrene,[78,80,85,248] methyl methacrylate,[78,85,248,249] 2-(dimethylamino)ethyl methacrylate,[80] sodium styrene sulfonate,[246,247] n-isopropylacrylamide,[75,76] and acrylonitrile.[77,80]

Although ATRP based surface grafting strategy has been already successfully applied to functionalize ordered mesoporous materials, there are still some major challenges. For example, most of the aforementioned ATRP reactions were initiated using bromoester based initiators,[76-78,80,85,245,246,248,249] which are very successful, but usually require multiple-steps syntheses. For instance, bromo-ester initiating sites can be introduced by reacting the bromoester-bearing acid halide with appropriate functional groups (amino or hydroxy) on the modified silica

surface.[76,239-242,244,246,249] Alternately they can be first integrated into an organosilane, e. g. through hydrosilylation, and then attached onto the silica surface through the reaction of organosilane with surface silanols.[77,78,80,85,248] It would be simpler if ATRP initiators could be selected among commercially available organosilanes, which can be directly immobilized onto the silicas surface and be ready to start polymerization. Moreover, typical ATRP reactions need high concentration of catalyst (transition metal based), which is costly, toxic and constitutes a contamination of the final product. Typical ATRP reactions also require strict and time-consuming degassing procedures to remove oxygen from the reaction system.

In this chapter, the research is focused on identifying alternative chemical reagents or pathways to address the aforementioned problems in order to simplify and improve ATRP-based surface-initiated grafting strategies. The proposed new methods meet the same standards as the reported successful syntheses of well-defined mesoporous polymer/silica composites (MPSC).[67,80] Such standards include: (i) controlled polymer film thickness on the mesopore surface, (ii) narrow molecular weight distribution of polymer brushes, (iii) accessibility of pores, and (iv) the preservation of the silica hosts' original structure. The proposed methods include:

1. The use of a readily available and cost-efficient 2-(4-chlorosulfonylphenyl) ethyltrichlorosilane (CTCS) as a potential replacement of bromoester-based initiators to graft polymers from the mesopore surface by using normal ATRP.

2. The application of ATRP with activators regenerated by electron transfer (ARGET) as a convenient and environmentally friendly pathway to well-defined MPSCs. The method is capable of polymerizing a large number of monomers under mild conditions with hundred

ppm level of catalyst and tolerance to limited amount of oxygen, thus being successfully preformed in capped vials instead of air-tight glassware and vacuum line.

3.2. Normal ATRP Using 2-(4-Chlorosulfonylphenyl)ethyltrichlorosilane as A Versatile ATRP Initiator

2-(4-chlorosulfonylphenyl)ethyltrichlorosilane (CTCS) with a chlorosulfonylphenyl (CSP) group [251-256] is a readily available and cost-effective organosilane and has already been widely used in ATRP to initiate monomers, including styrenes,[219,233,234,253,255] methacrylates,[221-227,230,231,253,255,257,258] acrylates[253,255] and *n*-isopropylacrylamide[232] from solutions,[251,253,255] silicon wafers,[220,222-227] magnetic nanoparticles,[230-234] quartz plates,[221] porous glasses,[257,258] etc. However, the application of CSP as an ATRP initiator in grafting from concave surfaces of mesoporous silicas is more challenging than the grafting from flat surfaces or spherical particle surfaces because the limited space inside the pores may decrease the local concentration and/or restricted diffusions of catalyst or deactivator. Moreover, sulfonyl-halide-based initiators have the nature of yielding about four orders of magnitude faster initiation than propagation, and they have tendency to dimerize to form disulfones.[40] As a consequence of these factors, polymerizations may lose control or even be self-terminated at an early stage if active species (radicals) cannot be promptly converted to dormant species.[259] Therefore, polymerization conditions, including temperature, time, solvents and amount of deactivators, must be carefully selected.

Herein we proposed the surface modification of ordered mesoporous silicas (SBA-15) with CTCS in a single step to introduce CSP groups onto the surface. The CSP-anchored SBA-15

was found to be a universal support to form well-defined MPSC including those formed by grafting poly(methyl methacrylate), polystyrene, poly(N-isopropylacrylamide) and poly(sodium *p*-styrenesulfonate).

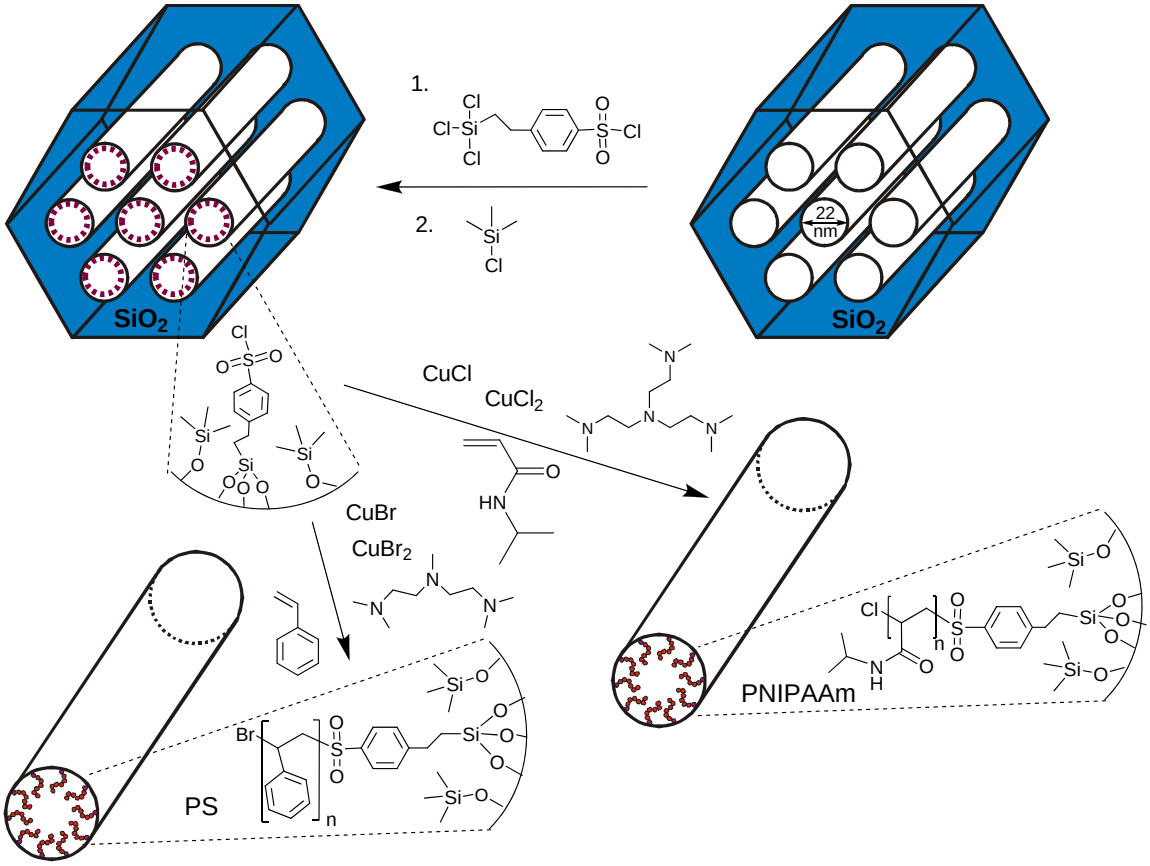

Scheme 3.1. Grafting poly (n-isopropylacrylamide) and polystyrene from concave surface of cylindrical mesopores of SBA-15 via atom transfer radical polymerization (ATRP) using the 2-(4-chlorosulfonylphenyl)ethylsilanyl group as an initiator.

3.2.1. Experimental section

3.2.1.1. Materials

Methyl methacrylate (MMA, 99%) and styrene (99%) were purchased from Aldrich and purified by passing through a column filled with basic alumina. N-isopropylacrylamide (NIPAAm) (Aldrich) was purified by recrystallization from a mixture of cyclohexane and acetone (50:50, volume%) and dried at 25°C under vacuum. The ligand tris[2-(dimethylamino)ethyl]amine (Me_6TREN) was purchased from ATRP Solutions, Inc. and used as received. All other chemicals, including 1,1,2,4,4-pentamethyldiethylenetriamine (PMDETA), sodium *p*-styrenesulfonate (SSNa), tetraethyl orthosilicate (TEOS), 1,3,5-triisopropylbenzene (TIPB), NH_4F, copper salts, pyridine, 2-(4-chlorosulfonylphenyl)ethyltrichlorosilane (CTCS) (50% in tolune), chlorotrimethylsilane and solvents were used as received. $EO_{20}PO_{70}EO_{20}$ block copolymer Pluronic P123 was provided by BASF.

3.2.1.2. Synthesis of ordered mesoporous large-pore SBA-15 silicas

The large-pore SBA-15 silica was synthesized as reported elsewhere.[50] 2.4 g P123 and 0.027 g NH_4F were dissolved in 84.0 mL of 1.30 M aqueous HCl solution at 12.75 °C. After at least one hour of stirring, a mixture of 5.5 mL TEOS and 2.4 mL (2.0 g) TIPB was added. The solution was stirred for 24 hours at 12.75 °C in an open container using a mechanical stirrer and then was transferred in a closed container heated at 130 °C for one day. As-synthesized material was isolated by filtering, washing with water and drying at ~60 °C in a vacuum oven. Finally, the sample (SBA-15) was calcined under air at 550 °C for 5 hours (heating ramp 2 °C min^{-1}).

3.2.1.3. Immobilization of CTCS on the LP-SBA-15 surface

1.0 g SBA-15 and 40 mL dry toluene was stirred for 30 minutes with purging nitrogen before 5 mL CTCS was added. The solution was stirred at room temperature for one day under nitrogen and then the solid sample was isolated by filtering, washing with toluene and acetone, and drying at ~40 °C in a vacuum oven overnight. The obtained sample was added to 40 mL of dry toluene and stirred for 30 minutes under nitrogen. Then 1.0 mL pyridine and 5 mL chlorotrimethylsilane was added and stirred at room temperature for one day under nitrogen. The product was isolated by filtering, washing with toluene and acetone, and drying at ~40 °C in a vacuum oven overnight, affording chlorosulfonylphenyl-modified SBA-15 (SBA-15-CSP). The modification with trimethylsilyl groups has the purpose of decreasing the possibility of adsorption of copper complexes on the silica surface.[80,85]

3.2.1.4. Procedure for surface initiated polymerizations

A typical polymerization of styrene was as follows: SBA-15-CSP, styrene, a pre-mixed solution of $CuBr_2$ and PMDETA ligand in N,N-dimethylformamide (DMF), and solvent anisole were added into a Schlenk flask. After the mixture was degassed by three freeze-pump-thaw cycles, CuBr was added under the nitrogen atmosphere. The final molar ratio of reactants was as follows: initiator: Cu(I): Cu(II): PMDETA: styrene=1 : 1 : 0.1 : 2.2: 100. The polymerization mixture was placed in an oil bath at 80 °C for the period of 13 to 49 hours under nitrogen. The reactions were terminated by opening the Schlenk flask and exposing the catalyst to air. The silica/polymer composites were isolated by filtration, washed with toluene, acetone and methanol, and dried in a vacuum oven.

The polymerizations of MMA were performed in anisole at 40 °C for 3 to 12 hours; polymerizations of NIPAAm were performed in isopropyl alcohol at 40 °C for the period of time from 1 to 3 days. CuCl, $CuCl_2$ and Me_6TREN were applied instead of CuBr, $CuBr_2$ and PMEDTA for better polymerization control in the case of polymerization of NIPAAm. The final molar ratio of reactants was as follows: initiator: Cu(I): Cu(II): Me_6TREN: NIPAAm=1 : 1 : 0.1 : 2.2: 100.; and polymerizations of SSNa were in methanol/water mixture (3:2 volume ratio) at room temperature for 30 minutes.

3.2.1.5. Characterization

Nitrogen adsorption measurements at -196 °C were carried out using a Micromeritics ASAP 2020 volumetric adsorption analyzer. Samples were degassed under vacuum at 200 °C (for silicas) or 80 °C (for modified silicas) before adsorption measurements. The specific surface area was determined using the BET method.[1] The total pore volume was calculated from the amount adsorbed at a relative pressure of 0.99.[1] The pore size distribution was calculated using the BJH method for cylindrical mesopores.[161] Thermogravimetric analysis (TGA) was performed under nitrogen with 5 °C/min ramping rate to 800 °C on Hi-Res 2950 thermogravimetric analyzer from TA Instruments. Molecular weight distributions were determined by gel permeation chromatography (GPC) on Alliance GPCV 2000 with refractive index detector and polystyrene standards. The cleavage of polymer from silica support was performed using 48% HF water solution mixed with THF in the volume ratio of one to ten. Small-angle X-ray scattering (SAXS) measurements were performed using a Bruker Nanostar small-angle/wide-angle X-ray scattering (SAXS/WAXS) instrument with a rotating anode X-ray source and Vantec-2000 two-

dimensional detector. FTIR spectra were collected by Bruker Vertex 70 FTIR spectrophotometer, operating at 4 cm^{-1} resolution and 32 scans.

3.2.2. Results and discussions

3.2.2.1. Immobilization of the ATRP initiator on the silicas surface

The selected ordered mesoporous silica SBA-15 had very large cylindrical mesopores (22 nm, as calculated using eq 1 in Chapter 2) and thus allowed us to more easily accommodate polymers than previously used silica templates with smaller pore size.[75,77,78,80,247-249] The commercially available CTCS was a toluene solution, which was directly used without any purification. The immobilization of CTCS was done in a single step in which trichlorosilane groups on one side of CTCS underwent condensation reactions with silanol groups on the silica surface to form Si-O-Si bonds while the CSP group (an ATRP initiator) on the other side was left intact. The reaction can be shortened to 3 hours,[231] but longer time (24 hours) was used here in order to achieve high coverage of initiating sites. The successful immobilization of CSP onto the silica surface was confirmed by FTIR spectrum (Figure. 3.1(a)), in which a new peak that appeared at 1380 cm^{-1} can be assigned to the symmetric stretch of the S=O bond in CSP and another peak at 1485 cm^{-1} is due to the benzene ring of CSP.[230,234] The asymmetric stretching of the S=O bond at 1136 cm^{-1} from CSP[230,234] is not observed because of the overlap with stronger peak of Si-O bonds from silica template at ~1100 cm^{-1} (data not shown). The amount of immobilized CSP determined by TGA was ~12 wt.%, corresponding to about 0.5 mmoles of initiator per gram and 0.88 groups per nm^2 based on the specific surface area of SBA-15 (333 m^2 g^{-1}) and molecular weight of the CSP group (236 g $mole^{-1}$). Such an initiator coverage is moderate and comparable with that previous reported for bromoester based initiators.[77,78,80,85,248]

The SAXS pattern of SBA-15-CSP (Figure 3.1(b)) is nearly identical to the pattern of unmodified SBA-15, indicating that the immobilization step did not change the structure of the silica support.

The successful introduction of CSP onto the surface of SBA-15 is also proven by nitrogen adsorption analysis as seen from the lowering of the capillary condensation pressure, which is indicative of the pore diameter decrease (Figure 3.2(b), 3.3(b) and 3.4(b)). However, no appreciable broadening of the adsorption-desorption hysteresis loop was observed, suggesting that the CSP groups formed a smooth monolayer on the surface of the cylindrical pores of SBA-15. The decrease of pore diameter was measured as ~3.6 nm, but actual decrease could be around ~2.5 nm because the BJH method used overestimates the diameter of large cylindrical pores.[33] Such a decrease is reasonable as the molecular modeling of 2-(4-chlorosulfonylphenyl)-ethyltrimethoxysilane, which is similar to ethyltrichlorosilane used in our case, indicates a length of ~1 nm.[227]

Table 3.1. Characteristics of mesoporous silicas template (SBA-15), the initiator-functionalized silicas (SBA-15-CSP), and silica/polymer composites.[a]

Sample	Reaction time (h)	M_n (g/mol)	PDI	S_{BET} (m^2 g^{-1})	V_t (cm^3 g^{-1})	w_{BJH} (nm)	Surface density (groups per nm^2)	Initiation efficiency (%)
SBA-15[b]				333.3	1.32	30.2		
SBA-15-CSP				206.9	0.92	26.6	0.88	
SBA-15-PSt 13%	13	4400	1.04	157.1	0.71	25.1	0.068	8.1%
SBA-15-PSt 23%	25	6800	1.03	113.8	0.48	23.0	0.088	10.5%
SBA-15-PSt 31%	49	9100	1.03	107.6	0.33	21.8	0.103	12.3%
SBA-15-PMMA 11%	3	4600	1.03	115.0	0.62	25.1	0.056	6.7%
SBA-15-PMMA 24%	6	7400	1.05	101.2	0.43	22.1	0.089	10.7%
SBA-15-PMMA 33%	9	9200	1.15	82.5	0.29	20.9	0.108	12.9%
SBA-15-PMMA 40%	12	10100	1.17	27.8	0.10	20.4	0.136	16.2%
SBA-15-PNIPAAm 12%	24	[c]	[c]	132.5	0.63	24.8	[d]	[d]
SBA-15-PNIPAAm 21%	48	2700	1.21	111.9	0.45	23.2	0.192	23.0%
SBA-15-PNIPAAm 34%	72	5500	1.12	19.0	0.09	23.3	0.186	22.3%
SBA-15-PSSNa 26%	0.5	[c]	[c]	14.0	0.06	21.1	[d]	[d]

[a] Notation: M_n, number average molecular weight estimated by GPC calibrated using polystyrene standards; PDI, polydispersity index evaluated by GPC; S_{BET}, BET specific surface area; V_t, total pore volume; w_{BJH}, BJH pore diameter; surface density estimated from M_n, content of polymer and S_{BET} of SBA-15 template; initiation efficiency estimated from M_n, content of polymer and amount of surface-bonded initiator; [b] More realistic pore diameter (~22 nm) was evaluated using equation 1 from Chapter 2; [c] cannot be measured by GPC or more than one peak in GPC curve; [d] cannot be calculated without molecular weight.

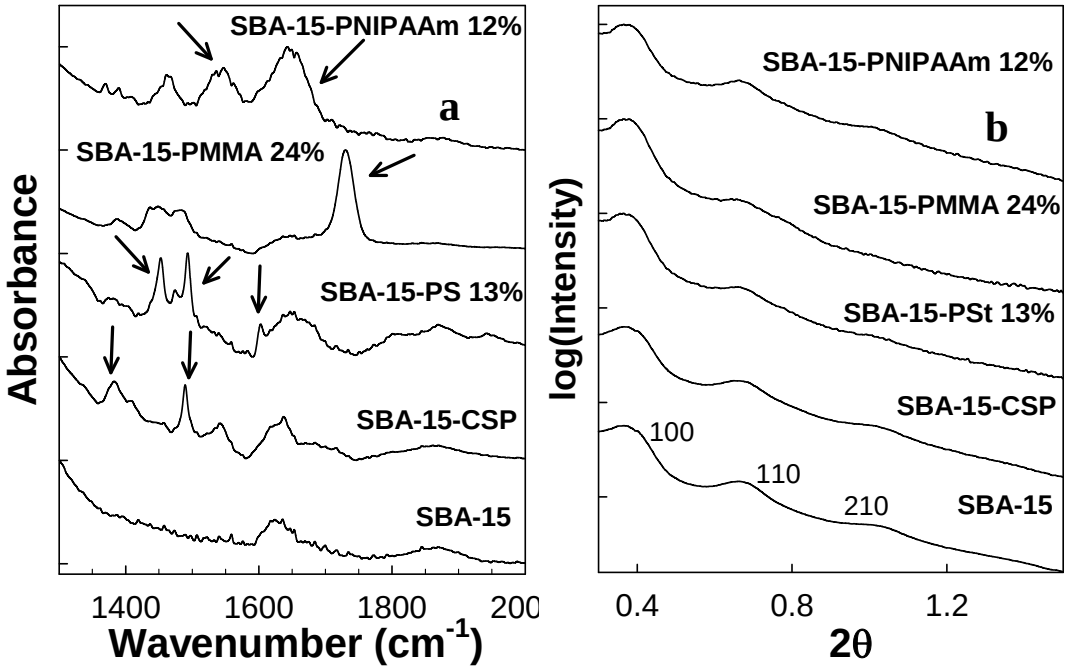

Figure 3.1. (a) FTIR and (b) SAXS of SBA-15 template, SBA-15-CSP and representative silica/polymers composites such as SBA-15-PSt 13%, SBA-15-PMMA 24% and SBA-15-PNIPAAm 12%. The loading of polymers in the composite is indicated in wt.%. The FTIR spectra were shown with selected wavenumber range because the intensity of peaks shown here are much weaker than the intensity of Si-O-Si peak at ~1100 cm^{-1} of the silica template. The FTIR spectra and SAXS patterns were offset vertically to facilitate comparison.

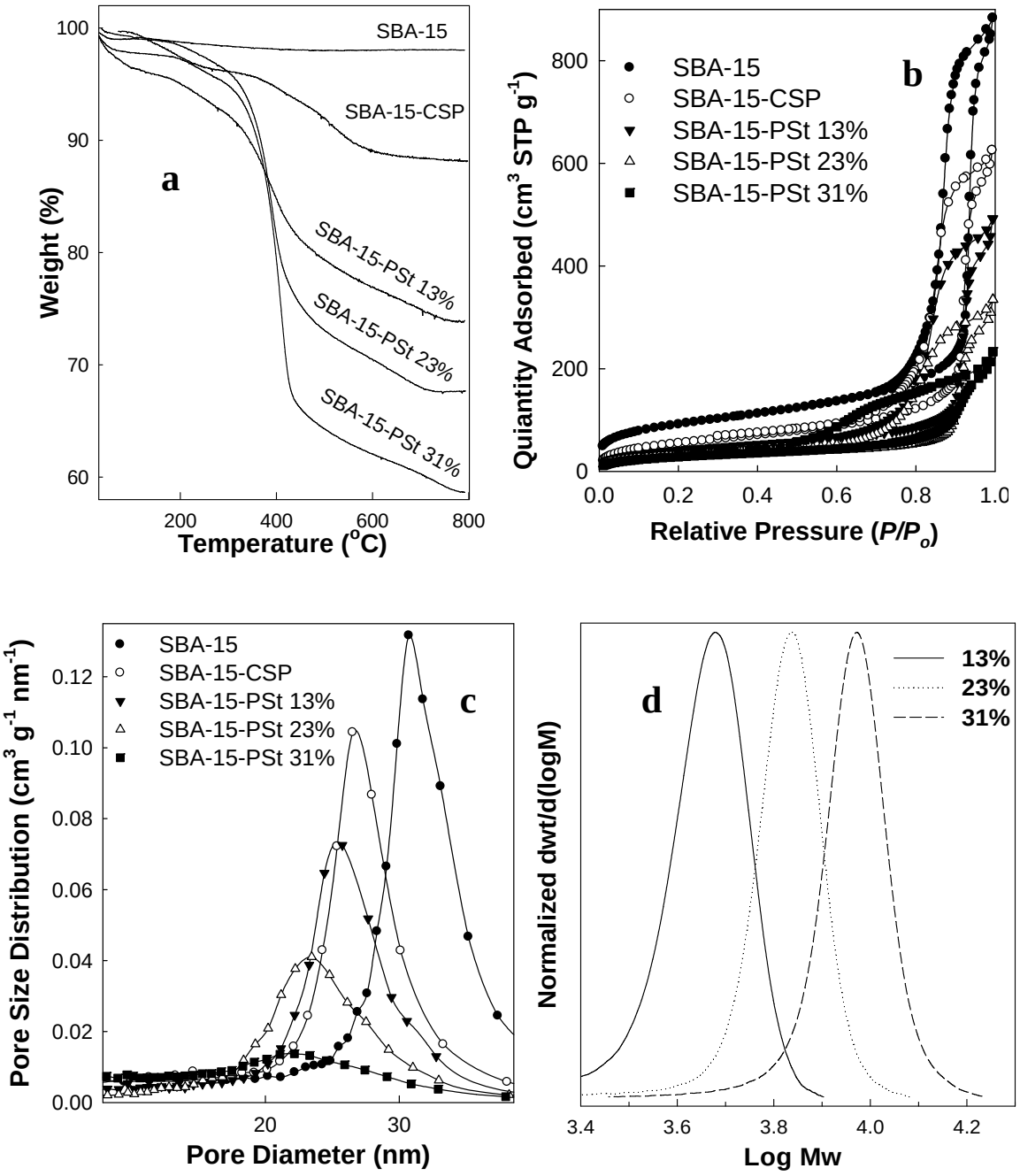

Figure 3.2. (a) Weight change patterns, (b) nitrogen adsorption isotherms and (c) pore size distributions for SBA-15 silica before and after attachment of initiation sites and polymerization of styrene; (d) GPC molecular weight distributions for PSt cleaved from the surface of SBA-15/PSt composites. (loading of PSt in the composites is indicated in wt.%).

3.2.2.2. Surface-initiated polymerization of styrene

Successful surface-initiated ATRP of styrene from flat surfaces, spherical particles and macroporous substrates using CSP as an initiator has been reported,[219,233,234] while such a polymerization in mesoporous structures has not been reported. In particular, PSt-modified mesoporous silicas prepared using ATRP technique are mostly derived from bromoester-based initiators,[78,80,85,248] which have been proven very efficient but often need multi-step syntheses. The commerically available CSP-based initiator was very successful to initiate polymerization of styrene from SBA-15 surface in anisole at 80 ^{o}C. Three parallel experiments were performed with different reaction time, ranging from 13 hours to 49 hours. To confirm successful grafting, all composites were characterized with FTIR spectroscopy. A spectrum with a selected wavenumber range for a representative sample was shown in Figure 3.1a, in which peaks at ~1450 cm^{-1}, ~1500 cm^{-1} and ~1600 cm^{-1} can be assigned to the benzene rings of PSt, suggesting that PSt coexisted with silica support. The intensity ratio of the peak at ~1500 cm^{-1} to the peak at ~1380 cm^{-1} (ratio of benzene rings to S=O bonds), was enhanced after grafting, indicating that the signal related to benzene rings were not only from CSP the initiator, but to a great extent from PSt polymer. Moreover, SAXS patterns in Figure 3.1b verified that the achieved SBA-15/PSt composite preserved ordered mesoporous structure of the support, because all peaks were visible and their relative peak positions were unchanged.

The controlled polymer loading was verified by TGA (Figure 3.2(a)). It is clear that polymer contents increased from 13, to 23 and 31 wt.% with reaction time increase from 13, to 25 and 49 hours. Accordingly, the molecular weight of polymer cleaved by etching silica/PSt composites with HF increased gradually from 4800, to 6500 and 8600 mol/g. More importantly, PSt chains

show extremely low polydispersity index (PDI) of 1.03-1.04, which to the best of our knowledge is the lowest PDI ever reported in grafting from surfaces of ordered mesoporous materials. It has been reported that bromoester initiated PSt grafted on SBA-15 surface had low value of PDI (1.08) at the beginning of the polymerization, but the PDI significantly increased (to 2.92) as polymerization proceeded.[80] In our case, however, the extremely low PDI remained throughout the whole polymerization even when mesopores were nearly total filled (see discussion in next paragraph) Such very well controlled polymerizations could be attributed to the high efficiency of initiating by CSP and low synthesis temperature (80 ^{o}C) to slow down polymerization and decrease the chance of thermal self-initiation of styrene, while normal ATRP polymerizations of styrene are performed in the temperature from 100 to 130 ^{o}C.[40] It was suggested that sacrificial initiators[78,220-227,231,234,248,257,258] added into surface-initiated polymerization systems can help to better control polymer growth. In our case, a certain amount of deactivator, 10% of Cu(II) relative to Cu(I), were applied instead.[80] The advantage of such a strategy is that it can eliminate polymers which was initiated by free initiators and physically adsorbed on the pore surface, resulting in pore volume decrease and the lack of strong attachment of polymer to the support. Moreover, herein the polymerizations were controlled by changing reaction time rather than the ratio of monomer to initiator;[249] that is, in our case the growth of the polymer was gradual and polymer thickness and loading could be controlled using the same composition of the reaction medium by simply stopping the reaction after appropriate time.

The successfully controlled surface initiated-polymerizations of styrene from SBA-15 surface are also evident from nitrogen adsorption isotherms shown in Figure 3.2(b). As the polymerization proceeded, polymer products occupied more and more space inside the pores, leading to lower and lower specific surface area (157-107 m^2g^{-1}) and pore volume (0.71-0.33 cm^3

g^{-1}). The shape of the adsorption-desorption hysteresis loop did not change until the loading of PSt in mesopores reached 31 wt.%, indicating that the grafted polymer was uniformly distributed along the mesoporous channels and did not block the pores to any appreciable extent. Pore size distributions shown in Figure 3.2(c) demonstrated that the pore diameters were systematically reduced with the increasing content of the polymer. The retention of the narrow pore size distribution indicated that PSt brushes formed a uniform layer on the surface of the silica. The thickness of the polymer layer corresponds to the pore radius decrease and was estimated on the basis of pore radius changes as 0.7, 1.7, 2.4 nm for 13, 23 and 31 wt.% PSt loading. It must be mentioned that such estimates could overestimate the polymer film thickness as the applied pore size distribution calculation method overestimates diameters of cylindrical pores by 10-25% in the considered size range. Thus, the maximum thickness of polymer film could be about 2 nm. It is obvious that the thickness of polymer film increased with polymerization time in a controlled manner.

Combining the results from TGA, GPC, and gas adsorption data discussed above, the grafting density was calculated as 0.07, 0.09 and 0.10 chains per nm^2, and the initiation efficiency was 8%, 11% and 12% for 13 wt.%, 23 wt.% and 31 wt.% PSt loading, respectively. The low efficiency could be due to the limited space inside mesopores leading to the steric hindrance for monomers and catalyst complex. It is also possible that some of the CSP groups were not accessible to initiate polymerization because they were located in micropores of SBA-15. But the low initiating efficiency is comparable with the results we published early in the case of polymerization of styrene via ARGET ATRP from SBA-15 surface[85] and with other results published earlier.[78,80]

3.2.2.3. Surface-initiated polymerization of MMA

MMA is another monomer extensively studied in the area of surface initiated ATRP. The grafting of PMMA brushes has been reported from particles and planar surface in case of CSP initiator[221-227,230,231,258] and from concave surface of ordered mesoporous silicas in case of bromoester based initiators.[78,85,248,249] As shown herein, CSP-initiated MMA grafting from the surface of SBA-15 was also very successful, when polymerization procedures similar to that of PSt was used, but at 40 ^{o}C as a reaction temperature. In the FTIR spectrum (Figure 3.3(a)) of the selected silica/PMMA sample, a new peak at 1730 cm^{-1} is assigned to the C=O bond of PMMA and indicates the formation of silica/PMMA composite. As expected from the SAXS pattern in Figure 3.1b, the silica/PMMA composite retained the ordered structure of the SBA-15 host.

The polymerization rates of MMA are much higher than those of styrene, as TGA results (Figure 3.3a) show that 3-hour polymerization could afford 21 wt.% organic moieties, corresponding to 11 wt.% PMMA content in the composite. The polymer loading kept gradually increasing to 40 wt.% (50 wt.% of organic moieties) as polymerization time was extended to 12 hours. In GPC traces, molecular weight increased from 4600, 7400, 9200 and 10100 g $mole^{-1}$ with polymerization times of 3, 6, 9 and 12 hours, indicating the living polymerization. PDI was very low at the initial stage (1.03-1.05), but it became higher (1.16), which is still quite low in comparison to the results published before.[78,85,248] The higher tendency to increase in polydispersity in the case of MMA in comparison to styrene could be due to the faster polymerization rate of MMA.[40]

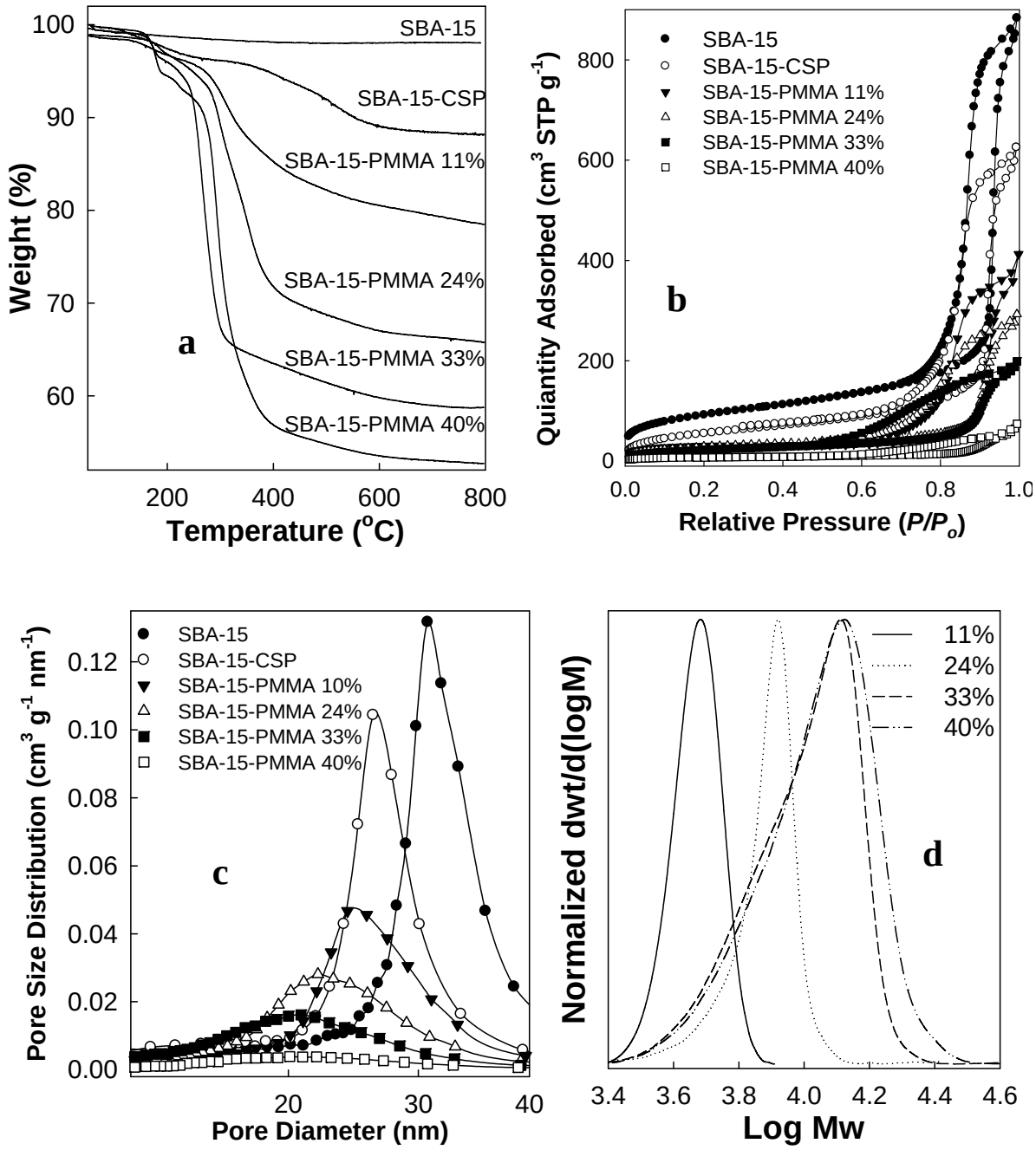

Figure 3.3. (a) Weight change patterns, (b) Nitrogen adsorption isotherms and (c) pore size distributions for SBA-15 silica before and after attachment of initiation sites and polymerization of MMA; (d) GPC molecular weight distributions for PMMA cleaved from the surface of SBA-15/PMMA composite. (loading of PMMA in the composites is indicated in wt.%).

The silica/PMMA composites showed a very good control of textural properties as proven by gas adsorption analysis. The BET specific surface area gradually decreased from 115 m^2 g^{-1} to 28 m^2 g^{-1} and the total pore volume decreased from 0.62 to 0.10 cm^3 g^{-1}, as the polymer content increased from 11 to 40 wt.%. The adsorption-desorption hysteresis loop in Figure 3.3(b) was not particularly broad with the loading of PMMA content in mesopores up to 33 wt.%, indicating that mesopores were not blocked by the grafted polymers. The mesopores were still at least partially accessible with very high polymer loading of 40 wt.%. Pore size distributions in Figure 3.3(c) demonstrated that the pore diameters were systematically reduced with the increasing polymer contents. The thicknesses of polymer layers were estimated as 0.7, 2.2, 2.8 and 3.1 nm for 11, 24, 33 and 40 wt.% PMMA loading, while actual polymer film thickness was likely to reach at least 2 nm, as discussed in the polymerization of PSt section. The grafting densities is calculated to be 0.06, 0.09 and 0.11 and 0.14 chains per nm^2 and the initiation efficiency is 7 %, 11 %, 13 % and 16 %, respectively. A similar efficiency were previously achieved in our study of ARGET ATRP surface-initiated polymerization of MMA[85] or in studies of other research groups. [78]

3.2.2.4. Surface-initiated polymerization of NIPAAm

PNIPAAm is a stimuli-responsive polymer well-known for its temperature-responsive properties as it exhibits a lower critical solution temperature (LCST) of ~32^{o}C.[75,76,232,260] Grafting PNIPAAm from mesopores via surface-initiated ATRP was studied before and the resulting composites have been evaluated in the area of adsorption and transport of molecular species[75] and drug release.[76] However, the structure of these materials is not clear. In our cases, ATRP polymerization of NIPAAm from CSP was conducted in isopropyl alcohol at 40 ^{o}C for

one to three days. The combination of CuCl and Me_6TREN gave a better control of polymerization than that of CuBr and PMDETA, as the Me_6TREN complex is more active than the PMDETA complex. The successful polymerization of NIPAAm (12 wt.%) within silica pores was confirmed by the FTIR spectrum of Figure 3.1 in which two new peaks at ~1640 and ~1540 cm^{-1} can be assigned to Amide I (C=O) and Amide II (N-H) vibrations of the PNIPAAm unit. Similarly to other polymerizations described, the herein polymerizations here did not alter the ordered mesoporous silica framework (see SAXS patterns in Figure 3.1).

The TGA results (Figure 3.4(a)) showed that polymer loadings gradually increased from 12, to 21 and 34 wt.% as the polymerization time increased from 24 to 48 and 72 hours. However, further GPC analysis of PNIPAAm cleaved from the surface showed multiple low-molecular weight tails on molecular weight distribution for the sample with 12 wt.% polymer loading, indicating that the growth of PNIPAAm was not under good control at the initial stage of polymerization. As the polymerizations progressed, monodispersity of the polymer was observed. The PDI was reduced to 1.32 with M_n=2700 g mol^{-1} and to 1.21 with M_n=5500 g mol^{-1} (Figure 3.4(d)). The reason is not clear, but it might be due to the interactions of nitrogen atom of NIPAAm with the copper catalyst in the initial period before reaching the equilibrium between dormant species and propagating species.

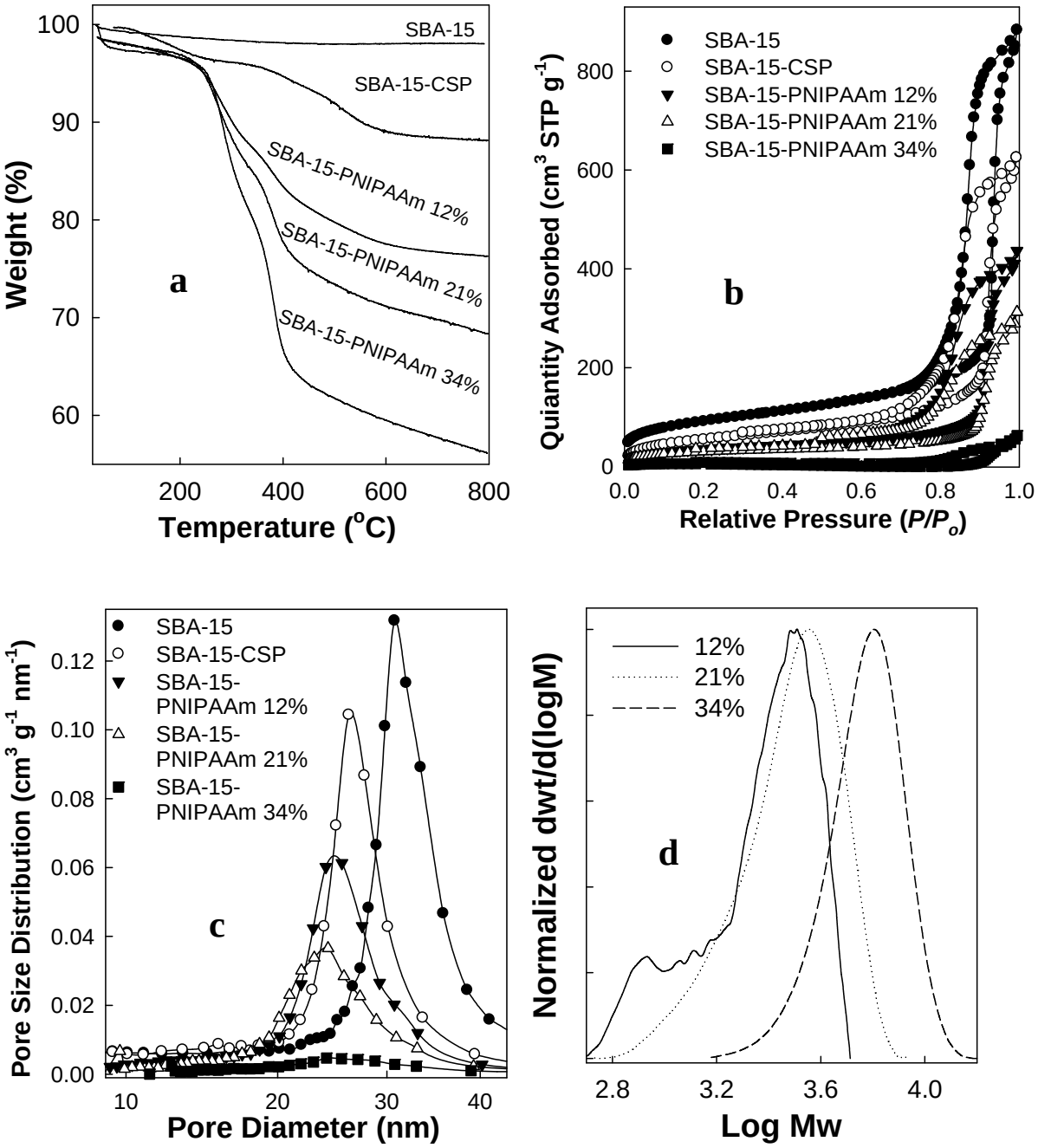

Figure 3.4. (a) Weight change patterns, (b) nitrogen adsorption isotherms and (c) pore size distributions for SBA-15 silica before and after attachment of initiation sites and polymerization of NIPAAm for SBA-15 silica; (d) GPC molecular weight distributions for PNIPam cleaved from the surface of SBA-15/PNIPAAm composites (loading of PNIPAAm in the composites is indicated in wt.%).

The silica/PNIPAAm composites also displayed tailorable textural properties as seen from nitrogen adsorption analysis which shows that BET specific surface areas were reduced from 130, to 120 and 19 m^2 g^{-1} with polymer loading 12, 21 and 34 wt.%, respectively. Accordingly, the pore volume decreased from 0.63, to 0.45 and 0.09 cm^3 g^{-1} and the BJH pore diameter was reduced to 23 nm (Figure 3.4(b) and (c)). The calculated PNIPAAm film thickness was ~1 nm.

3.2.2.5. Surface-initiated polymerization of other monomers

To verify the versatility of CSP as an ATRP initiator in the context of functionalization of nanoporous materials, the polymerization of another monomer sodium *p*-styrenesulfonate (SSNa) was attempted, which is a precursor of ion-exchange resins applied as solid acid catalysts.[247,261] Polymerizations of SSNa initiated from the surface of mesoporous materials were demonstrated by other research groups using chloromethylphenyl[247] or bromoester based initiators.[246] The ATRP polymerization of SSNa from CSP on the SBA-15 surface was very fast, as in thirty minutes the organic content reached ~40 wt.%. The mesopores were nearly totally filled or blocked with the polymer, because the measured BET specific surface area and the total pore volume were 14 m^2 g^{-1} and 0.06 cm^3 g^{-1}, respectively.

3.2.3. Conclusions

2-(4-chlorosulfonylphenyl)ethyltrichlorosilane-initiated atom transfer radical polymerizations from the concave surfaces of ordered mesoporous silicas, LP-SBA-15, allow one to achieve well defined MSPCs with various polymer components, such as poly(methyl methacrylate), polystyrene, poly(n-isopropylacrylamide) and poly(sodium p-styrenesulfonate). Pore structure

properties can be well tailored to achieve different surface areas (30-160 m^2 g^{-1}), pore volumes (0.10-0.71 cm^3 g^{-1}) and pore diameters. The grafted polymer brushes formed uniform polymer layers with controlled thickness from several tenths of a nanometer to more than 2 nm, as seen, for instance, from quite narrow adsorption/desorption hysteresis loops on adsorption isotherms for materials with the moderate polymer loadings. The cleaved polymer brushes exhibited a behavior characteristic for controlled growth of polymers as their molecular weight increased with polymerization time. The polydispersity remained extremely narrow (~1.05) in the case of polymerization of styrene throughout of the whole process, while in case of other polymerizations, the polydispersity became moderate at the end of polymerization. Due to its simplicity, the approach described herein for the syntheses of silica/polymer composites can be extended to other inorganic/polymer composites with wide variety of polymers.

3.3. Grafting of Polymer Brushes from Nanopore Surface via Atom Transfer Radical Polymerization with Activators Regenerated by Electron Transfer

Recently developed ATRP with activators regenerated by electron transfer (ARGET)[81-86] provides a major improvement over the normal ATRP (discussed in Chapter 3.2) in two important areas, because it can be performed using a closed vial instead of using air-tight glassware and a vacuum line, and it involves low concentrations of copper catalyst (~10-100 ppm vs. 1000-10000 ppm used in normal ATRP). In ARGET ATRP, a reducing agent (typically, tin(II) 2-ethylhexanoate, $Sn(EH)_2$, or vitamin C) is used to convert Cu(II) to Cu(I), the latter being component of ATRP catalyst complex (activator), and to remove the oxygen (radical trap) through a cycle involving oxidation and reduction of copper species. ARGET ATRP has been successfully used to grow polymer brushes on flat surfaces[83] and surfaces of nanoparticles.[84] However, its applicability to graft thin polymer films on surfaces of high-surface-area nanoporous materials has not been demonstrated. This is a very challenging case, because dimensions of the nanopores are comparable to the length of extended polymer chains even for low-molecular-weight polymers. Therefore, an uncontrolled growth of even a small fraction of chains to form high polymers may lead to the blocking of the nanopores. Moreover, a high-surface-area support may have a tendency to adsorb the ATRP catalyst,[262] which may make an effort to decrease the concentration of the catalyst inherently difficult. Herein, it is demonstrated that ARGET ATRP (see Scheme 3.2) is fully applicable to grafting from the surfaces of nanoporous hosts, allowing one to achieve a controlled polymer loading and film thickness. Polymer chains exhibit quite low polydispersity, unless the polymerization process is prolonged until the nanopores are nearly completely filled, which

resembles the performance of normal ATRP.[80] The present work demonstrates new opportunities in the synthesis of well-defined high-surface-area silica-polymer composites through simple and benign chemistry.[85]

3.3.1. Experimental section

3.3.1.1. Materials

SBA-15 silica with cylindrical pores of diameter ~14 nm, ~22 nm and ~23 nm (as estimated using a geometrical equation 1 from chapter 2) were synthesized as described elsewhere.[50] For SBA-15 with ~14 nm mesopores (d_{100} = 13.7 nm), 1.0 g TIPB per 2.4 g Pluronic P123 was used, the initial synthesis temperature was 17 °C and the hydrothermal treatment was performed for 2 days at 100 °C. For the SBA-15 with ~22 nm and ~23 nm mesopores, 2.0 g TIPB per 2.4 g Pluronic P123 was used, the initial synthesis temperature was 12.75 °C and the hydrothermal treatment was performed for 1 day at 130 °C. Methyl methacrylate (MMA, 99%), styrene (St, 99%) and 2-(dimethylamino)ethyl methacrylate (DMAEMA) were purchased from Aldrich and purified by passing through a column filled with basic alumina. N-isopropylacrylamide (NIPAAm) (Aldrich) was purified by recrystallization from a mixture of cyclohexane and acetone (50:50, volume%) and dried at 25 ^{o}C under vacuum. The ligand tris[(2-pyridyl)methyl]amine (TPMA) was purchased from ATRP Solutions, Inc. and used as received. The initiator, 3-(chlorodimethylsilyl)propyl 2-bromoisobutyrate, was synthesized and grafted on the surface of silica surface as described elsewhere.[77] All other chemicals including solvents, copper salt and reducing agent tin(II) 2-ethylhexanoate ($Sn(EH)_2$) were used as received.

3.3.1.2. Synthetic procedures

A typical ARGET ATRP of MMA from surface of mesoporous silica was as follows: initiator-modified silica (30 mg, with 0.012 mmol initiator), MMA monomer (0.13 mL, 1.2 mmol), a pre-mixed solution of $CuCl_2$ (0.033 mg, 0.00024 mmol) and TPMA ligand (0.69 mg, 0.0024 mmol) in anisole (0.17 mL) and anisole (3.10 ml) were added into a ~5 mL glass vial. Then the vial was sealed with a rubber septum and the solution was stirred for 20 minutes before a solution of $Sn(EH)_2$ (51 mg, 0.126 mmol) in anisole (0.3 mL) was injected. The molar ratio of reactants was as follows: Initiator: Cu(II) : TPMA : MMA = 1 : 0.02 : 0.2 : 100. The amount of reducing agent $Sn(EH)_2$ is related to free air space in the glass vial, which can be calculated as ~1.6 ml (~5 ml - 0.13 ml - 0.17 ml - 3.10 ml = ~1.6 ml). The mixtures for polymerization of MMA placed in an oil bath at 80 °C. The reaction was terminated by opening the vial and exposing the catalyst to air. The polymer/silica composites were isolated by filtration, washed with tetrahydrofuran (THF), acetone and methanol, and dried in a vacuum oven. In case of surface initiated polymerizations of St, similar conditions are applied but reaction temperature was 80 ^oC.[85]

A typical ARGET ATRP of NIPAAm from surface of mesoporous silica was as follows: initiator-modified silica (30 mg, with 0.016 mmol initiator), NIPAAm monomer (160 mg, 1.6 mmol), a pre-mixed solution of $CuCl_2$ (0.048 mg, 0.00032 mmol) and TPMA ligand (0.96 mg, 0.0032 mmol) in anisole (0.24 mL) and anisole (3.30 ml) were added into a ~5 mL glass vial. Then the vial was sealed with a rubber septum and the solution was stirred for 20 minutes before injecting a solution of $Sn(EH)_2$ (51 mg, 0.126 mmol) in anisole (0.3 mL). The molar ratio of reactants was as follows: Initiator: Cu(II) : TPMA : NIPAAm = 1 : 0.02 : 0.2 :

100. The amount of reducing agent $Sn(EH)_2$ is related to free air space in the glass vial, which can be calculated as ~1.46 ml (~5 ml - 0.24 ml - 3.30 ml = ~1.46 ml). The mixtures were placed in an oil bath at 40 °C. The reaction was terminated by opening the vial and exposing the catalyst to air. The polymer/silica composites were isolated by filtration, washed with tetrahydrofuran (THF), acetone and methanol, and dried in a vacuum oven.

In case of surface initiated polymerizations of DMAEMA, similar conditions are applied with ratio of reactants was Initiator: Cu(II) : TPMA : DMAEMA = 1 : 0.02 : 0.2 : 100. The solvent was anisole and reaction temperature was 40 °C.

3.3.1.3. Characterization[85]

Nitrogen adsorption measurements at -196 °C were carried out using a Micromeritics ASAP 2020 volumetric adsorption analyzer. Samples were degassed under vacuum at 200 °C (for silicas) or 80 °C (for modified silicas) before adsorption measurements. The specific surface area was determined using the BET method.[1] The total pore volume was calculated from the amount adsorbed at a relative pressure of 0.99.[1] The pore size distribution was calculated using the BJH method for cylindrical mesopores.[161] Thermogravimetric analysis (TGA) was performed under nitrogen with 5° C/min ramping rate to 800 °C on Hi-Res 2950 thermogravimetric analyzer from TA Instruments. Molecular weight distributions were determined by gel permeation chromatography (GPC) on Alliance GPCV 2000 model with refractive index detector and polystyrene standards. The cleavage of polymers from silica support was performed using 48% HF water solution mixed with THF in the volume ratio of one to ten.[80] Small-angle X-ray scattering (SAXS) measurements were performed using a Bruker Nanostar small-angle/wide-

angle X-ray scattering (SAXS/WAXS) instrument with a rotating anode X-ray source and Vantec-2000 two-dimensional detector.

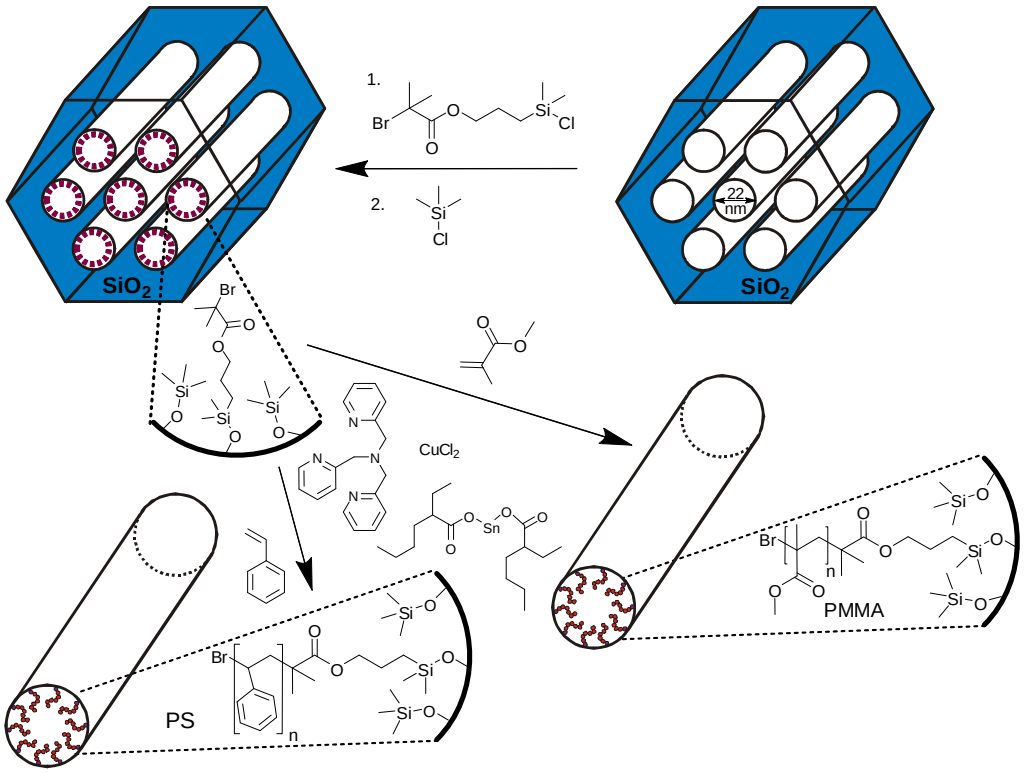

Scheme 3.2. Grafting poly(methyl methacrylate) and polystyrene in the cylindrical mesopores of SBA-15 silica using activators regenerated by electron transfer (ARGET) atom transfer radical polymerization (ATRP).[85]

Table 3.2 Structural properties of materials.[a]

SBA-15 support, grafted polymer and its weight %	S_{BET} (m^2 g^{-1})	V_t (cm^3 g^{-1})	w_{BJH} (nm)
SBA-15(22 nm)[b]	333	1.32	30.2
SBA-15(22 nm)-BiB	235	1.09	25.0
SBA-15(22 nm)-PMMA 13%	136	0.66	23.5
SBA-15(22 nm)-PMMA 29%	101	0.40	21.5
SBA-15(22 nm)-PMMA 36%	64	0.23	18.2
SBA-15(22 nm)-PS 14%	117	0.60	23.3
SBA-15(22 nm)-PS 19%	103	0.48	21.1
SBA-15(14 nm)[b]	582	1.31	14.3
SBA-15(14 nm)-BiB	309	0.82	12.4
SBA-15(14 nm)-PMMA 11%	192	0.49	11.1
SBA-15(14 nm)-PMMA 22%	82	0.17	8.4
SBA-15(14 nm)-PMMA 34%	~1	0.01	/[c]
SBA-15(23 nm)[b]	370	1.63	28.9
SBA-15(23 nm)-BiB	214	1.16	25.8
SBA-15(23 nm)-PNIPAAm 19%	145	0.66	23.6
SBA-15(23 nm)-PNIPAAm 26%	116	0.45	22.8
SBA-15(23 nm)-PNIPAAm 35%	46	0.11	/[c]
SBA-15(23 nm)-PDMAEMA 8%	138	0.52	23.8
SBA-15(23 nm)-PDMAEMA 16%	68	0.29	21.0
SBA-15(23 nm)-PDMAEMA 29%	21	0.11	19.3

[a] Notation: S_{BET}, BET specific surface area; V_t, total pore volume; w_{BJH}, BJH pore diameter. [b] Pore diameter evaluated using equation in Chapter 2; thus obtained pore diameter is expected to accurately reflect the pore diameter of the SBA-15 silica support; the considered equation is not applicable for surface-modified SBA-15, therefore the pore diameter for these materials was assessed using the BJH method, which is expected to reliably assess the shape and reasonably represent the width of the pore size distribution, but which is known to overestimate the pore diameter in the considered pore size range. [c] Could not be estimated because of lack of pore accessibility.

3.3.2. Results and discussion

3.3.2.1. Surface-initiated polymerization of MMA[85]

Ordered mesoporous silica support (SBA-15) with very large cylindrical pores[50] (22 nm, as calculated using eq 1) was selected to allow us to follow the grafting process up to the polymer layer thicknesses (in dry state) of several nanometers. The surface of silica was modified with 3-(2-bromoisobutyryloxy)propyldimethylsilyl groups (BiB, which serve as an ATRP initiator)) and trimethylsilyl groups (see Scheme 3.2).[77, 80] The surface coverage of the initiator was about 0.98 groups per nm^2, as estimated from TGA, which is consistent with the value reported earlier for regular SBA-15 (pore diameter ~10 nm).[77] Thus obtained initiator-functionalized SBA-15-BiB was placed in a glass vial to which monomer (methyl methacrylate, MMA), copper(II) chloride, tris[(2-pyridil)methyl]amine (TPMA) ligand, and anisole (solvent) were added. Subsequently, the vial was sealed with a septum and a reducing agent $Sn(EH)_2$ was added to convert Cu(II) to Cu(I). The molar ratio of reactants was: initiator: Cu(II) : TPMA : MMA = 1 : 0.02 : 0.2 : 100. It should be noted that the initiator : Cu ratio in normal ATRP is commonly about 1 : 1, so the present composition corresponds to 50-fold lowering of Cu concentration. The amount of reducing agent $Sn(EH)_2$ was determined relative to free air space in the vial. The mixture was placed in an oil bath at 40 °C. After a selected period of time, the reaction was terminated by opening the vial and exposing the catalyst to air to convert it to a deactivator form (that is, Cu(II) complex). The silica/PMMA composite was isolated by filtration, washed, and dried. The composites were white (Figure 3.5), being free from coloration due to residual Cu.

Figure 3.5. (left) SBA-15-PS synthesized via ARGET ATRP; (right) SBA-15-PS synthesized via normal ATRP. The preparation of both samples involved the same purification procedure including the washing with THF, acetone and methanol, and drying in a vacuum oven.[85]

The products after 6, 11, 24 and 48 hours of polymerization were analyzed by thermogravimetry (Figure 3.6(a)) and found to contain 13, 29, 36 and 48 wt.% of PMMA, respectively. Nitrogen adsorption isotherms (Figure 3.6(b)) showed that the mesopores were accessible for the polymer contents up to 36 wt.% (with BET specific surface area 60-140 m^2 g^{-1}, and total pore volume 0.23-0.66 cm^3 g^{-1}; see Table 3.2), while the sample with 48 wt.% of PMMA (content of organic moieties equal to 53 wt.%) had inaccessible mesopores. In the latter case, the inaccessibility of the pores is not surprising, because the composite contained the amount of organic moieties close to that needed to completely fill the mesopores of the silica support. Pore size distributions (PSDs) (Figure 3.6(c)) showed that the pore diameter systematically decreased as the loading of the polymer increased. The thickness of the polymer layer corresponds to the pore radius decrease and can be estimated on the basis of

pore radius changes as 0.7, 1.7 and 3.3 nm for 13, 29 and 36 wt% PMMA loading (see Figure 3.6(c)). While the method used herein to calculate the diameter of cylindrical pores is known to overestimate it by 10-25 % in the considered size range,[50] thus leading to an overestimation of the polymer film thickness, it is clear that the thickness of the polymer layer increased with time and reached at least 2 nm. The latter is comparable with the highest thicknesses achieved using normal ATRP without blocking of the nanopores in the considered diameter range.[77] Interestingly enough, the introduction of the loadings of the polymer up to 36 wt.%, the latter being higher than that achieved earlier using normal ATRP without pore blocking,[77] did not lead to any prominent broadening of hysteresis loops on the nitrogen adsorption isotherms (Figure 3.6(b)), indicating the polymer film did not form any major constrictions in the mesopores.[77] As expected, the polymerization did not induce any structural changes in the mesoporous host (see SAXS data in Figure 3.6(d)).

The grafted PMMA was detached from the surface of the silica support and analyzed by gel permeation chromatography (GPC) (Figure 3.7). The molecular weight was 4700, 7300, 8700 and 20800 g mol^{-1} for composites with 13, 29, 36 and 48 wt.% loading of PMMA, respectively. The PDI was 1.18, 1.28, 1.47 and 2.09, respectively. Clearly, the molecular weight of PMMA increased with the polymerization time thus providing strong evidence for the controlled growth of the polymer. PDI, which was initially quite low, became moderate or even quite high at high PMMA loadings. On the basis of GPC, TGA and gas adsorption data, the grafting density was calculated to be 0.06, 0.12, 0.14 and 0.09 chains per nm^2, whereas the initiation efficiency was 6, 12, 14 and 9 % for 4700, 7300, 8700 and 20800 g mol^{-1} PMMA, respectively. The apparent decrease in the grafting density and initiation efficiency for the highest-molecular-weight case may be related to the coupling of chains at

later stages of the grafting process where the pores are nearly completely filled with the polymer and the deactivator cannot readily diffuse to convert the propagating chains to the dormant species.[263] This contention is consistent with the more than two-fold increase in the molecular weight and the significant broadening of the molecular weight distribution at this stage. The grafting densities and initiation efficiencies were 2-3 times lower than those observed earlier for PAN grafted in nanopores via normal ATRP,[70] but one should keep in mind that the repeating unit of PMMA occupies the volume about two times larger than that occupied by PAN repeating unit.

Similar results were also obtained for PMMA grafting in 14 nm mesopores. The loadings of 11, 22 and 34 wt.% were achieved after polymerization times of 4.5, 7.5 and 17 hours. The mesopores were accessible for loadings up to 22 wt. %, and silica-PMMA composites with the BET specific surface areas 80-190 $m^2\ g^{-1}$, and total pore volumes 0.17-0.49 $cm^3\ g^{-1}$ were obtained. The molecular weight of PMMA was 2700, 4300 and 6000 g mol^{-1}, and PDI was 1.27, 1.32 and 1.50. The grafting density was calculated to be 0.06, 0.08, and 0.11 chains per nm^2, whereas the initiation efficiency was 6, 8, and 11 %, respectively. These data are similar to those for the larger-pore support discussed above.

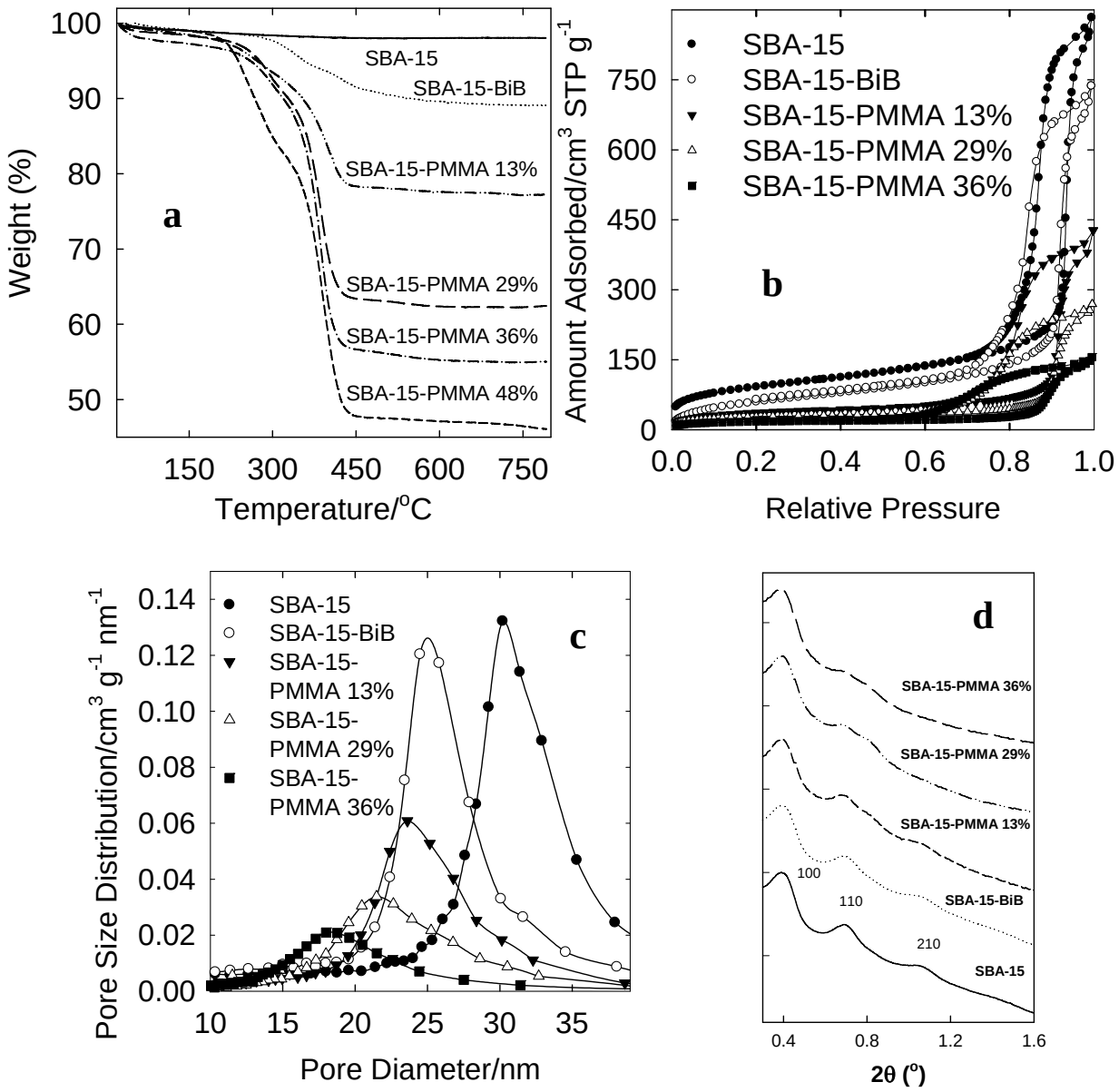

Figure 3.6. (a) Weight change patterns, (b) nitrogen adsorption isotherms, (c) pore size distributions and (d) small-angle X-ray scattering patterns for SBA-15 silica before and after attachment of initiation sites and polymerization of methyl methacrylate (loading of PMMA in the composites is indicated in wt.%).[85]

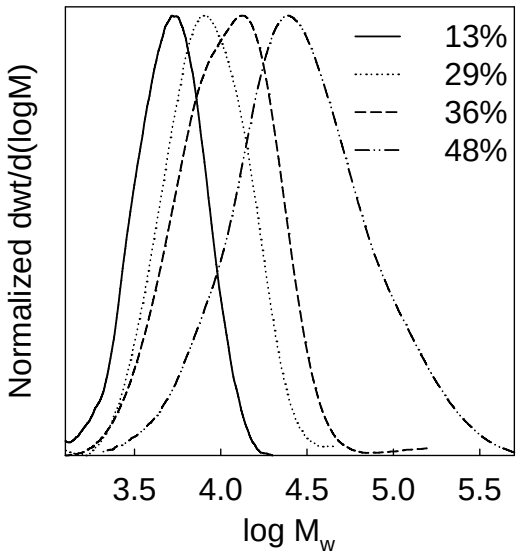

Figure 3.7. Gel permeation chromatography (GPC) molecular weight distributions for poly(methyl methacrylate) cleaved from the surface of SBA-15/PMMA composites (loading of PMMA in the composites is indicated in wt.%).[85]

3.3.2.2. Surface-initiated polymerization of styrene[85]

To verify the scope of this method in the context of functionalization of nanoporous materials, the polymerization of styrene was successfully performed. In this case, the polymerization temperature was 80 °C. After 24 and 30 hours of polymerization, PS loadings of 14 and 19 wt.% (Figure 3.8(a)) were achieved with retention of accessible porosity with BET surface area 100-120 $m^2\ g^{-1}$, and total pore volume 0.48-0.60 $cm^3\ g^{-1}$ (Figures 3.8(b), 3.8(c) and 3.8(d)). Molecular weights of 1150 and 2380 g mol^{-1} and PDIs of ~1.3 were observed for the PS graft. The grafting density was calculated to be ~0.24 chains per nm^2, whereas the initiation efficiency was ~25 %, which are similar to those achieved for PAN grafted in nanopores using normal ATRP.[77]

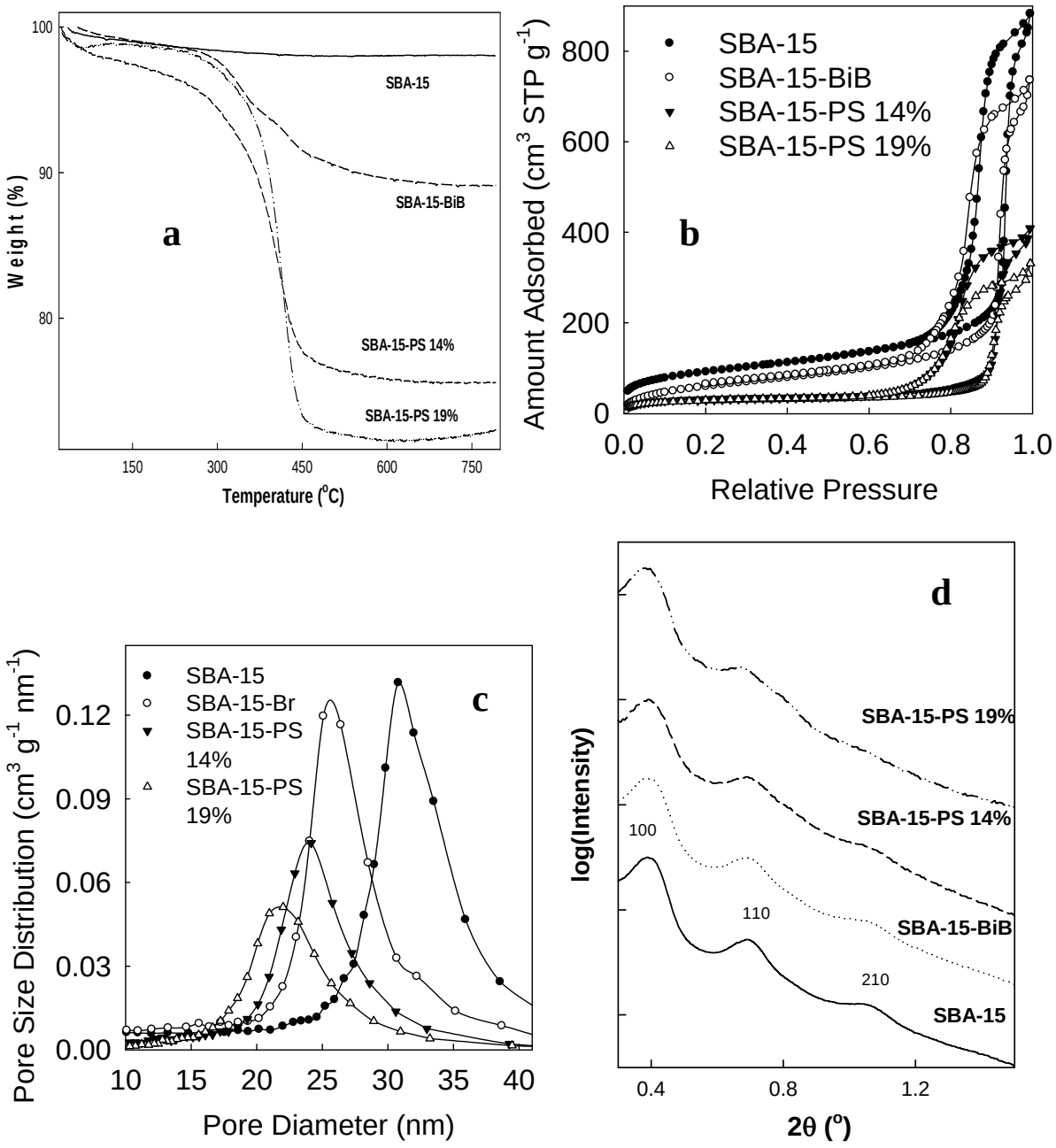

Figure 3.8. (a) Weight change patterns, (b) nitrogen adsorption isotherms, (c) pore size distributions and (d) small-angle X-ray scattering patterns for SBA-15 silica (22 nm pore diameter) before and after attachment of initiation sites and polymerization of styrene (loading of PS in the composite is indicated in wt.%).[85]

3.3.2.3. Surface-initiated polymerization of NIPAAm

ARGET ATRP polymerizations of NIPAAm were conducted in anisole at 40 ^{o}C for 12 to 48 hours. The TGA results (Figure 3.9(a)) show that the polymer loading gradually increased from 19 to 26 and 35 wt.% as the polymerization time proceeded from 12 to 24 and 48 hours. The silica/PNIPAAm composites displayed tailored textural properties, as seen from nitrogen adsorption analysis. The specific BET surface areas were systemically reduced from 145 to 116 and 46 $m^2 g^{-1}$ and the pore volume decreased from 0.66 to 0.45 and 0.11 $cm^3 g^{-1}$. (Figure 3.9(b)) On the basis of the decrease in BJH pore diameters from ~26 nm to ~23 nm, the calculated PNIPAAm thin film was ~1 nm (Figure 3.9(c)). GPC analysis of PNIPAAm cleaved from the surface indicated that the growth of PNIPAAm was under good control during the grafting, and the molecular weight continually increased from 1800 to 2300 and 3600 g mol^{-1}, while the PDIs were nearly constantly at ~1.25 (Figure 3.10).

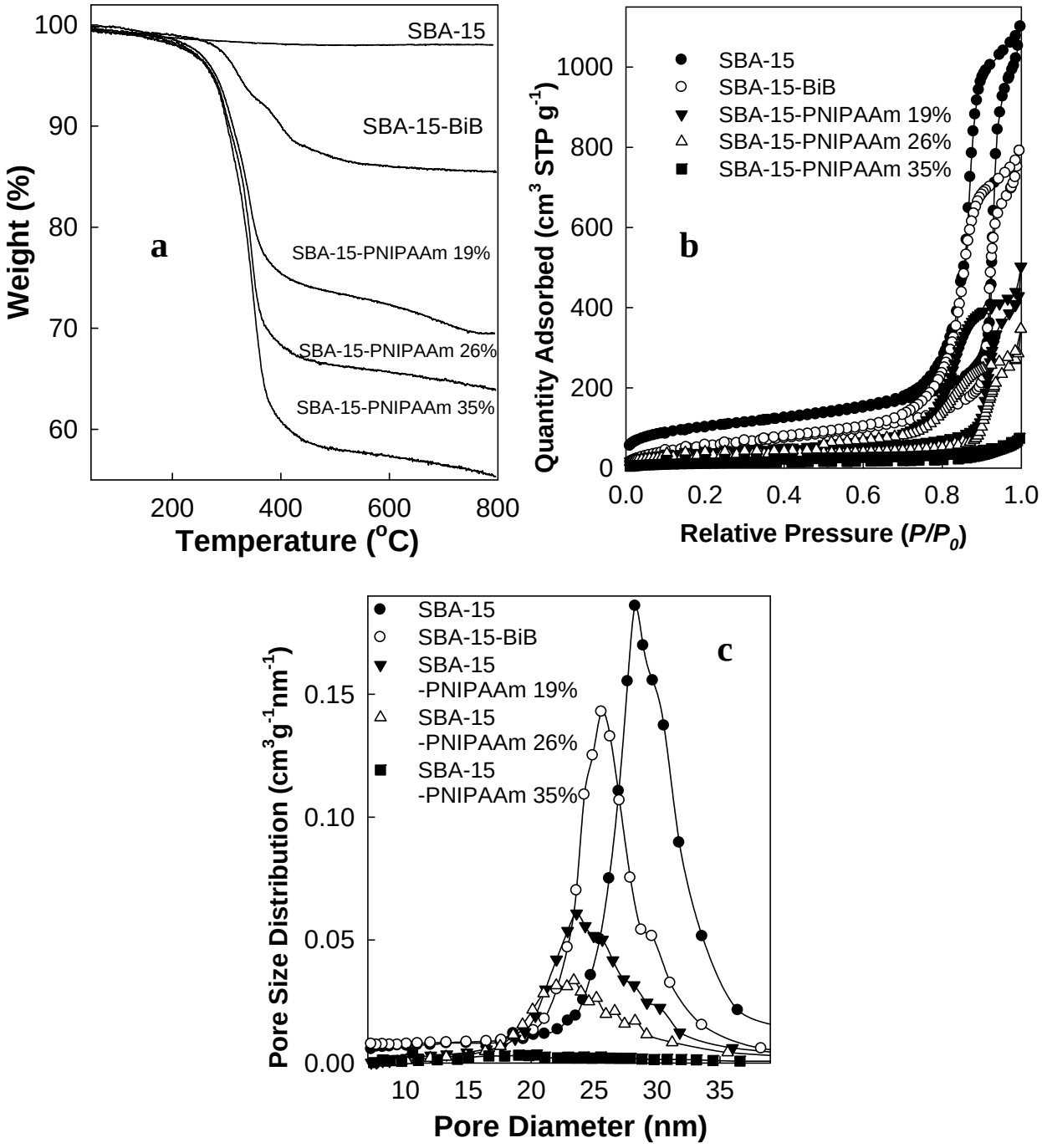

Figure 3.9. (a) Weight change patterns, (b) nitrogen adsorption isotherms and (c) pore size distributions for SBA-15 silica before and after attachment of initiation sites and polymerization of NIPAAm (loading of PNIPAAm in the composite is indicated in wt.%).

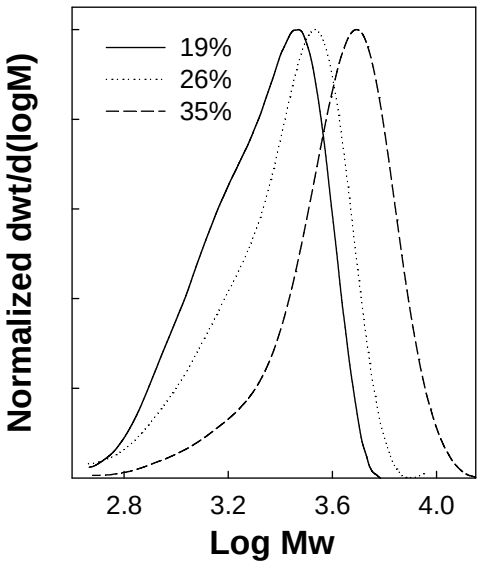

Figure 3.10. GPC molecular weight distributions for PNIPAAm cleaved from the surface of SBA-15/PNIPAAm composites (loading of PNIPAAm in the composites is indicated in wt.%).

3.3.2.4. Surface-initiated polymerization of DMAEMA

Poly[2-(dimethylamino)ethyl methacrylate)] (PDMAEMA), a pH-responsive and temperature-responsive polymer with lower critical solution temperature of 44 °C, was also successfully grafted from surfaces of SBA-15 silica. Polymerizations were performed at 40 ^{o}C for 24 to 72 hours using anisole as a solvent. As shown in Figure 3.11(a), TGA provided evidence of the systematic increases in the loading of PDMAEMA from 8 wt.% (1 day), to 16 wt.% (2 days) and 29 wt.% (3 days). It should be noted that the analysis of PDMAEMA by GPC was unsuccessful, presumably due to the protonation of the amino groups during the HF etching.[80] Gas adsorption (Figure 3.11(b)) showed that the SBA-15/PDMAEMA composites with 8, 16 and 29 wt. % of polymer exhibited accessible pores of volume 0.11-0.52 cm^3 g^{-1}, and specific surface areas of 21-140 m^2 g^{-1}. No appreciable broadening of the

pore size distribution was observed (Figure 3.11c) when PDMAEMA loading up to 16 wt.%, while with the higher content of 29 wt.%, the pores became almost inaccessible.

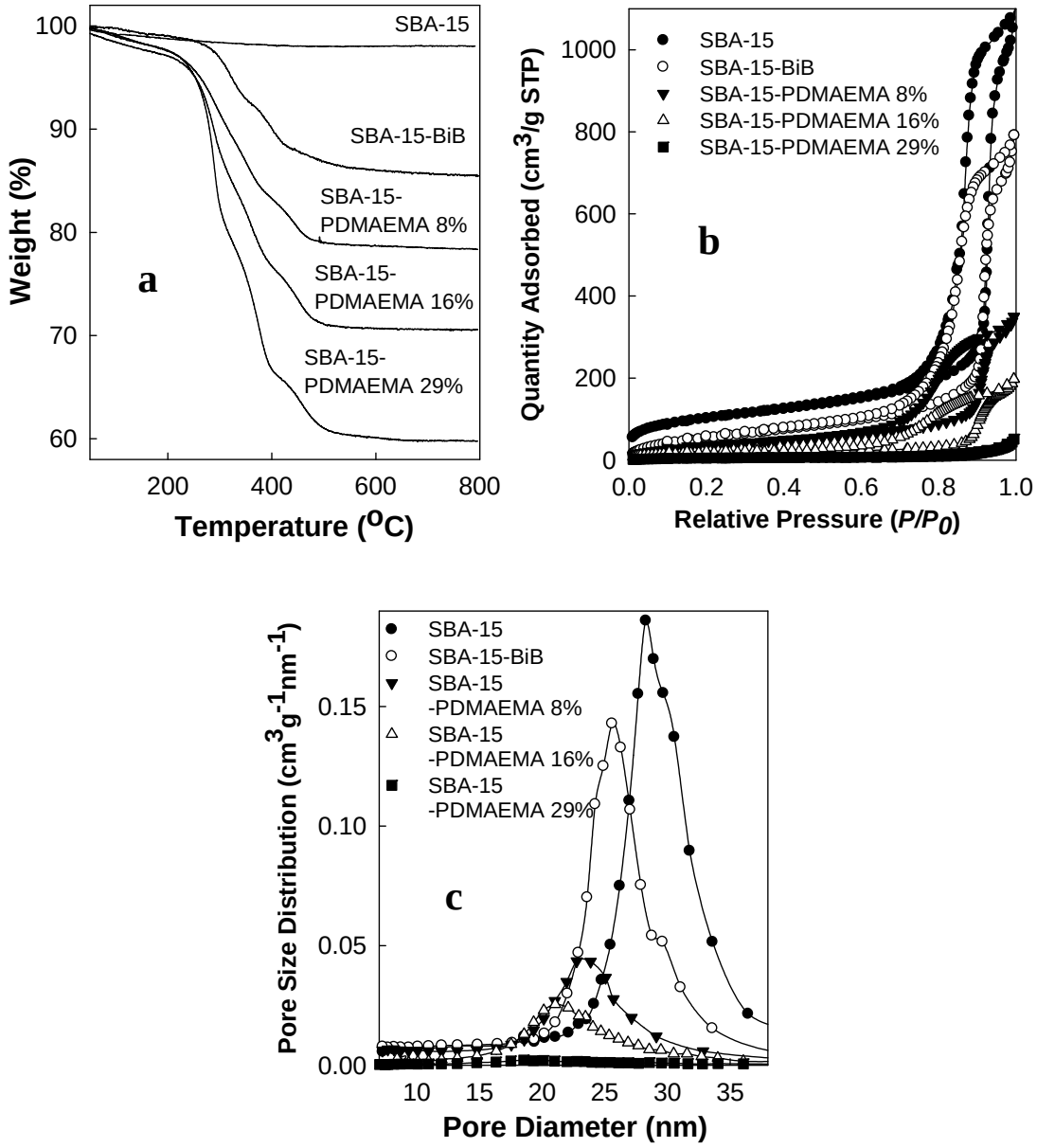

Figure 3.11. (a) Weight change patterns, (b) nitrogen adsorption isotherms and (c) pore size distributions for SBA-15 silica before and after attachment of initiation sites and polymerization of DMAEMA (loading of PDMAEMA in the composite is indicated in wt.%).

3.3.3. Conclusions

One can conclude that ARGET ATRP is highly suitable for the synthesis of high-surface-area mesoporous silica/polymer composites consisting of a large variaty of polymers. Adjustable polymer loadings, including very high ones, and appreciable polymer film thicknesses can be achieved. Due to its simplicity, ARGET ATRP emerges as a powerful, yet surprisingly straightforward way to synthesize well-defined polymer brushes in nanopores, opening a convenient avenue to a wide range of high-surface-area silica-polymer composites.

Chapter 4.

Synthesis of Nanoporous Carbons via the Hard-Templating Strategy

4.1 Introduction

Ordered mesoporous carbons (OMCs)[87-89] are unique porous carbonaceous materials due to their ordered nanoscale structures, pore sizes in the mesopore range (typically 2-12 nm), high specific surface areas and large pore volumes. OMCs have attracted a lot of research activity, mainly due to their potential advanced applications in the areas of heterogeneous catalysis, chromatography, electrochemical double-layer capacitors and gas storage.[88,89]

The mesoporous carbons are mostly synthesized via hard-templating (nano-casting method),[49,77,94,118,120-122,130,135,138-142,144,145,179,264-269] in which solid nanoporous structures are applied as templates to assist carbon precursors to form mesoporous structures. The strategy usually involves three major steps: (i) introduction of the carbon precursor to the pores of the template, (ii) the carbonation of the carbon precursor in the carbon/template composite and (iii) the removal of the template. In most of cases, resulting porous carbons keep the morphologies of the parent templates, but with inverse structures, as the framework and pores of template will turn into pores and framework of the produced carbon. The ordered mesoporous silicas have been proven as excellent templates for fabricating porous carbons, especially ordered mesoporous carbons (OMCs)[264] due to their highly ordered structures, outstanding thermal stability and chemical resistance. Large variety of OMC with diverse structures and pore sizes have been successfully produced, for example, the 2-D hexagonally cylindrical CMK-3 (rode-type)[118] and CMK-5 (tube-type)[94] templated by SBA-15, or cubic CMK-1 templated by MCM-48,[120] or bi-continuous mesoporous carbons templated by FDU-5[49] or KIT-6 silicas.[179]

In this chapter, the discussion will focus on the use of selected carbon precursors for the synthesis of a variety of well-defined OMCs. It is known that in the case of a particular silica

template, different carbon precursors afford porous carbon samples with different carbon framework and physical properties. The chapter includes two different carbons precursors:

1. Commercially available mesophase pitch (MP). A family of OMCs with a variety of structures, such as solid 2-D hexagonal arrays of nano-rods and cubic arrays of nano-dots fabricated via a simple MP imprinting method. The produced carbons show well-defined mesostructures and semi-graphitic frameworks.

2. Polyacrylonitrile via surface-initiated polymerizations. Well-defined silica/ polyacrylonitrile composites with controlled polyacrylonitrile loadings and film thickness were synthesized via the ATRP grafting of acrylonitrile from surfaces of OMSs. After stabilization and carbonization of PAN, and removal of the silica templates, carbon materials were obtained with highly ordered structures, often composed of hollow nanoscale features, and having high surface areas, and large mesopore volumes.

4.2. Nanoporous Carbons Derived from Mesophase Pitch[142]

Although mesophase pitch has been known as a precursor for carbon fibers for several decades, its utility to synthesize mesoporous carbons has been explored during the last decade.[138-141,145,265,267,269-272] Li and Jaroniec reported that by using colloidal silica particles to imprint in the mesophase pitch, one can achieve carbons with controlled mesopore size depending on the diameter of the silica particles.[140] The resulting mesoporous carbons had uniform spherical mesopores with narrow size distribution, quite high specific surface areas (up to 425 m^2 g^{-1}) and large pore volumes (up to 1.61cm^3 g^{-1}), and their heat treatment at 2400 °C under Ar afforded a graphitized carbon with quite narrow mesopore size distribution.[270] Later, the mesophase pitch has been proven useful in the synthesis of OMCs templated by SBA-15,[138,141,269] MCM-48,[144,273] KIT-6,[271] and SBA-16.[273] Moreover, the surfaces of some of these OMCs were functionalized by aryl or fluoro groups to tailor OMC pore diameter and surface properties.[139,269]

4.2.1. Experimental section

4.2.1.1. Materials

The synthesis and structural properties of SBA-15 with nominal (BJH) pore diameter ~16 nm and actual pore diameter 14 nm were described in detail elsewhere (the sample was denoted 15C1d+100C2d #2).[48] SBA-15 with nominal (BJH) pore diameter ~26 nm and actual pore diameter ~19 nm was synthesized at initial temperature of 14 °C and hydrothermally treated at 130 °C for 2 days. Due to the high hydrothermal treatment temperature and extended time, the mesopores of this material are likely to be connected by large mesoporous gaps in the walls.[50]

The synthesis of KIT-6 silica involved a procedure originally reported by Kim et al.[274] with the hydrothermal treatment at 100 °C for one day. The synthesis and characterization of LP-FDU-12 silica was described in detail elsewhere[189] (the sample was denoted 15C + 100C1d + A130C2d). SBA-16 was synthesized using the synthesis mixture composition reported by Kleitz et al.[275] with the hydrothermal treatment at 130 °C for 2 days. The mesophase pitch (AR-MP) was provided by Mitsubishi Gas Chemical Company. Ground MP was thoroughly mixed with silica template in ethanol (using sonication) and the mixture was dried in an open container until the solvent evaporated. The mixture was transferred into a ceramic boat and heated in a tube furnace under nitrogen atmosphere. The temperature was set at 460-550 ^{o}C for 8 hours (16 hours for SBA-16 replica) (with 5 ^{o}C/min ramp to the final temperature) for infiltration, and 850 ^{o}C for 3 hours (5 ^{o}C min^{-1} ramp) for carbonation. The carbon samples were isolated by dissolving the silica templates in HF solution overnight. The products were extensively washed with deionized water and acetone before drying under vacuum. The mass of MP used was calculated as a mass of the template used multiplied by its specific total pore volume and by the density of the mesophase pitch (1.23 g cm^{-3}), which corresponds to the mass of MP that would be capable of completely filling the mesopores and micropores of the template.

4.2.1.2. Characterization

Small-angle X-ray scattering (SAXS) measurements were performed at Station D1 of CHESS synchrotron facility at Cornell University. The samples were placed in a hole in an aluminum sample holder and secured from both sides using a Kapton tape. Powder X-ray diffraction measurements were performed using a PANalytical X-ray Diffractometer with step size of 0.05° and angular range of 10-90°. Transmission electron microscopy (TEM) images were recorded on

a Philips CM 100 microscope operated at 80 kV or on a FEI Tecnai G2 Twin microscope operated at 120 kV. Before the imaging, the samples were dispersed in ethanol through sonication and subsequently deposited on a carbon-coated copper grid. Nitrogen adsorption measurements at -196 °C were carried out using a Micromeritics ASAP 2020 volumetric adsorption analyzer. Samples were degassed under vacuum at 200 °C before adsorption measurements. The specific surface area was determined using the BET method[1] applied to the relative pressure range 0.04-0.20. The total pore volume was calculated from the amount adsorbed at a relative pressure of 0.99.[1] The pore size distribution was calculated from adsorption branches of isotherms using the Barrett-Joyner-Halenda (BJH) algorithm and the KJS relation between the pore diameter and the capillary condensation pressure.[161]

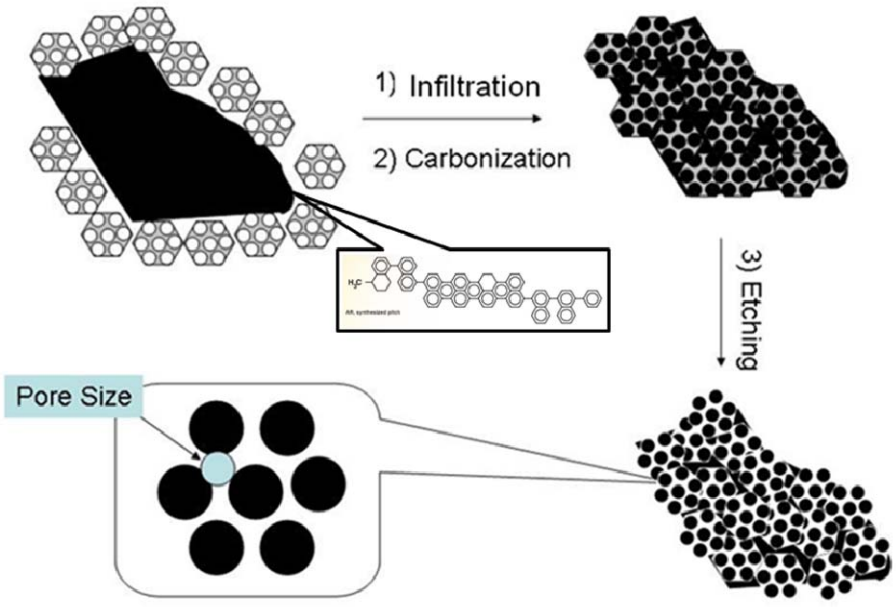

Scheme 4.1. The scheme of the process for preparing ordered mesoporous carbons using the template (e.g., large-pore SBA-15 silica) and the mesophase pitch carbon precursor. It is illustrated that the pore diameter of the 2-D hexagonal arrays of nanorods provides the information about the dimensions of the space between three adjacent nanorods.[142]

4.2.2. Results and discussions

4.2.2.1. Preparation of 2-D mesoporous carbon nano-rods.

SBA-15 with 2-D hexagonal structure of large cylindrical mesopores[21] is one of the most extensive studied and widely applied OMSs because of its facile synthesis and beneficial structural properties. SBA-15 has been proven as an excellent template to fabricate other ordered mesoporous materials, including carbons (CMK-3 and CMK-5),[77,94,118,130,135,138,141,144,269] via the inverse replication process. In spite of extensive activity in this area, the use of large-pore SBA-15 (LP-SBA-15; pore diameter > 12 nm) as a template has been nearly unexplored. To the best of our knowledge, only Sun et al.[276] applied macroporous-mesoporous LP-SBA-15 with d_{100} interplanar spacing of ~14 nm to synthesize an ordered mesoporous carbon (as seen from TEM) that retained the morphology of the template and exhibited narrow pore size distribution (pore diameter ~6 nm). However, XRD or SAXS data were not reported, so the crucial information about the periodicity and unit-cell size is not available. Straightforward syntheses of LP-SBA-15 with pore diameters up to ~26 nm have been reported recently,[46,48,50] and herein the applicability of these templates for the synthesis of CMK-3 carbons is demonstrated.

The LP-SBA-15 template applied in our study had a large (100) interplanar spacing (14.0 nm), a large pore diameter of 14.3 nm (nominal BJH pore diameter ~16 nm), high surface area (550 $m^2\ g^{-1}$) and large pore volume (1.36 $cm^3\ g^{-1}$).[48] The process of infiltration with the carbon precursor (MP) is illustrated in Scheme 4.1. When the temperature was raised above MPs softening temperature (~285 ^oC), MP became less viscous and infiltrated the cylindrical nanochannels of LP-SBA-15. The subsequent carbonation process at 850 ^oC was likely to facilitate intermolecular cross-linking to form semi-graphitic carbon framework (see below).

Finally, the silica template was removed by HF etching. The resulting carbon samples showed highly ordered 2-D hexagonal (CMK-3 type) structures, as seen from SAXS patterns (Figure 4.1(a)) with diffraction peaks indexed as (100), (110) and (200). The formation of inverse replicas of SBA-15 in the case of carbon and other framework compositions has been explained as a result of the micropore/mesopore connections between the ordered mesopores of SBA-15, as these connecting pores allow for the formation of connections between the nanorods in the structure of the inverse replica.[118] There is no obvious difference in (100) interplanar spacings (~ 13 nm) for all the CMK-3 samples synthesized with different infiltration temperatures, indicating a good reproducibility of the dimensions of the nanostructure. A low extent of contraction of the unit cell during the carbon formation process (from d_{100} = 14 nm for the silica template to 13 nm) can be attributed to a high carbon yield for the pitch carbonization and an excellent thermal stability of the silica template and the produced carbon nanostructure.

The obtained carbon samples were further analyzed by nitrogen adsorption. As shown in Figure 4.1(b), the carbon samples prepared at different infiltration temperatures had similar Type IV adsorption-desorption isotherms. The capillary condensation steps occurred in the relative pressure range from 0.45 to 0.65 and the isotherms leveled off at higher relative pressure, indicating uniform pore structures and low external surface areas. The adsorption isotherms of our carbons were similar to that reported by Sun et al.[276] for their macroporous-mesoporous carbon prepared using a similar template. However, these researchers did not report X-ray diffraction/scattering data, so overall periodicity of their carbon is not clear.

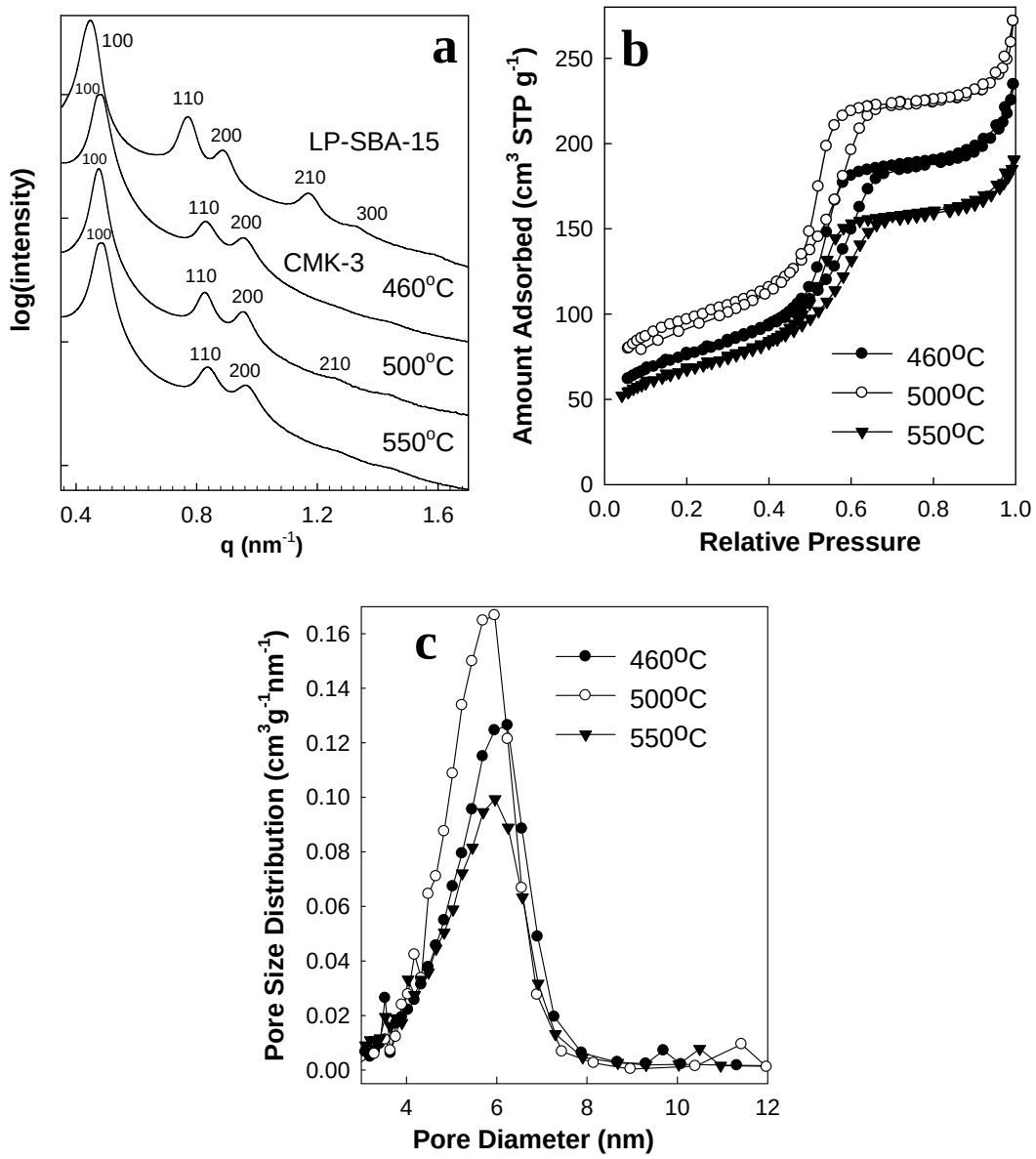

Figure 4.1. (a) SAXS patterns, (b) nitrogen adsorption isotherms and (c) pore size distributions of mesoporous carbon samples prepared using the LP-SBA-15 template and different MP infiltration temperatures.[142]

Interestingly, the BET specific surface area and pore volume of the CMK-3 samples reached the maximum (340 m^2 g^{-1} and 0.40 cm^3 g^{-1}, respectively) when the infiltration temperature was

500 °C. It is known that the viscosity of MP will gradually decrease with the rising temperature, so the higher temperature is likely to be beneficial for MP infiltration into LP-SBA-15 nano-channels and thus expected to lead to higher pore volume and specific surface area. However, the phenomenon observed here might be due to the cross-linking of pitch molecules when imprinting temperature is much higher (e.g., 550 °C) than the MP softening temperature, and close to the carbonation temperature (850 °C), and/or to the mesophase - isotropic phase transition[277] taking place at excessively high temperatures. Either possibility would lead to higher viscosity and reduced mobility of MP, which may have negative effect on the BET specific surface area and pore volume. To rule out the possibility of an effect specific to LP-SBA-15 template, another template (KIT-6) with 3-D cubic structure was studied and found to exhibit a similar trend (see data and discussion in the next section).

The BET specific surface area and pore volume of the obtained carbons are much less than carbons produced from many other carbon precursors, especially sucrose, as these precursors give rise to carbons with considerable amount of microporosity, leading to very high specific surface area and pore volume.[118] However, OMCs from mesophase pitch and some other precursors giving rise to semi-graphitic carbon frameworks with low microporosity[141,271] commonly exhibit specific surface areas and pore volumes comparable to the carbons from our optimized synthesis. The pore size distributions (PSDs) in Figure 4.1(c) indicated that the pore diameters of the carbon samples were independent of the imprinting temperature. PSDs were relatively narrow and had a maximum around 5.8 nm. This pore size is larger than pore wall thickness of the LP-SBA-15 template (~2 nm) because the pore diameter shown on PSD reflects primarily the dimensions of the pore space between three adjacent carbon nanorods (see Figure 1).[278] The pore diameter of CMK-3 prepared from MP using large-pore SBA-15 was larger than

the pore diameter of CMK-3 templated by regular SBA-15 silica derived from MP[141] or petroleum pitch.[135] This is consistent with Equation 3 of Ref.[278], which indicates that the pore diameter of CMK-3 scales with the (100) interplanar spacing.

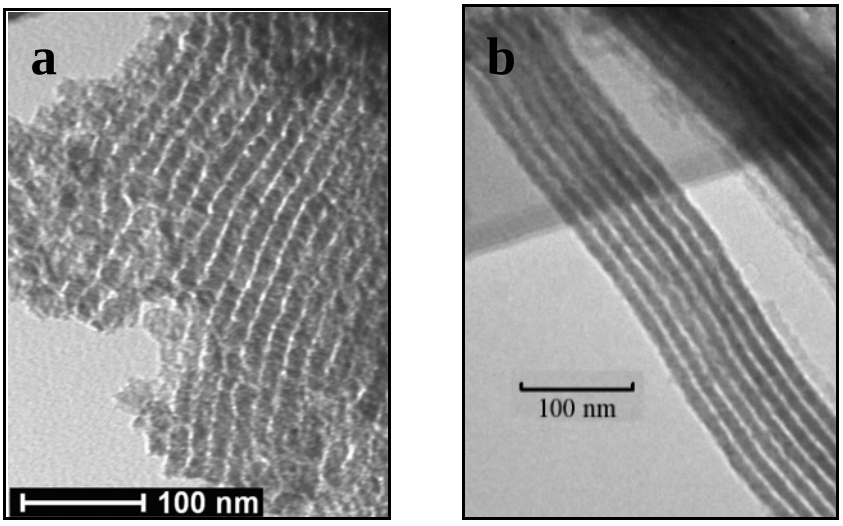

Figure 4.2. TEM images of mesoporous carbons prepared using LP-SBA-15 templates of pore diameter (a) ~19 nm, and (b) 14 nm. The infiltration temperature was 500 ^{o}C.[142]

SBA-15 with even larger pore diameter (19 nm, nominal BJH pore diameter 26 nm) was also used to obtain ordered array of carbon nano-rods. TEM images in Figure 4.2(a) revealed that both kinds of the SBA-15 inverse replicas contained arrays of uniform nano-rods, which are replicas of the ordered cylindrical mesopores of the SBA-15 templates. The diameters of nano-rods were roughly estimated from TEM as ~12 nm and ~16 nm for carbons template by the silicas with pore diameters of 14 nm and 19 nm, respectively. It must be pointed out that most of the carbon nanostructures observed in TEM images were nanorods rather than hollow tubes or broken rods, indicating that the MP infiltration process can introduce high loading of carbon to nearly totally fill the mesopores. This provides an insight as to why the tendency to create

secondary porosity was not observed and the contraction of the lattice during the inverse replication process was low. The present results show that LP-SBA-15 is a facile template for the synthesis of CMK-3 carbons, which was mentioned elsewhere without presenting the experimental results,[48] the latter being reported here for the first time.

4.2.2.2. Preparation of mesoporous carbons from 3-D OMS templates

The MP infiltration process described above is also capable of producing OMCs using KIT-6[179,274] template with 3-D bicontinuous structure and *Ia3d* symmetry, as well as SBA-16[21] with body-centered cubic structure and *Im3m* symmetry, and large-pore FDU-12 (LP-FDU-12)[188,189] with face centered cubic structure and *Fm3m* symmetry.

The KIT-6 template featured the pore diameter of 9.4 nm, specific surface area of 941 m^2 g^{-1} and total pore volume of 1.14 cm^3 g^{-1}. The preparation of the carbon samples using KIT-6 templates was similar to that for LP-SBA-15 templates. The resulting carbon samples preserved the *Ia3d* symmetry of the template, as seen from peaks or shoulders on SAXS patterns that can be associated with 211, 220, 321/400 and 420/332 reflections (Figure 4.3(a)). Therefore, these carbons can be referred to as CMK-8 carbons.[271] Compared to the carbons prepared using LP-SBA-15 template, the preparation of KIT-6-templated carbons (unit cell parameter 20 nm) involved larger shrinkage (unit cell parameter for the template was 25.4 nm). The infiltration temperature did not have any appreciable effect on the unit cell parameter of the carbons.

Type IV nitrogen adsorption isotherms were obtained for the CMK-8 carbons (Figure 4.3(b)). The isotherms were similar to those reported earlier for CMK-8 derived from MP.[271] Depending on the infiltration temperature (from 460 ^oC to 550 ^oC), the specific surface area and

pore volume varied, but it reached 400 m^2 g^{-1}, and 0.43 cm^3 g^{-1}, respectively, for the sample prepared at 500 °C. Although the best structural properties of CMK-3 and CMK-8 were achieved herein for the optimized infiltration temperature of 500 ^oC, it should be noted that the softening points of MPs are different for different manufactures and MP preparation techniques.[277] The pore diameters were narrowly distributed and centered as 5-6 nm (inset of Figure 4.3(b)).

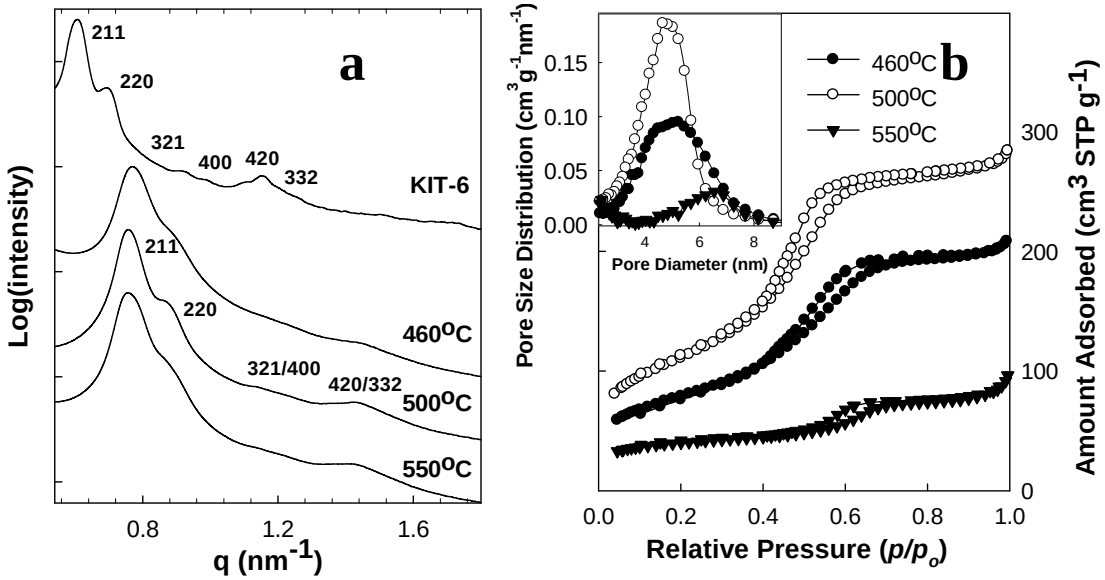

Figure 4.3. (a) SAXS spectra and (b) nitrogen adsorption isotherms with inset pore size distributions of OMC prepared from the template KIT-6 with different imprinting temperatures.[142]

LP-FDU-12 is OMS with face-centered cubic structure of spherical pores of diameter up to 27 nm, which are connected with one another through passages that can be made large in size.[188,189] The successful preparation of OMC using LP-FDU-12 template was indicated by the SAXS pattern that featured peaks and shoulders that can be identified as (111), (220) and (311) reflections of the face-centered cubic structure (*Fm3m* symmetry) (Figure 4.4(a)). Previously, FDU-1, FDU-12 and LP-FDU-12 were used as templates for OMCs,[77,178,188] but the resulting

carbons never featured such a well-resolved and indexable XRD or SAXS pattern. The calculated unit cell size was 32.9 nm, which is 9% lower than the unit cell size of 36.3 nm for the silica template. The unit cell size for the considered carbon is particularly large, and exceeds the unit-cell size for LP-FDU-12 carbon described in some detail earlier.[188] The BET specific surface area, pore volume and pore diameter of the LP-FDU-12-templated carbon were 297 m^2 g^{-1}, 0.40 cm^3 g^{-1} and 10.8 nm (Figure 4.4(a)), respectively. The adsorption isotherm was similar to that reported earlier for FDU-1 replica prepared using polyacrylonitrile as a carbon precursor.[77] The TEM image for the LP-FDU-12 inverse replica carbon showed a well-ordered structure composed of nanospheres of size ~20 nm (Figure 4.4(b)). OMC was also successfully synthesized using SBA-16 template, which had body-centered cubic structure and spherical mesopores of diameter ~11 nm (which is likely to be underestimated by ~2 nm based on prior studies).[169] The resulting OMC obtained via the infiltration with MP at 500 ^oC for extended period of time had a pore diameter of 6.6 nm, the specific surface area of 500 m^2 g^{-1} and pore volume of 0.62 cm^3 g^{-1} (Figure 4.4(c)). The adsorption isotherm of our carbon is similar to the isotherms reported earlier for the carbon inverse replicas of SBA-16,[178,279] but in our case, the capillary condensation step was much more pronounced and the isotherm sharply leveled off after the capillary condensation was completed. This indicates that the MP affords SBA-16 carbon inverse replicas that are comparable to or even of better quality than those from other carbon sources. The carbon featured a rather narrow single peak on its SAXS pattern. From TEM image (Figure 4.4(d)), the estimated diameter of highly ordered nanospheres was ~11 nm, very close to the pore size of its SBA-16 template.

4.2.2.3. Framework properties of carbon samples

To confirm that MP has an advantage of affording semi-graphitic structures,[138,271] one of the carbons templated by KIT-6 was examined by XRD. The diffraction pattern featured characteristic (002) reflection at ~25^{o} corresponding to 0.36 nm graphite layer spacing, a less intense peak at ~44^{o} for (100) and/or (101) reflection and a weak (110) reflection at ~79^{o} (Figure 4.5).[130] It is clear that the MP-derived carbon had an appreciable ordering on atomic scale (despite rather low carbonation temperature), but the carbon was still far from a perfectly graphitized structure (d_{002}=0.343 nm). It is known that in the case of templated pitch-based carbons, graphene sheets have preferred perpendicular orientation with respect to the template's mesopore surface.[138]

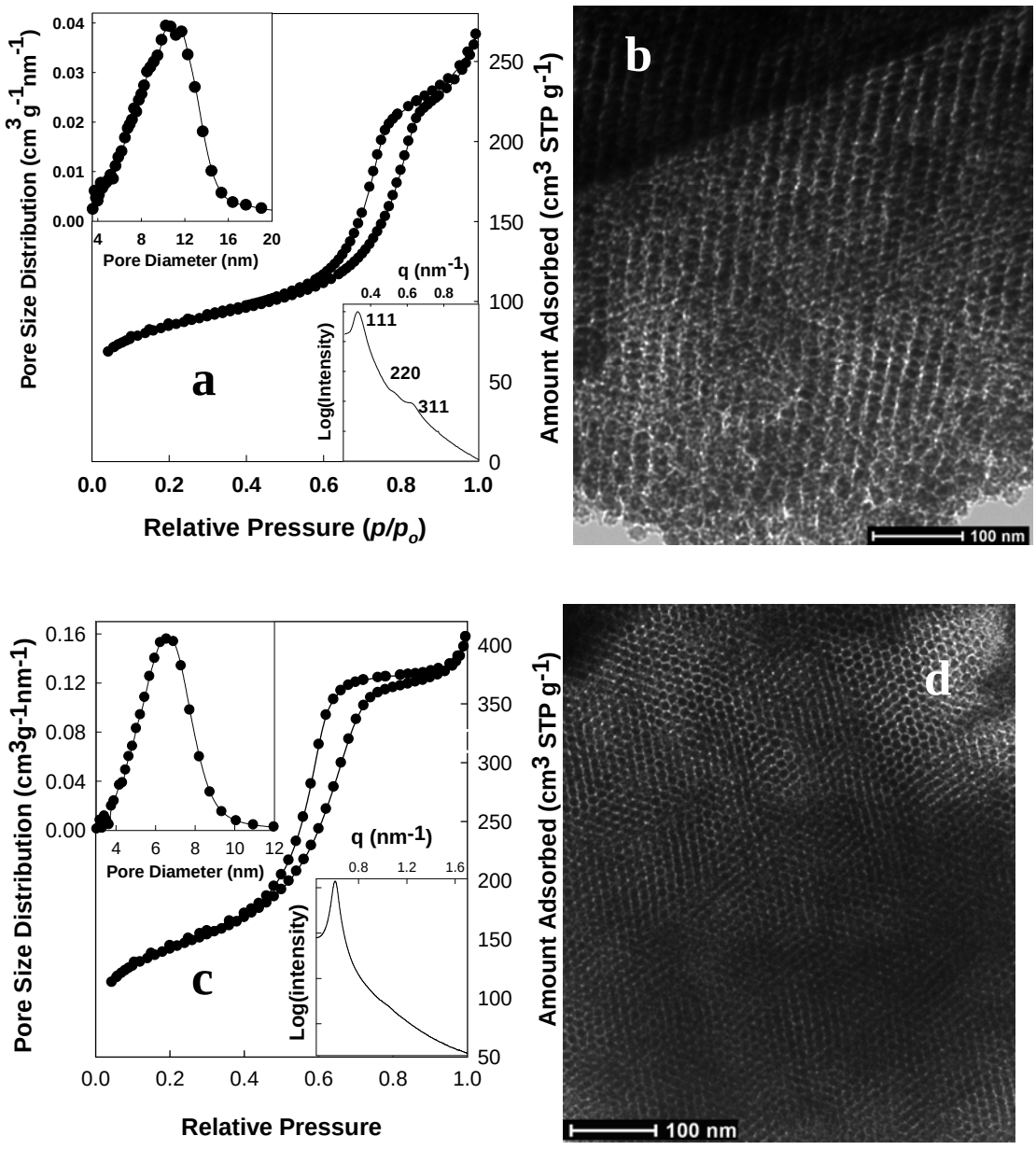

Figure 4.4. (a) The nitrogen adsorption isotherm with inset SAXS spectrum and pore size distribution, and (b) TEM image of OMC prepared from the template LP-FDU-12 with imprinting temperatures at 500 ^{o}C; (c) The nitrogen adsorption isotherm with inset SAXS spectrum and pore size distribution, and (d) TEM image of OMC prepared from the template SBA-16 with imprinting temperatures at 500 ^{o}C.[142]

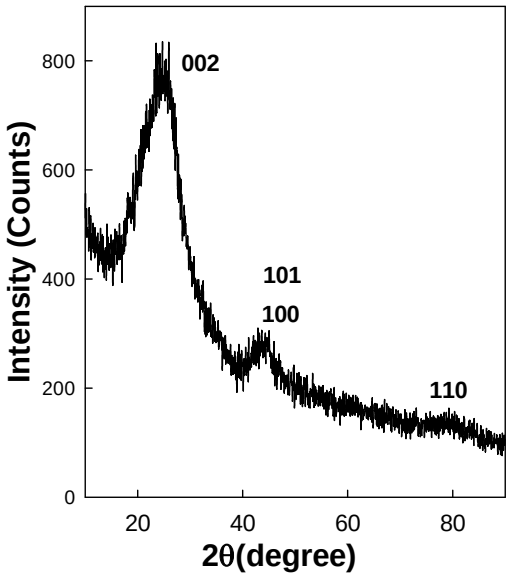

Figure 4.5. XRD pattern of KIT-6-templated carbon (infiltration temperature of 500 ^{o}C).[142]

4.2.3. Conclusions

The results presented here demonstrated that the MP infiltration method provided a simple way to synthesize high-quality ordered mesoporous carbons. The method is effective for synthesis of carbons with desired pore geometries, such as 2-D hexagonal arrays of nanorods, or 3-D cubic structures templated by KIT-6, LP-FDU-12 and SBA-16 silicas. The resulting carbons show quite high specific surface areas (up to 500 m^2 g^{-1}) and moderate pore volumes (up to 0.62 cm^3 g^{-1}). It is interesting that there was an optimal infiltration temperature under which the resulting carbon sample has the highest surface area and pore volume, which appears to be independent of the type of the template. XRD showed that the produced mesoporous carbons have semi-graphitic frameworks.

4.3. Nanoporous Carbons Derived from Polyacrylonitrile

Polyacrylonitrile (PAN) is a unique carbon precursor and has been proven to produce mesoporous carbons when mesoporous silicas served as templates.[114,130,131] ATRP grafting of acrylonitrile from surfaces of ordered mesoporous silicas has been demonstrated as a powerful strategy to fabricate well-defined silica/PAN composites with controlled PAN loading and film thickness. After stabilization and carbonization of the composites, and the silica template removal, one obtain mesoporous carbons showing ordered pore structure, high surface area and large pore volume. (See Scheme 4.2)

4.3.1. Experimental section

4.3.1.1. Materials

The syntheses of ordered mesoporous silicas including KIT-6,[179] and SBA-15[50] were described elsewhere. The synthesis of LP-FDU-12 was performed similarly to the procedure developed by others,[202] but the inorganic salt was not added and mechanical stirring was used. The synthesis was as follows: 1.0 g of P127 was dissolved in 60 ml of 2.0 M aqueous HCl solution at 14 ^{o}C under mechanical stirring for 3 hours, then 2.0 g of xylene was added and stirring was continued for 1 day at the same temperature in polypropylene container. Afterwards, 4.1 g TEOS was added and solution was stirred for 1 day. Later, the precipitate was isolated by filtration and re-dispersed in 2.0 M aqueous HCl solution in a closed Teflon-lined autoclave at 130 ^{o}C for 2 days. The product was isolated by filtering and calcined under air at 550 °C for 5 hours (heating ramp 5 °C min^{-1}).

Acrylonitrile (AN) monomer was purchased from Aldrich and purified by passing through a column filled with basic alumina. The initiator, 1-(chlorodimethylsilyl)propyl 2-bromoisobutyrate (BiB), was synthesized and grafted on the surface of silica as described elsewhere.[77,80] Other chemicals including solvents, copper salts and ligand bipyridine were used as received.

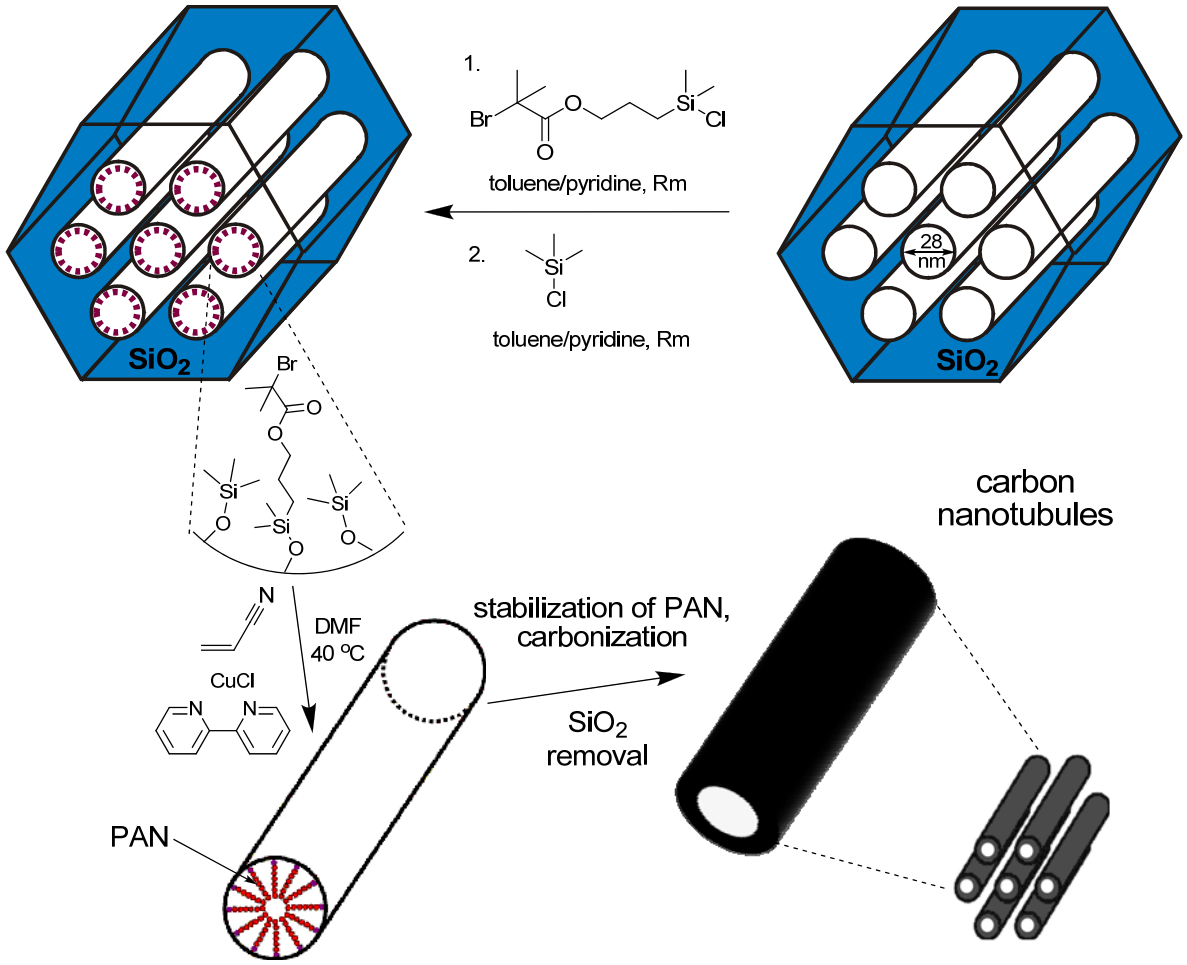

Scheme 4.2. Synthesis of silica/PAN composites via surface initiated ATRP polymerizations and fabrication of ordered mesoporous carbons with ordered arrays of nanotubules from the composites. The procedure is illustrated for large-pore SBA-15 as a template (See discussion of 4.3.2.2).

4.3.1.2. Synthesis of PAN/silica composites

The polymerization conditions were similar to those described earlier.[77,80] Initiator-modified silica, AN monomer, a pre-mixed solution of $CuCl_2$ and bipyridine (Bpy) ligand in N,N-dimethylformamide (DMF) were added into a Schlenk flask. After the mixture was degassed by three freeze-pump-thaw cycles, CuCl was added under nitrogen atmosphere. The final molar ratio of reactants was as follows: initiator: Cu(I): Cu(II) : bpy : AN=1 : 1 : 0.1 : 2.2: 300. The polymerizations were placed in an oil bath at 40 °C for 2 days under nitrogen. The reaction was terminated by opening the glassware and exposing the catalyst to air. The silica/polymer composites were isolated by filtration, washed with DMF, acetone and methanol, and dried in a vacuum oven.

4.3.1.3. Synthesis of mesoporous carbon replica

Silica/PAN composite was stabilized by heating under air to 300 ^{o}C at a rate of 2 ^{o}C min^{-1} and maintaining at 300 ^{o}C for 2 hours; subsequent carbonation was performed under nitrogen to final temperature 800 ^{o}C at a rate of 2 ^{o}C min^{-1} with dwelling at this final temperature for 3 hours and cooling to room temperature. The silica template was removed by hydrofluoric acid etching.

4.3.1.4. Characterization

Same as 4.2.1.2

4.3.2. Results and discussion

4.3.2.1. The KIT-6 template[280]

The mesoporous silica KIT-6 was chosen as a template with cubic *Ia3d* structure and pore diameter ~11 nm. The successful polymerization of AN via ATRP and the formation of silica/PAN composite (KIT-6-PAN) was evident from TGA. The weight change curves for KIT-6, KIT-6-BiB and KIT-6-PAN are shown in Figure 4.6. In comparison to pure silica KIT-6 with ~2 wt.% weight loss and KIT-6-BiB with ~23 wt.% weight loss, KIT-6-PAN had a significant weight loss (~45 wt.%), which was primarily related to PAN grafted from the surface of the silica host. The content of PAN was estimated as ~29 wt.%.

Based on the nitrogen adsorption isotherms in Figure 4.7, the original KIT-6 template had BET specific surface area of 670 m^2 g^{-1} and total pore volume of 1.10 cm^3 g^{-1}, while initiator-functionalized KIT-6-BiB had 290 m^2 g^{-1} and 0.56 cm^3 g^{-1}, respectively. On the other hand, KIT-6-PAN sample had rather low specific surface area (~5 m^2 g^{-1}) and the total pore volume (~0.03 cm^3 g^{-1}) because the mesopores were filled or blocked by large contents of PAN and were not accessible to nitrogen gas. After stabilization and carbonization of KIT-6-PAN composite, sample KIT-6-Carbon was obtained, and the removal of the silica template by HF etching produced mesoporous carbon (C-KIT-6) that showed BET specific surface area of 750 m^2 g^{-1} and total pore volume of 1.44 cm^3 g^{-1}. the latter being higher than that of the KIT-6 template. Although the specific surface area of C-KIT-6 was lower than that of other silica-templated mesoporous carbons made from other carbon precursors,[120] it is due to the fact that the material has relatively low microporosity.[77]

The KIT-6 template had a narrow pore size distribution centered at ~11 nm (Figure 4.8), consistent with earlier work.[179] The initiator-functionalized KIT-6-BiB had ~9 nm pore diameter. There were no mesopores accessible to nitrogen adsorbate in the KIT-6-PAN sample, indicating that pores were either filled with PAN or the access to them was blocked by PAN. After carbonization, no pores of diameter similar to that of the KIT-6 template were seen, thus indicating a uniform infiltration of the pores of the silica template by carbon. Interestingly enough, the C-KIT-6 material showed structure with bi-modal pore size distribution centered at ~6 and ~9 nm, as reported earlier by others in the case of KIT-6 replica derived from other carbon precursors.[281] The bimodality is related to the fact that some parts of the carbon framework shifted with respect to one another, resulting in the lowering of the symmetry of the part of the material (as seen from the appearance of the SAXS peak at 0.57°, see Figure 4.9), while other parts of the carbon structure retain their original symmetry.

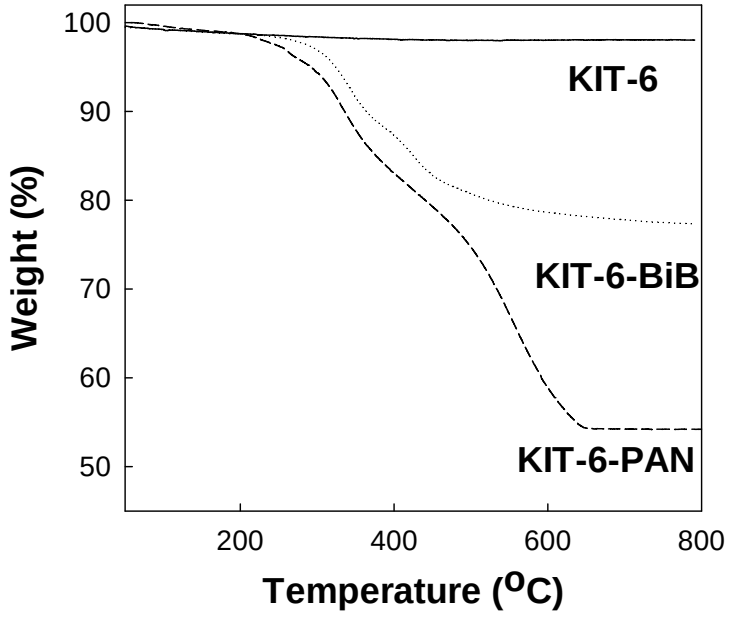

Figure 4.6. TGA curve (weight loss) of KIT-6 silica, KIT-6-BiB and KIT-6-PAN.[280]

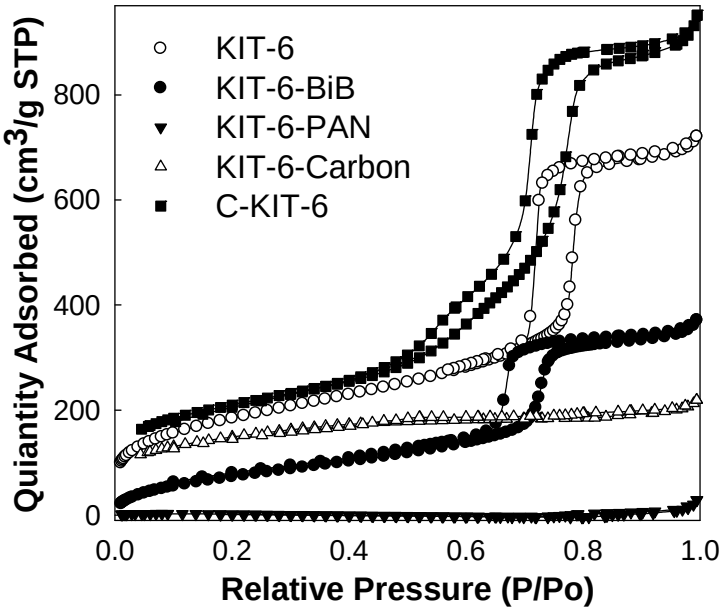

Figure 4.7. Nitrogen adsorption isotherms of KIT-6 silica, KIT-6-BiB, KIT-6-PAN composite, KIT-6-Carbon composite and C-KIT-6 Carbon.[278]

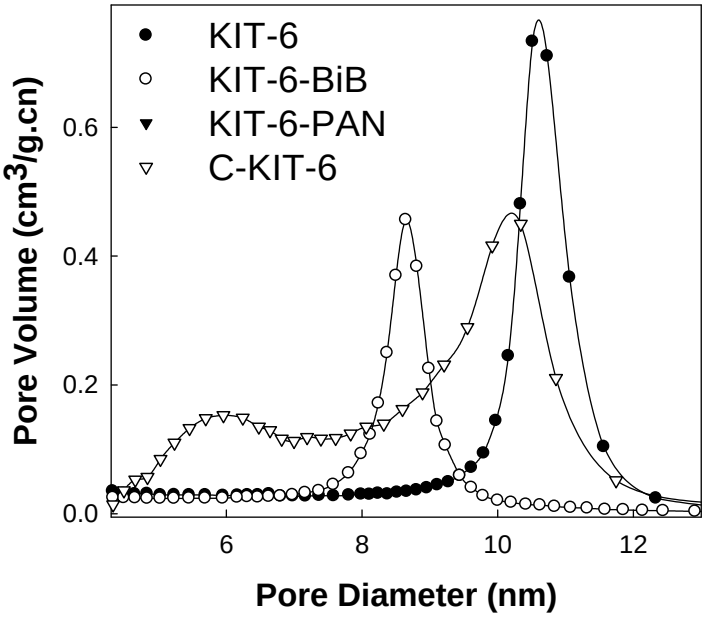

Figure 4.8. Pore size distributions for KIT-6 silica, KIT-6-BiB, KIT-6-PAN composite, and C-KIT-6 Carbon.[278]

The SAXS patterns (Figure 4.9) for KIT-6-PAN and C-KIT-6 were similar to those of KIT-6 templates, providing evidence for the retention of ordering after polymerization and conversion to carbon. Obvious peaks or shoulders that can be indexed as (211), (220), and (420)/(332) (the latter absent for carbon) indicated the cubic *Ia3d* structure in all samples, although as discussed above, the symmetry of a part of the carbon framework may be lower. The unit cell parameter of KIT-6-Carbon was 21.9 nm, less than that of KIT-6-PAN (24.5 nm) and KIT-6 (24.5 nm) because carbonation in high temperature led to the shrinkage of the structure.[77] TEM image (Figure 4.10) of C-KIT-6 shows a large domain of highly ordered structure.

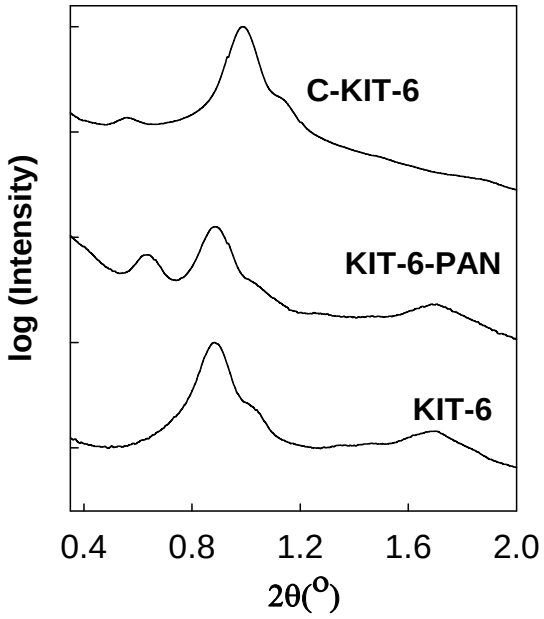

Figure 4.9. Small-angle X-ray scattering patterns for KIT-6 silica, KIT-6-PAN composite, and C-KIT-6.[278]

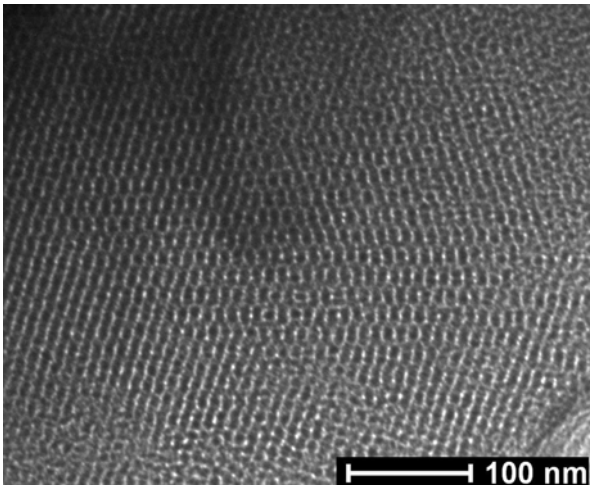

Figure 4.10. Transmission electron microscopy image for C-KIT-6.[278]

4.3.2.2. The FDU-12 template

Large-pore FDU-12 silica (LP-FDU-12) has face-centered cubic structure of spherical pores with quite high BET specific surface area (420 m^2 g^{-1}), large pore volume (1.06 cm^3 g^{-1}) and large BJH pore size of 28 nm. Surface-initiated ATRP allowed us to graft PAN up to 40 wt.% within the porous hosts (FDU-12-PAN), which almost totally filled the mesopores resulting in no accessibility, as evidenced by the negligible adsorption of nitrogen (Figure 4.11). After the composite's stabilization at 300 ^oC and carbonizations at 800 ^oC, the cross-linked and carbonized PAN shrank and formed layers of carbon coating on the surface of the LP-FDU-12 template. Therefore, the increased pore volume (0.33 cm^3 g^{-1}) and BET specific surface area (350 m^2 g^{-1}) were observed for silica/carbon composite. The silica/carbon composite (FDU-12-Carbon) had a large pore diameter of ~23 nm. After the template removal, the resulting carbons (C-FDU-12) had high BET specific surface area (805 m^2 g^{-1}), large total pore volume (1.98 cm^3 g^{-1}), and bi-modal pore size distributions centered at 15 nm and 22 nm. (Figure 4.11 and 4.12)

In Figure 4.13, all samples including FDU-12, FDU-12~PAN, FDU-12-Carbon and C-FDU-12 have similar SAXS patterns, revealing a characteristics of face-centered cubic structure and providing evidence for the retention of ordering after polymerization and carbon formation as well as its isolation. The C-FDU-12 has a slightly smaller unit cell parameter (47.1 nm) than the FDU-12 template (47.8 nm) because the carbonation at high temperature led to the shrinkage of the structure.

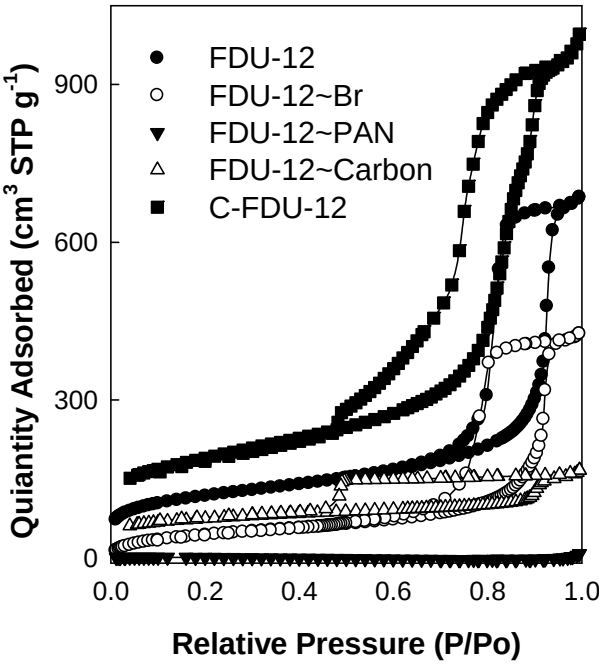

Figure 4.11. Nitrogen adsorption isotherms of FDU-12, FDU-12-BiB, FDU-12-PAN, FDU-12-Carbon and C-FDU-12.

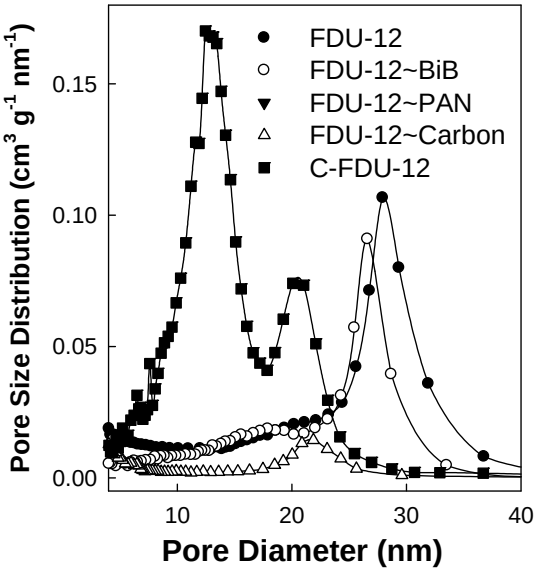

Figure 4.12. Pore size distributions of FDU-12, FDU-Br, FDU-12-PAN, FDU-12-Carbon and C-FDU-12.

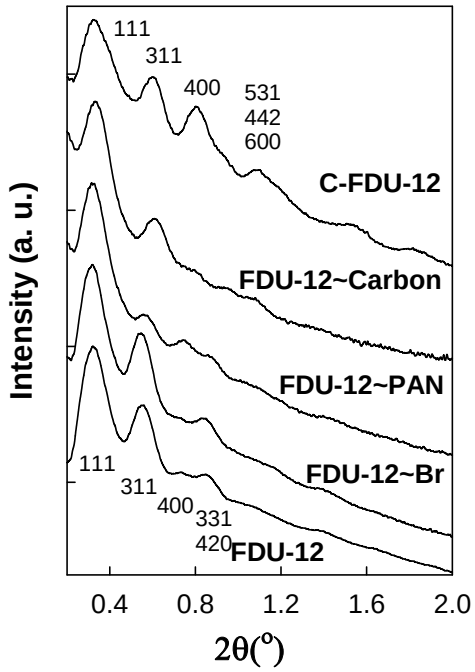

Figure 4.13. SAXS patterns of FDU-12, FDU-12-BiB, FDU-12-PAN, FDU-12-Carbon and C-FDU-12.

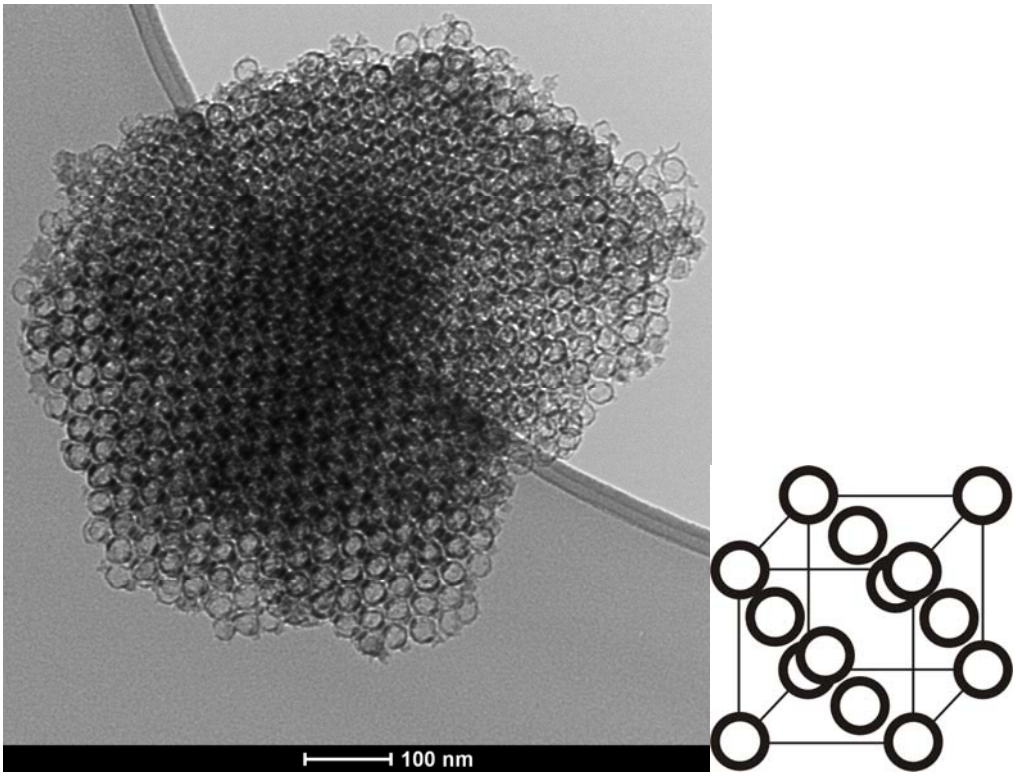

Figure 4.14. Transmission electron microscopy image of C-FDU-12 and the corresponding structure model.

TEM image (Figure 4.14) not only confirms that C-FDU-12 is an ordered array of spheres, but also provides information that these spheres are hollow. The pore diameter estimated from TEM is ~23 nm, which is very close to one of the pore diameters (~22 nm) measured from gas adsorption, while another pore diameter is believed to correspond to the cavity between spheres. This identification is consistent with the fact that ~ 20 nm pores are present both in the silica-carbon composite and in the final carbon material, and thus are related to internal voids in the carbon framework. On the other hand, the ~13 nm pores appeared after the removal of the template and thus are likely to be related to spaces once occupied by the silica template.

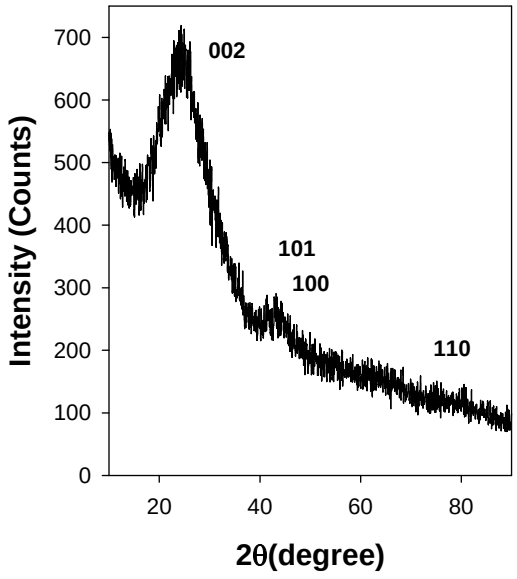

Figure 4.15. WAXS patterns of C-FDU-12 with carbonization temperature at 850 ^{o}C.

The semi-graphitic property of C-FDU-12 is evident from the XRD pattern (Figure 4.15) which featured characteristic broad peak (002) at ~25^{o} corresponding to 0.36 nm spacing between graphite layers, a less intense peak at ~44^{o} for either (100) or (101) reflection and a weak peak (110) at ~79 ^{o}. It is clear that under such moderate carbonation conditions (800 ^{o}C), carbon sample had not reached the fully graphitized structure (d_{002}=0.343 nm). Semi-graphitic carbons can be graphitized at 2300 ^{o}C to improve their ordering, but ordered mesoporous structures are hard to preserve under such conditions.[130]

4.3.2.2. The large pore SBA-15 template

A similar strategy to produce mesoporous carbons was applied to large-pore SBA-15 (LP-SBA-15) template, which has 2-D hexagonal structure and large cylindrical pores. The selected LP-SBA-15 had a BET specific surface area of 320 m^2 g^{-1}, total pore volume of 1.31 cm^3 g^{-1} and large BJH pore size of 28 nm. The mesopores were still accessible after loading 37 wt.% PAN

(SBA-15-PAN), After stabilization and carbonization of SBA-15-PAN, pore volume increased to 0.61 cm^3 $g^{-1}$and BET surface area to 280 m^2 g^{-1} in the silica/carbon composites (SBA-15-Carbon). After the template removal, the produced mesoporous carbon (C-SBA-15) had a pore volume of 2.43 cm^3 g^{-1} and BET specific surface area of 855 m^2 g^{-1}. Bi-modal distribution of pores was also observed as ~22 nm and ~8 nm, which represent the diameter of empty nanotubules and the dimensions of the spaces between nanotubules (Figure 4.17). The ordered structure of C-SBA-15 resembled that of LP-SBA-15 template (see the SAXS pattern showing similar peak position in Figure 4.18). TEM image confirmed ordered hexagonal array (Figure 4.19 (a)) of cylindrical nanotubules (Figure 4.19 (b)).

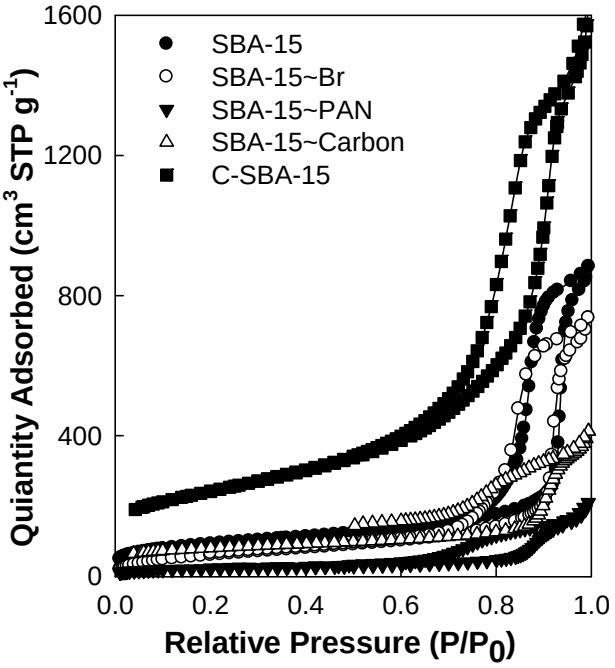

Figure 4.16. Nitrogen adsorption isotherms of SBA-15, SBA-15-Br, SBA-15~PAN, SBA-15-Carbon and C- SBA-15.

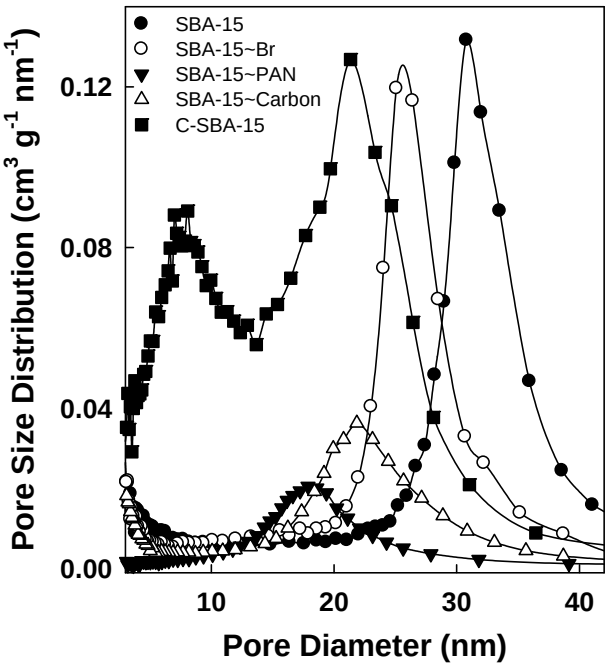

Figure 4.17. Pore size distributions of SBA-15, SBA-15-Br, SBA-15~PAN, SBA-15-Carbon and C-SBA-15.

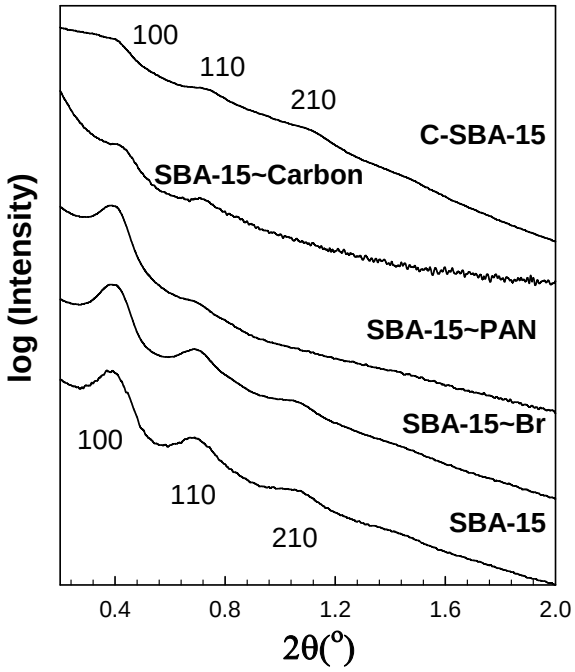

Figure 4.18. SAXS of SBA-15, SBA-15-Br, SBA-15~PAN, SBA-15-Carbon and C-SBA-15.

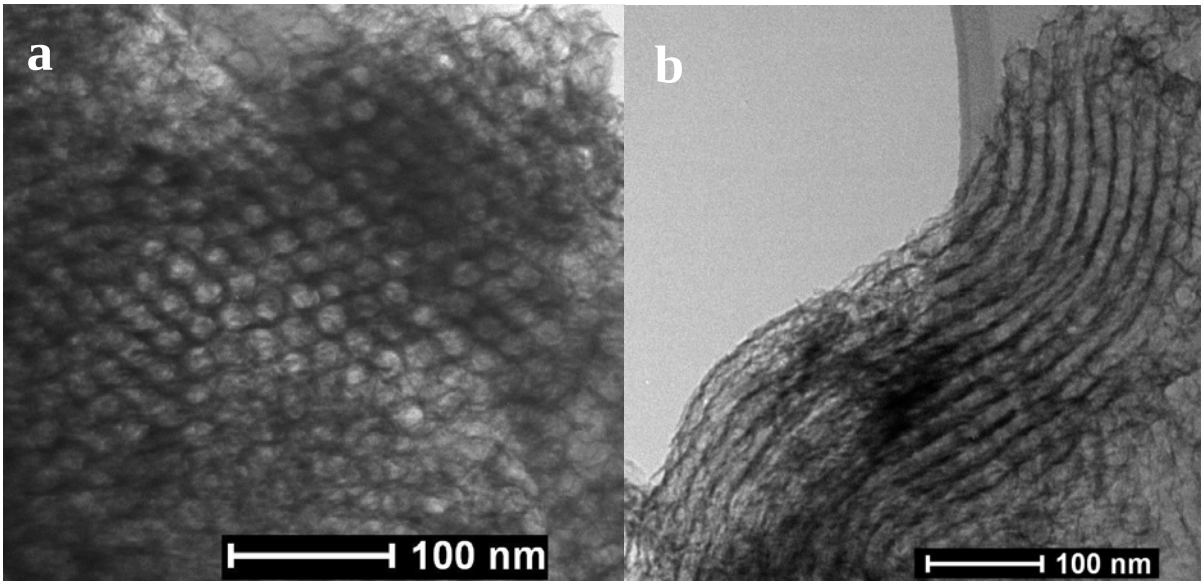

Figure 4.19. Transmission electron microscopy image of C-SBA-15.

4.3.3. Conclusions

Ordered mesoporous silica/PAN composites were produced by the surface-initiated ATRP technique. High loadings of PAN were confirmed by TGA. Subsequent carbonization of PAN and removal of the silica template successfully generated mesoporous carbon materials showing high surface areas and large pore volumes. SAXS and TEM proved that the carbons were ordered and well replicated their templates. In cases of carbons templated by large-pore SBA-15 and FDU-12, hollow nanotubules and nanospheres, respectively, were produced. These results illustrate new opportunities in the synthesis of ordered mesoporous carbons with high surface area and large pore volume that consist of hollow nanostructure elements.

Chapter 5.

General Conclusions

This dissertation is devoted to synthesizing novel families of ordered mesoporous materials including silicas (Chapter 2), silica/polymer composites (Chapter 3) and carbons (Chapter 4). The achieved materials have designable structures, tunable structural and/or surface properties, large and accessible pores, high surface areas and large pore volumes. The methods developed herein are often simple, cost-effective and versatile.

Our specific aims at ordered mesoporous silicas were to create large (or ultra large) and still ordered pores in SBA-15, which has 2-D hexagonal structures of cylindrical mesopores. Using the commercially available surfactant P123 and identifying suitable micelle expanders (primarily triisopropylbenzene), we managed to tailor SBA-15 pore diameters in a wide range from 10 to 30 nm. Well-tunable large-pore SBA-15 was produced with pore diameters up to 15 nm by using hexane as a micelle expander, while in the case of using triisopropylbenzene, large and ultra-large-pore SBA-15 were achieved with pore diameters from about 10 up to 30 nm. In combination with triisopropylbenzene, two silica precursors, tetraethylorthosilicate (preferred) and tetramethylorthosilicate, were both found suitable to afford high-quality large-pore SBA-15. Moreover, a rapid synthesis strategy was proposed to fabricate large-pore SBA-15, and was further extended to large-pore FDU-12 silica with face-centered cubic structures and spherical mesopores. The syntheses were as short as 6 hours, in many cases the achieved materials had similar high quality as materials produced by standard methods. By using static conditions, the particle morphology of large-pore SBA-15 can be adjusted to platelet morphology with highly ordered mesopores in very large domains and short pore lengths in the order of half a micrometer.

The well-defined mesoporous polymer/silica composites were produced by using the surface-initiated atom transfer radical polymerization (ATRP). The commercially available 2-(4-

chlorosulfonylphenyl)ethyltrichlorosilane was identified as a versatile initiator to polymerize a large number of monomers. ATRP with activators regenerated by electron transfer (ARGET) was proven as a very convenient and environmentally friendly pathway to achieve materials comparable to those achievable by normal ATRP. The method can be conducted under mild conditions with hundred ppm levels of copper catalyst and tolerance of limited amount of air. Overall, both of the methods were capable of achieving mesoporous composites with remarkable properties, such as controlled polymer film thickness on the mesopore surface, narrow molecular weight distribution of polymer brushes, accessibility of pores, quite high surface areas and pore volumes and preservation of the silica hosts' original structures. The composites are expected to provide a synergistic performance in comparison to individual components of organic polymer and inorganic silica backbone.

In the study of ordered mesoporous carbons with high surface areas and large pore volumes, two carbon precursors, mesophase pitch (MP) or polyacrylonitrile (PAN), were investigated in details. The simple MP infiltration method was effective for synthesis of carbons with semi-graphitic frameworks at low carbonization temperature (850 ^{o}C), and desired pore geometries, such as 2-D hexagonal arrays of nanorods or cubic structures of spheres were obtained from selected templates. Silica/PAN composites with controlled PAN loadings prepared via surface-initiated ATRP were proven to produce unique mesoporous carbons with hollow structures. Ordered arrays of hollow nanospheres with the face-centered cubic structure were replicated from large-pore FDU-12, while ordered arrays of hollow nanotubules with the 2-D hexagonal structure were obtained from large pore SBA-15.

Bibliography

(1) Sing, K. S. W.; Everett, D. H.; Haul, R. A. W.; Moscou, L.; Pierotti, R. A.; Rouquerol, J.; Siemieniewska, T. *Pure Appl. Chem.* **1985**, *57*, 603.

(2) Lester, E.; Hilal, N.; Henderson, J. *Surf. Interface Anal.* **2004**, *36*, 1323.

(3) Yanagisawa, T.; Shimizu, T.; Kuroda, K.; Kato, C. *Bull. Chem. Soc. Jpn.* **1990**, *63*, 988.

(4) Kresge, C. T.; Leonowicz, M. E.; Roth, W. J.; Vartuli, J. C.; Beck, J. S. *Nature* **1992**, *359*, 710.

(5) Vartuli, J. C.; Schmitt, K. D.; Kresge, C. T.; Roth, W. J.; Leonowicz, M. E.; McCullen, S. B.; Hellring, S. D.; Beck, J. S.; Schlenker, J. L.; Olson, D. H.; Sheppard, E. W. *Chem. Mat.* **1994**, *6*, 2317.

(6) Vartuli, J. C.; Kresge, C. T.; Leonowicz, M. E.; Chu, A. S.; McCullen, S. B.; Johnsen, I. D.; Sheppard, E. W. *Chem. Mat.* **1994**, *6*, 2070.

(7) Beck, J. S.; Vartuli, J. C.; Roth, W. J.; Leonowicz, M. E.; Kresge, C. T.; Schmitt, K. D.; Chu, C. T. W.; Olson, D. H.; Sheppard, E. W.; McCullen, S. B.; Higgins, J. B.; Schlenker, J. L. *J. Am. Chem. Soc.* **1992**, *114*, 10834.

(8) Wan, Y.; Shi, Y.; Zhao, D. *Chem. Commun.* **2007**, 897

(9) Wan, Y.; Zhao, D. *Chem. Rev.* **2007**, *107*, 2821.

(10) Fujita, S.; Inagaki, S. *Chem. Mater.* **2008**, *20*, 891.

(11) Hoffmann, F.; Cornelius, M.; Morell, J.; Fröba, M. *Angew. Chem. Int. Ed.* **2006**, *45*, 3216.

(12) Chen, C. Y.; Burkett, S. L.; Li, H. X.; Davis, M. E. *Microporous Mater.* **1993**, *2*, 27.

(13) Chen, C. Y.; Xiao, S. Q.; Davis, M. E. *Microporous Mater.* **1995**, *4*, 1.

(14) Marlow, F.; Zhao, D. Y.; Stucky, G. D. *Microporous Mesoporous Mat.* **2000**, *39*, 37.

(15) Steel, A.; Carr, S. W.; Anderson, M. W. *Chem. Commun.* **1994**, 1571.

(16) Ying, J. Y.; Mehnert, C. P.; Wong, M. S. *Angew. Chem.Int. Ed.* **1999**, *38*, 56.

(17) Sun, T.; Ying, J. Y. *Nature* **1997**, *389*, 704.

(18) Firouzi, A.; Kumar, D.; Bull, L. M.; Besier, T.; Sieger, P.; Huo, Q.; Walker, S. A.; Zasadzinski, J. A.; Glinka, C.; Nicol, J.; Margolese, D.; Stucky, G. D.; Chmelka, B. F. *Science* **1995**, *267*, 1138.

(19) Huo, Q. S.; Margolese, D. I.; Stucky, G. D. *Chem. Mater.* **1996**, *8*, 1147.

(20) Huo, Q. S.; Margolese, D. I.; Ciesla, U.; Feng, P. Y.; Gier, T. E.; Sieger, P.; Leon, R.; Petroff, P. M.; Schuth, F.; Stucky, G. D. *Nature* **1994**, *368*, 317.

(21) Zhao, D. Y.; Huo, Q. S.; Feng, J. L.; Chmelka, B. F.; Stucky, G. D. *J. Am. Chem. Soc.* **1998**, *120*, 6024.

(22) Zhao, D. Y.; Feng, J. L.; Huo, Q. S.; Melosh, N.; Fredrickson, G. H.; Chmelka, B. F.; Stucky, G. D. *Science* **1998**, *279*, 548.

(23) Shen, S.; Garcia-Bennett, A. E.; Liu, Z.; Lu, Q.; Shi, Y.; Yan; Yu, C.; Liu, W.; Cai, Y.; Terasaki, O.; Zhao, D. *J. Am. Chem. Soc.* **2005**, *127*, 6780.

(24) Tan, B.; Dozier, A.; Lehmler, H.-J.; Knutson, B. L.; Rankin, S. E. *Langmuir* **2004**, *20*, 6981.

(25) Sakamoto, Y. H.; Kaneda, M.; Terasaki, O.; Zhao, D. Y.; Kim, J. M.; Stucky, G.; Shim, H. J.; Ryoo, R. *Nature* **2000**, *408*, 449.

(26) Kruk, M.; Jaroniec, M.; Sayari, A. *J. Phys. Chem. B* **1999**, *103*, 4590.

(27) Kruk, M.; Jaroniec, M.; Ryoo, R.; Joo, S. H. *Chem. Mater.* **2000**, *12*, 1414.

(28) Lettow, J. S.; Han, Y. J.; Schmidt-Winkel, P.; Yang, P.; Zhao, D.; Stucky, G. D.; Ying, J. Y. *Langmuir* **2000**, *16*, 8291.

(29) Schmidt-Winkel, P.; Lukens, W. W.; Zhao, D.; Yang, P.; Chmelka, B. F.; Stucky, G. D. *J. Am. Chem. Soc.* **1998**, *121*, 254.

(30) Goltner, C. G.; Berton, B.; Kramer, E.; Antonietti, M. *Chem. Commun.* **1998**, 2287.

(31) Chan, Y.-T.; Lin, H.-P.; Mou, C.-Y.; Liu, S.-T. *Chem. Commun.* **2002**, 2878.

(32) Chan, Y. T.; Lin, H. P.; Mou, C. Y.; Liu, S. T. *Stud. Surf. Sci. Catal.* **2003**, *146*, 113.

(33) Lin, C.-F.; Lin, H.-P.; Mou, C.-Y.; Liu, S.-T. *Microporous and Mesoporous Mater.* **2006**, *91*, 151.

(34) Yu, C.; Yu, Y.; Zhao, D. *Chem. Commun.* **2000**, 575.

(35) Van Der Voort, P.; Ravikovitch, P. I.; De Jong, K. P.; Benjelloun, M.; Van Bavel, E.; Janssen, A. H.; Neimark, A. V.; Weckhuysen, B. M.; Vansant, E. F. *J. Phys. Chem. B* **2002**, *106*, 5873.

(36) Kruk, M.; Jaroniec, M.; Joo, S. H.; Ryoo, R. *J. Phys. Chem. B* **2003**, *107*, 2205.

(37) Deng, Y.; Yu, T.; Wan, Y.; Shi, S.; Meng, Y.; Gu, D.; Zhang, L.; Huang, Y.; Liu, C.; Wu, X.; Zhao, D. *J. Am. Chem. Soc.* **2007**, *129*, 1690.

(38) Bloch, E.; Phan, T.; Bertin, D.; Llewellyn, P.; Hornebecq, V. *Microporous and Mesoporous Mater.* **2008**, *112*, 612.

(39) Wang, J.-S.; Matyjaszewski, K. *J. Am. Chem. Soc.* **1995**, *117*, 5614.

(40) Matyjaszewski, K.; Xia, J. *Chem. Rev.* **2001**, *101*, 2921.

(41) Cao, L.; Dong, H.; Huang, L.; Matyjaszewski, K.; Kruk, M. *Adsorption* **2009**, *15*, 156.

(42) Chan, Y.-T.; Lin, H.-P.; Mou, C.-Y.; Liu, S.-T. *Microporous Mesoporous Mater.* **2009**, *123*, 331.

(43) Feng, P.; Bu, X.; Stucky, G. D.; Pine, D. J. *J. Am. Chem. Soc.* **2000**, *122*, 994.

(44) Feng, P.; Bu, X.; Pine, D. J. *Langmuir* **2000**, *16*, 5304.

(45) Sörensen, M. H.; Corkery, R. W.; Pedersen, J. S.; Rosenholm, J.; Alberius, P. C. *Microporous Mesoporous Mater.* **2008**, *113*, 1.

(46) Sun, J.; Zhang, H.; Ma, D.; Chen, Y.; Bao, X.; Klein-Hoffmann, A.; Pfaender, N.; Su, D. S. *Chem. Commun.* **2005**, 5343.

(47) Zhang, H.; Sun, J.; Ma, D.; Weinberg, G.; Su, D. S.; Bao, X. *J. Phys. Chem. B* **2006**, *110*, 25908.

(48) Kruk, M.; Cao, L. *Langmuir* **2007**, *23*, 7247.

(49) Liu, X.; Tian, B.; Yu, C.; Gao, F.; Xie, S.; Tu, B.; Che, R.; Peng, L.-M.; Zhao, D. *Angew. Chem. Int. Ed.* **2002**, *41*, 3876.

(50) Cao, L.; Man, T.; Kruk, M. *Chem. Mater.* **2009**, *21*, 1144.

(51) Schmidt-Winkel, P.; Lukens, W. W., Jr.; Yang, P.; Margolese, D. I.; Lettow, J. S.; Ying, J. Y.; Stucky, G. D. *Chem. Mater.* **2000**, *12*, 686.

(52) Nagarajan, R.; Barry, M.; Ruckenstein, E. *Langmuir* **1986**, *2*, 210.

(53) Nagarajan, R. *Colloids Surf., B* **1999**, *16*, 55.

(54) Cao, L.; Kruk, M. *Colloids Surf., A* **2010**, 91.

(55) Kojima, Y.; Usuki, A.; Kawasumi, M.; Okada, A.; Kurauchi, T.; Kamigaito, O.; Kaji, K. *J. Polym. Sci. Part B: Polym. phys.* **1995**, *33*, 1039.

(56) Huang, K.-Y.; Weng, C.-J.; Huang, L.-T.; Cheng, T.-H.; Wei, Y.; Yeh, J.-M. *Microporous Mesoporous Mater.*, *131*, 192.

(57) Zhang, F.-A.; Lee, D.-K.; Pinnavaia, T. J. *Polymer* **2009**, *50*, 4768.

(58) Ogoshi, T.; Kim, K. M.; Chujo, Y.; *J. Mater. Chem.* **2003**, 2202.

(59) Posudievsky, O. Y.; Telbiz, G. M.; Rossokhaty, V. K. *J. Mater. Chem.* **2006**, *16*, 2485.

(60) Schlossbauer, A.; Schaffert, D.; Kecht, J.; Wagner, E.; Bein, T. *J. Am. Chem. Soc.* **2008**, *130*, 12558.

(61) Nakazawa, J.; Stack, T. D. P. *J. Am. Chem. Soc.* **2008**, *130*, 14360.

(62) Malvi, B.; Sarkar, B. R.; Pati, D.; Mathew, R.; Ajithkumar, T. G.; Sen Gupta, S. *J. Mater. Chem.* **2009**, *19*, 1409.

(63) Huang, L.; Dolai, S.; Raja, K.; Kruk, M. *Langmuir* **2009**, *26*, 2688.

(64) Barbey, R.; Lavanant, L.; Paripovic, D.; Schuwer, N.; Sugnaux, C.; Tugulu, S.; Klok, H.-A. *Chem. Rev.* **2009**, *109*, 5437.

(65) Acosta, E. J.; Carr, C. S.; Simanek, E. E.; Shantz, D. F. *Adv. Mater.* **2004**, *16*, 985.

(66) Reynhardt, J. P. K.; Yang, Y.; Sayari, A.; Alper, H. *Chem. Mater.* **2004**, *16*, 4095.

(67) Choi, M.; Kleitz, F.; Liu, D.; Lee, H. Y.; Ahn, W.-S.; Ryoo, R. *J. Am. Chem. Soc.* **2005**, *127*, 1924.

(68) Coutinho, D.; Yang, Z.; Ferraris, J. P.; Balkus Jr, K. J. *Microporous Mesoporous Mat.* **2005**, *81*, 321.

(69) Cho, M. S.; Choi, H. J.; Kim, K. Y.; Ahn, W. S. *Macromol. Rapid Commun.* **2002**, *23*, 713.

(70) Sasidharan, M.; Mal, N. K.; Bhaumik, A. *J. Mater. Chem.* **2007**, *17*.

(71) Advincula, R.; Zhou, Q.; Park, M.; Wang, S.; Mays, J.; Sakellariou, G.; Pispas, S.; Hadjichristidis, N. *Langmuir* **2002**, *18*, 8672.

(72) Zhou, Q.; Fan, X.; Xia, C.; Mays, J.; Advincula, R. *Chem. Mater.* **2001**, *13*, 2465.

(73) Zhou, Q.; Wang, S.; Fan, X.; Advincula, R.; Mays, J. *Langmuir* **2002**, *18*, 3324.

(74) Rovira-Truitt, R.; Patil, N.; Castillo, F.; White, J. L. *Macromolecules* **2009**, *42*, 7772.

(75) Q. Fu, G. V. R. R., L.K. Ista, Y. Wu, B.P. Andrzejewski, L.A. Sklar, T.L. Ward, G.P. Lopez, *Adv. Mater.* **2003**, *15*, 1262.

(76) Zhou, Z.; Zhu, S.; Zhang, D. *J. Mater. Chem.* **2007**, *17*, 2428.

(77) Kruk, M.; Dufour, B.; Celer, E. B.; Kowalewski, T.; Jaroniec, M.; Matyjaszewski, K. *J. Phys. Chem. B* **2005**, *109*, 9216.

(78) Save, M.; Granvorka, G.; Bernard, J.; Charleux, B.; Boissiere, C.; Grosso, D.; Sanchez, C. *Macromol. Rapid Commun.* **2006**, *27*, 393.

(79) Audouin, F.; Blas, H.; Pasetto, P.; Beaunier, P.; Boissiere, C.; Sanchez, C.; Save, M.; Charleux, B. *Macromol. Rapid Commun.* **2008**, *29*, 914.

(80) Kruk, M.; Dufour, B.; Celer, E. B.; Kowalewski, T.; Jaroniec, M.; Matyjaszewski, K. *Macromolecules* **2008**, *41*, 8584.

(81) Jakubowski, W.; Matyjaszewski, K. *Angew. Chem. Int. Ed.* **2006**, *45*, 4482.

(82) Jakubowski, W.; Min, K.; Matyjaszewski, K. *Macromolecules* **2006**, *39*, 39.

(83) Matyjaszewski, K.; Dong, H.; Jakubowski, W.; Pietrasik, J.; Kusumo, A. *Langmuir* **2007**, *23*, 4528.

(84) Bombalski, L.; Dong, H.; Listak, J.; Matyjaszewsk, K.; Bockstaller, M. R. *Adv. Mater.* **2007**, *19*, 4486.

(85) Cao, L.; Kruk, M. *Polymer Chemistry* **2010**, *1*, 97.

(86) Cao, L.; Kruk, M. *In Preparation*.

(87) Ryoo, R.; Joo, S. H.; Kruk, M.; Jaroniec, M. *Adv. Mater.* **2001**, *13*, 677.

(88) Lee, J.; Kim, J.; Hyeon, T. *Adv. Mater.* **2006**, *18*, 2073.

(89) Liang, C.; Li, Z.; Dai, S. *Angew. Chem. Int. Ed.* **2008**, *47*, 3696.

(90) Han, S.; Sohn, K.; Hyeon, T. *Chem. Mater.* **2000**, *12*, 3337.

(91) Vinu, A.; Streb, C.; Murugesan, V.; Hartmann, M. *J. Phys. Chem. B* **2003**, *107*, 8297.

(92) Choi, M.; Ryoo, R. *Nature Mater.* **2003**, *2*, 473.

(93) Ahn, W. S.; Min, K. I.; Chung, Y. M.; Rhee, H. K.; Joo, S. H.; Ryoo, R. *Stud. Surf. Sci. Catal.* **2001**, *135*, 4710.

(94) Joo, S. H.; Choi, S. J.; Oh, I.; Kwak, J.; Liu, Z.; Terasaki, O.; Ryoo, R. *Nature* **2001**, *412*, 169.

(95) Chai, G. S.; Yoon, S. B.; Yu, J. S.; Choi, J. H.; Sung, Y. E. *J. Phys. Chem. B* **2004**, *108*, 7074.

(96) Chan, K. Y.; Ding, J.; Ren, J.; Cheng, S.; Tsang, K. Y. *J. Mater. Chem.* **2004**, *14*, 505.

(97) Yang, H.; Shi, Q.; Liu, X.; Xie, S.; Jiang, D.; Zhang, F.; Yu, C.; Tu, B.; Zhao, D. *Chem. Commun.* **2002**, 2842.

(98) Yoon, S.; Lee, J.; Hyeon, T.; Oh, S. M. *J. Electrochem. Soc.* **2000**, *147*, 2507.

(99) Lee, J.; Kim, J.; Lee, Y.; Yoon, S.; Oh, S. M.; Hyeon, T. *Chem. Mater.* **2004**, *16*, 3323.

(100) Lee, J.; Yoon, S.; Oh, S. M.; Shin, C. H.; Hyeon, T. *Adv. Mater.* **2000**, *12*, 359.

(101) Zhou, H.; Zhu, S.; Hibino, M.; Honma, I. *J. Power Sources* **2003**, *122*, 219.

(102) Furukawa, H.; Hibino, M.; Zhou, H. S.; Honma, I. *Chem. Lett.* **2003**, *32*, 132.

(103) Vix-Guterl, C.; Saadallah, S.; Jurewicz, K.; Frackowiak, E.; Reda, M.; Parmentier, J.; Patarin, J.; Beguin, F. *Mater. Sci. Eng. B* **2004**, *B108*, 148.

(104) Jurewicz, K.; Vix-Guterl, C.; Frackowiak, E.; Saadallah, S.; Reda, M.; Parmentier, J.; Patarin, J.; Beguin, F. *J. Phys. Chem. Solids* **2004**, *65*, 287.

(105) Liang, C.; Hong, K.; Guiochon, G. A.; Mays, J. W.; Dai, S. *Angew. Chem. Int. Ed.* **2004**, *43*, 5785.

(106) Liang, C.; Dai, S. *J. Am. Chem. Soc.* **2006**, *128*, 5316.

(107) Tanaka, S.; Nishiyama, N.; Egashira, Y.; Ueyama, K. *Chem. Commun.* **2005**, 2125

(108) Meng, Y.; Gu, D.; Zhang, F.; Shi, Y.; Cheng, L.; Feng, D.; Wu, Z.; Chen, Z.; Wan, Y.; Stein, A.; Zhao, D. *Chem. Mater.* **2006**, *18*, 4447.

(109) Zhang, F.; Meng, Y.; Gu, D.; Yan; Chen, Z.; Tu, B.; Zhao, D. *Chem. Mater.* **2006**, *18*, 5279.

(110) Meng, Y.; Gu, D.; Zhang, F.; Shi, Y.; Yang, H.; Li, Z.; Yu, C.; Tu, B.; Zhao, D. *Angew. Chem. Int. Ed.* **2005**, *44*, 7053.

(111) Zhang, F.; Meng, Y.; Gu, D.; Yan; Yu, C.; Tu, B.; Zhao, D. *J. Am. Chem. Soc.* **2005**, *127*, 13508.

(112) Zhang, F.; Gu, D.; Yu, T.; Zhang, F.; Xie, S.; Zhang, L.; Deng, Y.; Wan, Y.; Tu, B.; Zhao, D. *J. Am. Chem. Soc.* **2007**, *129*, 7746.

(113) Huang, Y.; Cai, H.; Yu, T.; Zhang, F.; Zhang, F.; Meng, Y.; Gu, D.; Wan, Y.; Sun, X.; Tu, B.; Zhao, D. *Angew. Chem. Int. Ed.* **2007**, *46*, 1089.

(114) Kruk, M.; Dufour, B.; Celer, E. B.; Kowalewski, T.; Jaroniec, M.; Matyjaszewski, K. *Chem. Mater.* **2006**, *18*, 1417.

(115) Ho, R.-M.; Wang, T.-C.; Lin, C.-C.; Yu, T.-L. *Macromolecules* **2007**, *40*, 2814.

(116) Peng, M.; Li, D.; Shen, L.; Chen, Y.; Zheng, Q.; Wang, H. *Langmuir* **2006**, *22*, 9368.

(117) Yang, H.; Zhao, D. *J. Mater. Chem.* **2005**, *15*.

(118) Jun, S.; Joo, S. H.; Ryoo, R.; Kruk, M.; Jaroniec, M.; Liu, Z.; Ohsuna, T.; Terasaki, O. *J. Am. Chem. Soc.* **2000**, *122*, 10712.

(119) Lee, J.; Yoon, S.; Hyeon, T.; Oh, S. M.; Kim, K. B. *Chem. Commun.* **1999**, 2177.

(120) Ryoo, R.; Joo, S. H.; Jun, S. *J. Phys. Chem. B* **1999**, *103*, 7743.

(121) Knox, J. H.; B. Kaur; Millward, G. R. *J. Chromatogr.* **1986**, *352*, 3.

(122) Knox, J. H.; Unger, K. K.; Mueller, H. *J. Liq. Chromatogr.* **1983**, *6*, 1.

(123) Kruk, M.; Jaroniec, M.; Ryoo, R.; Joo, S. H. *J. Phys. Chem. B* **2000**, *104*, 7960.

(124) Fuertes, A. B.; Nevskaia, D. M. *J. Mater. Chem.* **2003**, *13*, 1843.

(125) Lu, A. H.; Schmidt, W.; Spliethoff, B.; Schueth, F. *Adv. Mater.* **2003**, *15*, 1602.

(126) Che, S.; Garcia-Bennett, A. E.; Liu, X.; Hodgkins, R. P.; Wright, P. A.; Zhao, D.; Terasaki, O.; Tatsumi, T. *Angew. Chem., Int. Ed.* **2003**, *42*, 3930.

(127) Fuertes, A. B.; Nevskaia, D. M. *Microporous Mesoporous Mater.* **2003**, *62*, 177.

(128) Yoon, S. B.; Kim, J. Y.; Yu, J. S. *Chem. Commun.* **2002**, 1536.

(129) Moriguchi, I.; Koga, Y.; Matsukura, R.; Teraoka, Y.; Kodama, M. *Chem. Commun.* **2002**, 1844.

(130) Kruk, M.; Kohlhaas, K. M.; Dufour, B.; Celer, E. B.; Jaroniec, M.; Matyjaszewski, K.; Ruoff, R. S.; Kowalewski, T. *Microporous Mesoporous Mater.* **2007**, *102*, 178.

(131) Lu, A.; Kiefer, A.; Schmidt, W.; Schueth, F. *Chem. Mater.* **2004**, *16*, 100.

(132) Fuertes, A. B.; Alvarez, S. *Carbon* **2004**, *42*, 3049.

(133) Kim, T. W.; Park, I. S.; Ryoo, R. *Angew. Chem., Int. Ed.* **2003**, *42*, 4375.

(134) Kim, C. H.; Lee, D. K.; Pinnavaia, T. J. *Langmuir* **2004**, *20*, 5157.

(135) Vix-Guterl, C.; Saadallah, S.; Vidal, L.; Reda, M.; Parmentier, J.; Patarin, J. *J. Mater. Chem.* **2003**, *13*, 2535.

(136) Parmentier, J.; Saadhallah, S.; Reda, M.; Gibot, P.; Roux, M.; Vidal, L.; Vix-Guterl, C.; Patarin, J. *J. Phys. Chem. Solids* **2004**, *65*, 139.

(137) Lu, A. H.; Schmidt, W.; Matoussevitch, N.; Bonnemann, H.; Spliethoff, B.; Tesche, B.; Bill, E.; Kiefer, W.; Schuth, F. *Angew. Chem., Int. Ed.* **2004**, *43*, 4303.

(138) Yang, H.; Yan; Liu, Y.; Zhang, F.; Zhang, R.; YanMeng, Y.; Li, M.; Xie, S.; Tu, B.; Zhao, D. *J. Phys. Chem. B* **2004**, *108*, 17320.

(139) Li, Z.; Del Cul, G. D.; Yan, W.; Liang, C.; Dai, S. *J. Am. Chem. Soc.* **2004**, *126*, 12782.

(140) Li, Z.; Jaroniec, M. *J. Am. Chem. Soc.* **2001**, *123*, 9208.

(141) Li, Z.; Jaroniec, M. *J. Phys. Chem. B* **2004**, *108*, 824.

(142) Cao, L.; Kruk, M. *Adsorption* **2010**, *Accepted*.

(143) Jun, S.; Choi, M.; Ryu, S.; Lee, H. Y.; Ryoo, R. *Stud. Surf. Sci. Catal.* **2003**, *146*, 37.

(144) Li, Z.; Yan, W.; Dai, S. *Langmuir* **2005**, *21*, 11999.

(145) Gierszal, K. P.; Yoon, S. B.; Yu, J.-S.; Jaroniec, M. *J. Mater. Chem.* **2006**, *16*, 2819

(146) Yang, C.-M.; Weidenthaler, C.; Spliethoff, B.; Mamatha, M.; Schuth, F. *Chem. Mater.* **2005**, *17*, 355.

(147) Yoon, S. B.; Kim, J. Y.; Yu, J.-S.; Gierszal, K. P.; Jaroniec, M. *Ind. Eng. Chem. Res.* **2005**, *44*, 4316.

(148) Liang, C.; Dai, S.; Guiochon, G. *Anal. Chem.* **2003**, *75*, 4904.

(149) Han, S.; Yun, Y.; Park, K.-W.; Sung, Y.-E.; Hyeon, T. *Adv. Mater.* **2003**, *15*, 1922.

(150) Sevilla, M.; Fuertes, A. B. *Carbon* **2006**, *44*, 468.

(151) Wang, J. N.; Zhang, L.; Niu, J. J.; Yu, F.; Sheng, Z. M.; Zhao, Y. Z.; Chang, H.; Pak, C. *Chem. Mater.* **2007**, *19*, 453.

(152) Lei, Z.; Xiao, Y.; Dang, L.; You, W.; Hu, G.; Zhang, J. *Chem. Mater.* **2006**, *19*, 477.

(153) Ryoo, R.; Ko, C. H.; Kruk, M.; Antochshuk, V.; Jaroniec, M. *J. Phys. Chem. B* **2000**, *104*, 11465.

(154) Kruk, M.; Jaroniec, M.; Ko, C. H.; Ryoo, R. *Chem. Mater.* **2000**, *12*, 1961.

(155) Schueth, F. *Angew. Chem. Int. Ed.* **2003**, *42*, 3604.

(156) Hartmann, M. *Chem. Mater.* **2005**, *17*, 4577.

(157) Yang, H. F.; Zhao, D. Y. *J. Mater. Chem.* **2005**, *15*, 1217.

(158) Tiemann, M. *Chem. Mater.* **2007**, *20*, 961.

(159) Li, B.; Inagaki, S.; Miyazaki, C.; Takahashi, H. *Chemical Research in Chinese Universities* **2002**, *18*, 200.

(160) Jaroniec, M.; Kruk, M.; Olivier, J. P. *Langmuir* **1999**, *15*, 5410.

(161) Kruk, M.; Jaroniec, M.; Sayari, A. *Langmuir* **1997**, *13*, 6267.

(162) Barrett, E. P.; Joyner, L. G.; Halenda, P. P. *J. Am. Chem. Soc.* **1951**, *73*, 373.

(163) Sayari, A.; Kruk, M.; Jaroniec, M. *Catal. Lett.* **1997**, *49*, 147.

(164) Kruk, M.; Jaroniec, M.; Sayari, A. *Chem. Mater.* **1999**, *11*, 492.

(165) Sayari, A.; Liu, P.; Kruk, M.; Jaroniec, M. *Chem. Mater.* **1997**, *9*, 2499.

(166) Kruk, M.; Jaroniec, M. *Chem. Mater.* **2003**, *15*, 2942.

(167) Ravikovitch, P. I.; Neimark, A. V. *Langmuir* **2002**, *18*, 9830.

(168) Celer, E. B.; Kruk, M.; Zuzek, Y.; Jaroniec, M. *J. Mater. Chem.* **2006**, *16*, 2824.

(169) Matos, J. R.; Kruk, M.; Mercuri, L. P.; Jaroniec, M.; Zhao, L.; Kamiyama, T.; Terasaki, O.; Pinnavaia, T. J.; Liu, Y. *J. Am. Chem. Soc.* **2003**, *125*, 821.

(170) Kim, T. W.; Ryoo, R.; Kruk, M.; Gierszal, K. P.; Jaroniec, M.; Kamiya, S.; Terasaki, O. *J. Phys. Chem. B* **2004**, *108*, 11480.

(171) Chen, D.; Li, Z.; Yu, C.; Shi, Y.; Zhang, Z.; Tu, B.; Zhao, D. *Chem. Mater.* **2005**, *17*, 3228.

(172) Gobin, O. C.; Wan, Y.; Zhao, D.; Kleitz, F.; Kaliaguine, S. *J. Phys. Chem. C* **2007**, *111*, 3053.

(173) Morishige, K.; Tateishi, M.; Hirose, F.; Aramaki, K. *Langmuir* **2006**, *22*, 9220.

(174) Fulvio, P. F.; Pikus, S.; Jaroniec, M. *J. Mater. Chem.***2005**, *15*, 5049.

(175) Blin, J. L.; Otjacques, C.; Herrier, G.; Su, B.-L. *Langmuir* **2000**, *16*, 4229.

(176) Karkamkar, A.; Kim, S.-S.; Pinnavaia, T. J. *Chem. Mater.* **2003**, *15*, 11.

(177) Galarneau, A.; Cambon, H.; DiRenzo, F.; Ryoo, R.; Choi, M.; Fajula, F. *New J. Chem.* **2003**, *27*, 73.

(178) Fan, J.; Yu, C.; Gao, F.; Lei, J.; Tian, B.; Wang, L.; Luo, Q.; Tu, B.; Zhou, W.; Zhao, D. *Angew. Chem. Int. Ed.* **2003**, *42*, 3146.

(179) Kleitz, F.; Choi, S. H.; Ryoo, R. *Chem. Commun.* **2003**, 2136.

(180) Fan, J.; Yu, C.; Wang, L.; Tu, B.; Zhao, D.; Sakamoto, Y.; Terasaki, O. *J. Am. Chem. Soc.* **2001**, *123*, 12113.

(181) Sayari, A.; Kruk, M.; Jaroniec, M.; Moudrakovski, I. L. *Adv, Mater.* **1998**, *10*, 1376.

(182) Melosh, N. A.; Lipic, P.; Bates, F. S.; Wudl, F.; Stucky, G. D.; Fredrickson, G. H.; Chmelka, B. F. *Macromolecules* **1999**, *32*, 4332.

(183) Jaroniec, M.; Solovyov, L. A. *Langmuir* **2006**, *22*, 6757.

(184) Kim, S. S.; Karkamkar, A.; Pinnavaia, T. J.; Kruk, M.; Jaroniec, M. *J. Phys. Chem. B* **2001**, *105*, 7663.

(185) Chenite, A.; Le Page, Y.; Sayari, A. *Chem. Mater.* **1995**, *7*, 1015.

(186) Jana, S. K.; Nishida, R.; Shindo, K.; Kugita, T.; Namba, S. *Microporous Mesoporous Mater.* **2004**, *68*, 133.

(187) Sun, J.; Ma, D.; Zhang, H.; Wang, C.; Bao, X.; Su, D. S.; Klein-Hoffmann, A.; Weinberg, G.; Mann, S. *J. Mater. Chem.***2006**, *16*, 1507.

(188) Fan, J.; Yu, C.; Lei, J.; Zhang, Q.; Li, T.; Tu, B.; Zhou, W.; Zhao, D. *J. Am. Chem. Soc.* **2005**, *127*, 10794.

(189) Kruk, M.; Hui, C. M. *Microporous Mesoporous Mater.* **2008**, *114*, 64.

(190) Wang, L.-Z.; Shi, J.-L.; Tang, F.-Q.; Yu, J.; Ruan, M.-L.; Yan, D.-S. *J. Mater. Chem.* **1999**, *9*, 643

(191) Luo, Y.; Hou, Z.; Li, R.; Zheng, X. *Microporous Mesoporous Mater.* **2008**, *109*, 585.

(192) Mukhopadhyay, K.; Ghosh, A.; Kumar, R. *Chem. Commun.* **2002**, 2404

(193) Celer, E. B.; Jaroniec, M. *J. Am. Chem. Soc.* **2006**, *128*, 14408.

(194) Newalkar, B. L.; Komarneni, S.; Katsuki, H. *Chem. Commun.* **2000**, 2389

(195) Tian, B.; Liu, X.; Yu, C.; Gao, F.; Luo, Q.; Xie, S.; Tu, B.; Zhao, D. *Chem. Commun.* **2002**, 1186

(196) Boote, B.; Subramanian, H.; Ranjit, K. T. *Chem. Commun.* **2007**, 4543

(197) Liu, X.; Sun, H.; Yang, Y. *J. Colloid Interface Sci.* **2008**, *319*, 377.

(198) Vercaemst, C.; Ide, M.; Allaert, B.; Ledoux, N.; Verpoort, F.; Van Der Voort, P. *Chem. Commun.* **2007**, 2261

(199) Fulvio, P. F.; Pikus, S.; Jaroniec, M. *J. Colloid Interface Sci.* **2005**, *287*, 717.

(200) Ravikovitch, P. I.; Neimark, A. V. *Langmuir* **2002**, *18*, 1550.

(201) Xiao, N.; Wang, L.; Liu, S.; Zou, Y.; Wang, C.; Ji, Y.; Song, J.; Li, F.; Meng, X.; Xiao, F.-S. *J. Mater. Chem.* **2009**, *19*, 661

(202) Huang, L.; Yang, X.; Kruk, M. *Langmuir* **submitted**

(203) Li, F.; Wang, J.-G.; Liu, Y.-P.; Zhou, H.-J.; Chen, T.-H. *J. Mater. Sci.* **2009**, *44*, 6505.

(204) Fan, J.; Lei, J.; Wang, L.; Yu, C.; Tu, B.; Zhao, D. *Chem. Commun.* **2003**, 2140

(205) Liu, J.; Li, C.; Yang, Q.; Yang, J.; Li, C. *Langmuir* **2007**, *23*, 7255.

(206) Sujandi; Park, S.-E.; Han, D.-S.; Han, S.-C.; Jin, M.-J.; Ohsuna, T. *Chem. Commun.* **2006**, 4131

(207) Yu, C.; Fan, J.; Tian, B.; Zhao, D.; Stucky, G. D. *Adv. Mater.* **2002**, *14*, 1742.

(208) Sayari, A.; Han, B.-H.; Yang, Y. *J. Am. Chem. Soc.* **2004**, *126*, 14348.

(209) Ji, X.; Lee, K. T.; Monjauze, M.; Nazar, L. F. *Chem. Commun.* **2008**, 4288

(210) Wang, Y.; Zhang, F.; Wang, Y.; Ren, J.; Li, C.; Liu, X.; Guo, Y.; Guo, Y.; Lu, G. *Mater. Chem. Phys.* **2009**, *115*, 649.

(211) Zhang, H.; Sun, J.; Ma, D.; Bao, X.; Klein-Hoffmann, A.; Weinberg, G.; Su, D.; Schlogl, R. *J. Am. Chem. Soc.* **2004**, *126*, 7440.

(212) Cui, X.; Moon, S.-W.; Zin, W.-C. *Mater. Lett.* **2006**, *60*, 3857.

(213) Chen, S.-Y.; Tang, C.-Y.; Chuang, W.-T.; Lee, J.-J.; Tsai, Y.-L.; Chan, J. C. C.; Lin, C.-Y.; Liu, Y.-C.; Cheng, S. *Chem. Mater.* **2008**, *20*, 3906.

(214) Chen, B.-C.; Lin, H.-P.; Chao, M.-C.; Mou, C.-Y.; Tang, C.-Y. *Adv. Mater.* **2004**, *16*, 1657.

(215) Kosuge, K.; Sato, T.; Kikukawa, N.; Takemori, M. *Chem. Mater.* **2004**, *16*, 899.

(216) Zhao, D.; Sun, J.; Li, Q.; Stucky, G. D. *Chem. Mater.* **2000**, *12*, 275.

(217) Brinks, M. K.; Studer, A. *Macromol. Rapid Commun.* **2009**, *30*, 1043.

(218) Tsujii, Y.; Ohno, K.; Yamamoto, S.; Goto, A.; Fukuda, T. *Adv. Polym. Sci.* **2006**, *197*, 1.

(219) Xu, F. J.; Yuan, Z. L.; Kang, E. T.; Neoh, K. G. *Langmuir* **2004**, *20*, 8200.

(220) Ejaz, M.; Ohno, K.; Tsujii, Y.; Fukuda, T. *Macromolecules* **2000**, *33*, 2870.

(221) Aoki, H.; Kitamura, M.; Ito, S. *Macromolecules* **2008**, *41*, 285.

(222) Ejaz, M.; Yamamoto, S.; Ohno, K.; Tsujii, Y.; Fukuda, T. *Macromolecules* **1998**, *31*, 5934.

(223) Tsujii, Y.; Ejaz, M.; Yamamoto, S.; Fukuda, T.; Shigeto, K.; Mibu, K.; Shinjo, T. *Polymer* **2002**, *43*, 3837.

(224) Urayama, K.; Yamamoto, S.; Tsujii, Y.; Fukuda, T.; Neher, D. *Macromolecules* **2002**, *35*, 9459.

(225) Yamamoto, S.; Ejaz, M.; Tsujii, Y.; Fukuda, T. *Macromolecules* **2000**, *33*, 5608.

(226) Yamamoto, S.; Ejaz, M.; Tsujii, Y.; Matsumoto, M.; Fukuda, T. *Macromolecules* **2000**, *33*, 5602.

(227) Ejaz, M.; Yamamoto, S.; Tsujii, Y.; Fukuda, T. *Macromolecules* **2002**, *35*, 1412.

(228) Zhao, B.; Brittain, W. J. *Macromolecules* **2000**, *33*, 8813.

(229) Edmondson, S.; Vo, C.-D.; Armes, S. P.; Unali, G.-F. *Macromolecules* **2007**, *40*, 5271.

(230) Garcia, I.; Zafeiropoulos, N. E.; Janke, A.; Tercjak, A.; Eceiza, A.; Stamm, M.; Mondragon, I. *J. Polym. Sci. Part A: Polym. Chem.* **2007**, *45*, 925.

(231) Marutani, E.; Yamamoto, S.; Ninjbadgar, T.; Tsujii, Y.; Fukuda, T.; Takano, M. *Polymer* **2004**, *45*, 2231.

(232) Wuang, S.; Neoh, K.; Kang, E.-T.; Pack, D.; Leckband, D. *Adv. Funct. Mater.* **2006**, *16*, 1723.

(233) Garcia, I.; Tercjak, A.; Zafeiropoulos, N. E.; Stamm, M.; Mondragon, I. *Macromol. Rapid Commun.* **2007**, *28*, 2361.

(234) Garcia, I.; Tercjak, A.; Zafeiropoulos, N. E.; Stamm, M.; Mondragon, I. *J. Polym. Sci. Part A: Polym. Chem.* **2007**, *45*, 4744.

(235) von Werne, T.; Patten, T. E. *J. Am. Chem. Soc.* **2001**, *123*, 7497.

(236) Kong, H.; Gao, C.; Yan, D. *J. Am. Chem. Soc.* **2003**, *126*, 412.

(237) Mulvihill, M. J.; Rupert, B. L.; He, R.; Hochbaum, A.; Arnold, J.; Yang, P. *J. Am. Chem. Soc.* **2005**, *127*, 16040.

(238) Qin, S.; Qin, D.; Ford, W. T.; Resasco, D. E.; Herrera, J. E. *J. Am. Chem. Soc.* **2003**, *126*, 170.

(239) Smith, J. J.; Zharov, I. *Chem. Mater.* **2009**, *21*, 2013.

(240) Yameen, B.; Kaltbeitzel, A.; Langer, A.; Mulller, F.; Gosele, U.; Knoll, W.; Azzaroni, O. *Angew. Chem. Int. Ed.* **2009**, *48*, 3124.

(241) Yameen, B.; Ali, M.; Neumann, R.; Ensinger, W.; Knoll, W.; Azzaroni, O. *Small* **2009**, *5*, 1287.

(242) Yameen, B.; Kaltbeitzel, A.; Langner, A.; Duran, H.; Muller, F.; Gosele, U.; Azzaroni, O.; Knoll, W. *J. Am. Chem. Soc.* **2008**, *130*, 13140.

(243) Huang, X.; Wirth, M. J. *Anal. Chem.* **1997**, *69*, 4577.

(244) Friebe, A.; Ulbricht, M. *Langmuir* **2007**, *23*, 10316.

(245) Guo, F.; Jankova, K.; Schulte, L.; Vigild, M. E.; Ndoni, S. *Langmuir* **2010**, *26*, 2008.

(246) Calvo, A.; Yameen, B.; Williams, F. J.; Azzaroni, O.; Soler-Illia, G. J. A. A. *Chem. Commun.* **2009**, 2553

(247) Li, C.; Yang, J.; Wang, P.; Liu, J.; Yang, Q. *Microporous Mesoporous Mater.* **2009**, *123*, 228.

(248) Pasetto, P.; Blas, H.; Audouin, F.; Boissiere, C.; Sanchez, C.; Save, M.; Charleux, B. *Macromolecules* **2009**, *42*, 5983.

(249) Moreno, J.; Sherrington, D. C. *Chem. Mater.* **2008**, *20*, 4468.

(250) Lenarda, M.; Chessa, G.; Moretti, E.; Polizzi, S.; Storaro, L.; Talon, A. *J. Mater. Sci.* **2006**, *41*, 6305.

(251) Grimaud, T.; Matyjaszewski, K. *Macromolecules* **1997**, *30*, 2216.

(252) Percec, V.; Barboiu, B. *Macromolecules* **2002**, *28*, 7970.

(253) Percec, V.; Barboiu, B.; Kim, H. J. *J. Am. Chem. Soc.* **1998**, *120*, 305.

(254) Percec, V.; Kim, H. J.; Barboiu, B. *Macromolecules* **1997**, *30*, 8526.

(255) Percec, V.; Kim, H. J.; Barboiu, B. *Macromolecules* **1997**, *30*, 6702.

(256) Robello, D. R.; Andre, A.; McCovick, T. A.; Mourey, T. H. *Macromolecules* **2002**, *35*, 9334.

(257) Ejaz, M.; Tsujii, Y.; Fukuda, T. *Polymer* **2001**, *42*, 6811.

(258) Kawakita, H.; Masunaga, H.; Nomura, K.; Uezu, K.; Akiba, I.; Tsuneda, S. *J. Porous Mater.* **2007**, *14*, 387.

(259) Percec, V.; Kim, H. J.; Barboiu, B. *Macromolecules* **1997**, *30*, 8526.

(260) Zha, L. S.; Zhang, Y.; Yang, W. L.; Fu, S. K. *Adv. Mater.* **2002**, *14*, 1090.

(261) Martín A; Morales G; Martínez F; Grieken R van; Cao L; Kruk M *J. Mater. Chem.*, *Accepted*.

(262) Nguyen, J. V.; Jones, C. W. *Macromolecules* **2004**, *37*, 1190.

(263) Kruk, M.; Dufour, B.; Celer, E. B.; Kowalewski, T.; Jaroniec, M.; Matyjaszewsk, K. *Polym. Mater. Sci. Eng. Preprints* **2007**, *97*.

(264) Wu, C. G.; Bein, T. *Science* **1994**, *266*, 1013.

(265) Qiao, W. M.; Song, Y.; Hong, S. H.; Lim, S. Y.; Yoon, S. H.; Korai, Y.; Mochida, I. *Langmuir* **2006**, *22*, 3791.

(266) Li, Z.; Jaroniec, M. *Chem. Mater.* **2003**, *15*, 1327.

(267) Adelhelm, P.; Hu, Y.-S.; Chuenchom, L.; Antonietti, M.; Smarsly, B. M.; Maier, J. *Adv. Mater.* **2007**, *19*, 4012.

(268) Gierszal, K. P.; Jaroniec, M. *Chem. Commun.* **2004**, 2576

(269) Li, Z.; Dai, S. *Chem. Mater.* **2005**, *17*, 1717.

(270) Li, Z.; Jaroniec, M.; Lee, Y.-J.; Radovic, L. R. *Chem. Commun.* **2002**, 1346.

(271) Gierszal, K. P.; Jaroniec, M.; Kim, T.-W.; Kim, J.; Ryoo, R. *New J. Chem.* **2008**, *32*, 981.

(272) Mohanty, P.; Fei, Y.; Landskron, K. *J. Am. Chem. Soc.* **2009**, *131*, 9638.

(273) Gierszal, K. P.; Jaroniec, M. *Stud. Surf. Sci. Catal.* **2005**, *156*, 581.

(274) Kim, T.-W.; Kleitz, F.; Paul, B.; Ryoo, R. *J. Am. Chem. Soc.* **2005**, *127*, 7601.

(275) Kleitz, F.; Kim, T.-W.; Ryoo, R. *Langmuir* **2006**, *22*, 440.

(276) Sun, J.; Ma, D.; Zhang, H.; Bao, X.; Weinberg, G.; Su, D. *Microporous Mesoporous Mater.* **2007**, *100*, 356.

(277) Mochida, I.; Korai, Y.; Ku, C.-H.; Watanabe, F.; Sakai, Y. *Carbon* **2000**, *38*, 305.

(278) Joo, S. H.; Ryoo, R.; Kruk, M.; Jaroniec, M. *J. Phys. Chem. B* **2002**, *106*, 4640.

(279) Fulvio, P. F.; Vinu, A.; Jaroniec, M. *J. Phys. Chem. C* **2009**, *113*, 13565.

(280) Cao, L.; Kruk, M. *Polym. Prepr.* **2010**, *51*, 409.

(281) Kim, T.-W.; Solovyov, L. A. *J. Mater. Chem.* **2006**, 1445.